



HAL
open science

Active control applied to offshore structures: positioning and attenuation of vortex induced vibrations

Eugênio Fortaleza

► **To cite this version:**

Eugênio Fortaleza. Active control applied to offshore structures: positioning and attenuation of vortex induced vibrations. Mathematics [math]. École Nationale Supérieure des Mines de Paris, 2009. English. NNT: . pastel-00006011

HAL Id: pastel-00006011

<https://pastel.hal.science/pastel-00006011>

Submitted on 20 Apr 2010

HAL is a multi-disciplinary open access archive for the deposit and dissemination of scientific research documents, whether they are published or not. The documents may come from teaching and research institutions in France or abroad, or from public or private research centers.

L'archive ouverte pluridisciplinaire **HAL**, est destinée au dépôt et à la diffusion de documents scientifiques de niveau recherche, publiés ou non, émanant des établissements d'enseignement et de recherche français ou étrangers, des laboratoires publics ou privés.



ED n°432 : SMI –
Sciences des Métiers de l'Ingénieur

T H E S E

pour obtenir le grade de

DOCTEUR DE L'ECOLE NATIONALE SUPERIEURE DES MINES DE PARIS

Spécialité “Mathématique et Automatique”

présentée et soutenue publiquement par
Eugênio FORTALEZA

le 24 Juin 2009

**Active Control Applied to Offshore Structures: Positioning and Attenuation
of Vortex Induced Vibrations**

Directeur de thèse : Jean Lévine

Jury

MM. Bernard Molin	Président
Celso Morooka	Rapporteur
Kurt Schalcher	Rapporteur
Daniel Averbuch	Examineur
Yann Creff	Examineur
Jean Lévine	Examineur
Claude Samson	Examineur

À minha família

Acknowledgements

I would like to thank Bernard Molin, president of the jury, Celso Morooka and Kurt Schlacher for their work as reporters, as well as Daniel Averbuch, Claude Samson for their participation in the jury. I also thank Jean Lévine for his work as thesis advisor.

Special thanks to Yann Creff, that trusted in my potential to graduate this PhD and guided me in this work until the end.

I would also like to thank Katja Wulf, Sebastien da Veiga, Claude Guillet, Olivier Lepreux, Jean-Pierre Wild that in different ways helped me during this period.

Résumé

Contrôle Actif de Structures Offshores: Positionnement et Réduction des Vibrations Induites par Vortex

L'exploration pétrolière en eaux profondes crée aujourd'hui de nouveaux défis technologiques. Plusieurs problèmes sont liés aux très longues structures servant à relier la plate-forme à la tête de puits. L'augmentation de la profondeur implique des structures plus longues et, par conséquent, plus souples. Deux problèmes liés à ce type de structure sont étudiés dans ce rapport : le positionnement de la structure pour sa connexion à la tête de puits (opération de ré-entrée), et les vibrations induites par vortex. La première partie de ce rapport est consacrée au contrôle de l'opération de ré-entrée. Deux stratégies différentes de planification sont proposées. La première est basée sur un modèle obtenu par une approche modale. La seconde approxime le comportement de la structure par l'équation d'un câble de Bernoulli avec amortissement. Les solutions approximées de cette EDP sont directement utilisées dans la conception du contrôleur. Deux types de contrôle en boucle fermée sont proposés : un système de suivi de trajectoire utilisant une fonction de Lyapunov, et un autre qui utilise l'inverse du système. La deuxième partie de ce rapport est consacrée à l'étude des vibrations induites par vortex (VIV) et à leur contrôle. Elle présente une première stratégie de contrôle afin de réduire les VIV. Cette stratégie est basée sur une analyse modale des équations du système. La loi de commande génère un déplacement en opposition de phase par rapport aux VIV, l'atténuation résultant d'un effet d'antirésonance. Les résultats de simulation sont confirmés par des expériences réalisées sur une maquette en modèle réduit.

Abstract

The petroleum exploration in deep water induces many challenges. Several problems are due to the extremely long structure that links the platform to the wellhead (risers). The depth increase makes the structure more slender, and consequently much more flexible. Its dynamical behavior can be described by an infinite dimensional system. Two associated problems are studied in this report: the positioning of the bottom end of structure, to connect it to the wellhead (reentry operation), and the vortex induced vibrations of these slender structures. The first part of this thesis is dedicated to the control of the reentry operation. Two different strategies are proposed. The first one is based on a finite dimensional model obtained by a modal approach. The other one considers that the behavior of the structure is close to the behavior of the Bernoulli's historical cable equation, completed with a damping factor. The proposed approximate solutions of this PDE are directly used in the control design. Two different closed loop controls are proposed: one using a Lyapunov function, and another tracking system that uses the system inversion to calculate the tracking feedback. The second part is dedicated to the study of the structure's undergoing vortex induced vibrations (VIV) and to their control. It presents a first control strategy to reduce the VIV. This control strategy is based on a modal analysis of the system equations. The control system generates a displacement in phase opposition to the VIV, attenuating the VIV because of an anti-resonance effect. The simulation results are confirmed by experiments done on a reduced scale setup.

Contents

- I Reentry control** **21**

- 1 Introduction and background** **27**

- 2 Modelling** **31**
 - 2.1 Structure forces 31
 - 2.1.1 General case 31
 - 2.1.2 Small angle assumption 34
 - 2.2 Hydrodynamic forces 35
 - 2.3 Boundary conditions 36
 - 2.4 Discretization of the physical model 37
 - 2.4.1 Finite difference method 37
 - 2.4.2 Finite element method 39
 - 2.4.3 Discrete model 43

- 3 Control designs** **45**
 - 3.1 Control using the modal reduction 46

3.1.1	Modal reduction of the discrete model	46
3.1.2	Control system	52
3.2	Analytical reentry control	56
3.2.1	Motion planning	56
3.2.2	Lyapunov design	60
3.2.3	Inverse model control	65
4	Conclusion for the reentry control part	69
II	VIV control	71
5	VIV background	77
5.1	Vortex Induced Vibrations	77
5.2	Passive VIV limitation	79
5.3	Vibration control	80
5.4	Active VIV limitation	82
6	Wake model	87
6.1	Phenomenological model	89
6.2	First harmonic approximation	91
6.3	VIV limit cycle: non resonant case	94
6.4	VIV limit cycle: resonant case	102

7	VIV control	107
7.1	VIV modal analysis	108
7.2	Control system	110
7.3	Mechanical fatigue	114
7.4	Numerical simulations	116
8	Reduced scale system	123
8.1	Experimental set description	123
8.1.1	Hydraulic plant	123
8.1.2	Structure undergoing VIV	125
8.1.3	Control system	126
8.2	Comparative analysis between numerical and experimental re- sults	127
8.3	Numerical simulations	128
8.4	Experimental results and discussion	130
9	Conclusion for the VIV control part	135
	Bibliography	137
A	Computations for the wake model in the resonant case	141

List of Figures

1.1	Platform during the reentry operation	28
2.1	Forces schema	32
2.2	a) Fixed support b) Rotary joint	36
2.3	Discretization schema	40
3.1	Dynamic response of the different models	51
3.2	Dynamic response of the different models (zoom)	52
3.3	Block diagram of the tracking system	53
3.4	Closed loop system output	55
3.5	System input	59
3.6	System output	60
3.7	Undisturbed case. Reference trajectory and system response.	61
3.8	Structure under constant disturbance due to the current.	64
3.9	Block diagram of the tracking system.	65
3.10	Structure under disturbances due to waves and sea current.	67

5.1	System under analysis	78
5.2	Transversal section and lateral view of devices to suppress VIV	85
5.3	Simplified model of building undergoing an earthquake	86
5.4	Tensioned cable	86
6.1	VIV amplitudes for different vortex shedding frequencies	88
6.2	VIV frequencies for different vortex shedding frequencies	89
6.3	Flexible structure undergoing VIV	92
6.4	Real part of matrix A eigenvalues. Zero values are associated to the non-resonant case.	97
6.5	Rigid cylinder undergoing vortex induced vibration in a non resonant case: structure displacement Υ (continuous line), wake variable Q (dashed line)	105
6.6	Rigid cylinder undergoing vortex induced vibration in a resonant case: Structure displacement Υ (continuous line), wake variable Q (dashed line)	106
7.1	Bode diagrams of the structure (continuous line) and the single mode model	111
7.2	Typical example of Wöhler curve	115
7.3	Cross-flow displacement for a constant sea current: open loop (dashed line) closed loop (continuous line)	117
7.4	Cross-flow displacement for a variable sea current: open loop (dashed line) closed loop (continuous line)	118
7.5	Cross-flow speed for a constant sea current: open loop (dashed line) closed loop (continuous line)	119

7.6	Cross-flow speed for a variable sea current: open loop (dashed line) closed loop (continuous line)	119
7.7	Cross-flow highest vibration Fourier transform for a constant sea current: open loop (dashed line) closed loop (continuous line)	120
7.8	Cross-flow highest vibration Fourier transform for a variable sea current: open loop (dashed line) closed loop (continuous line)	120
7.9	Cross-flow highest displacement for a constant sea current: open loop (dashed line) closed loop (continuous line)	121
7.10	Cross-flow highest displacement for a variable sea current: open loop (dashed line) closed loop (continuous line)	121
8.1	Experimental set overview	124
8.2	Stereovision system diagram	126
8.3	Open loop cross-flow displacement: numerical simulation and measured data	127
8.4	Fourier transform of the cross-flow displacement (open loop): numerical simulation and measured data	128
8.5	Closed loop cross-flow displacement: numerical simulation and measured data	129
8.6	Fourier transform of the cross-flow displacement (closed loop): numerical simulation and measured data	130
8.7	Cross-flow mean displacement amplitude (open and closed loop): numerical simulation	131
8.8	Cross-flow mean speed amplitude (open and closed loop): numerical simulation	132

8.9	Fourier transform of the cross-flow bottom end vibration (open and closed loop): numerical simulation	132
8.10	Cross-flow bottom end displacement (open and closed loop): numerical simulation	133
8.11	Measured cross-flow displacement: open and closed loop . . .	133
8.12	Fourier transform of the measured cross-flow displacement: open and closed loop	134

Introduction

This report presents the work made during the three years of a PhD program between IFP and the École des Mines de Paris, with the support of the French council of research (ANRT, French acronym), according to the program of partnership between industries and academic institutions (CIFRE, French acronym).

The research is dedicated to the control of long flexible structures used in offshore applications. The interest of studying offshore structures is linked to the discovery of large oil and gas reserves in deep water regions, and to the technological challenges associated to the drilling and exploration in these areas.

Two different problems are studied: the reentry operation and the vortex induced vibrations. The reentry operation consists in positioning the riser bottom end above the wellhead in order to connect it to a petroleum well. The objective of an active control is to minimize the time required for this operation, and to extend the range of meteorological conditions within which the connection is possible. To reach this goal, it is necessary to move the riser bottom end to the wellhead as fast as possible, and to make it stop accurately above the wellhead.

The vortex induced vibrations (VIV) are vibrations occurring for slender structures submerged in a flow, within a given range of Reynolds numbers. Within this range, the periodic vortex shedding generates an oscillating lift force. A lock-in phenomenon can appear and change the frequency of this force into one or more low damped natural frequencies of the structure. In these special cases the structure enters in resonance, generating vibrations that can drastically reduce its service life.

Unfortunately, offshore structures as the mooring cables and risers are extremely slender and often have low damped modes in the same frequency range than the periodic vortex shedding. That is the reason why the VIV study is interesting from an economical point of view, and many research groups dedicated to the subject around the world have been founded.

The studied subjects are presented in two different parts, each one dedicated to the modelling of the studied system and to the design of dedicated control laws.

Reentry control

This part is dedicated to the control of the reentry operation. The equations that define the behavior of slender structures are presented in chapter 2:

- The structure internal forces are defined and some assumptions are proposed to simplify the model, without any important loss of precision.
- The hydrodynamics forces, in this chapter, are defined by the linearized Morison's equation.
- A brief description of the methods to spatially discretize the model partial differential equation (PDE) is given.

In chapter 3, the reentry problem is analyzed and two different control strategies are proposed. The first one improves the control strategy developed by Sabri [33]. It is based on a discrete model that is reduced through a modal approach. Subsection 3.1.1 explains the method to rewrite a system into a modal base, and the principle of the modal reduction of high order systems (interests and drawbacks). The direct transfer generated by this reduction is replaced by a delay that tends to improve the model accuracy. The feedback control is obtained by model inversion.

The other control strategy considers that the behavior of several flexible structures is close to the behavior of the Bernoulli's historical cable equation, completed with a damping factor, that is associated to the hydrodynamic force described by the linearized Morison's equation. Approximate solutions are directly used in the control design, providing an extension to previous

works by Petit and Rouchon [35] on the control of heavy chains systems, in the framework of flatness as proposed by Fliess et al [12]. Two different closed loop control laws are proposed in this case: a tracking system using a Lyapunov function, following the idea of Thull et al [41], and another tracking system that uses the system inversion to calculate the tracking feedback.

These control systems can achieve the reentry with high precision, even in the presence of disturbances (sea current and marine waves).

VIV control

This part is dedicated to the study of structures undergoing vortex induced vibrations (VIV) and to their control. The main characteristics of this phenomenon and the current solutions are presented in chapter 5. The structure forces are considered as similar to the forces presented in chapter 2. However the hydrodynamic forces are represented with a more complex model proposed by Facchinetti [10]. This model contains a linear term inspired by the Morison's equation, plus a second term described by a non linear differential equation. Chapter 6 presents this wake model and the study of the limit cycle described by it.

Chapter 7 presents a first control strategy to reduce the vortex induced vibrations. This control strategy is based on the system equations and on a modal analysis. This modal analysis shows that, for low damped resonant frequencies, there is a phase shift of $\pm 90^\circ$ between a periodic external force at the riser top end, and the generated vibration along the structure. This phase shift is used in the design of the control law to reduce the VIV along the structure. The control system generates a displacement in phase opposition to the VIV, attenuating the VIV because of an anti-resonance effect.

Two different control laws are proposed to produce this displacement in the same frequency of the main vibration, but in phase opposition. The first one uses a series association of a bandpass filter with an adaptive gain and a phase shifter. The second one uses a dedicated observer especially designed to observe periodic disturbances and decompose it into sine and cosine, then the control is computed considering the adaptive gain and the phase shift.

The advantages of these strategies are the small displacements required to

reduce VIV, and the fact that no structural change is required along the structure submerged part. However, a displacement sensor close to the structure bottom is required.

For some operating conditions, simulations show a mechanical fatigue reduction of more than 70%. An interesting point of this technique is the small top displacement amplitude required to reduce the vibration along the entire riser. The current technique uses a top displacement of about 10% of the maximum riser displacement, for a 35% reduction of the vibration along the riser. These simulations results are confirmed by experiments done on a reduced scale system, presented in chapter 8.1.

Part I

Reentry control

Main Nomenclature

Capital letters.

A	State matrix.
B	Input matrix.
B_m	Input matrix of modal base.
B'_m	Reduced input matrix of modal base.
B'_{m2}	Delay system input matrix.
C	Output matrix.
C_m	Output matrix of modal base.
C'_m	Reduced output matrix of modal base.
D	Direct transfer.
D_2	Delay system direct transfer.
E	Elastic modulus.
F	Hydrodynamic force.
F_n	Normal force.
F_t	Tangential force.
H	Lyapunov function.
I	Identity matrix.
J	Second moment of area.
K	Stiffness matrix.
L	Region or subspace of a vector field.
N	Number of discretisation points.
O	Damping matrix.
P	disturbance.
R	Surface riser section.
S	Shearing force.
T	Tension.
U	Flow speed.
V	Eigenvector matrix.
\tilde{V}	Modified eigenvector matrix.
X	Structure state vector.

W	Modal state vector.
W'	Reduced modal state vector.
W'_2	State vector of the system with delay.
Y	Transverse riser displacement vector.
\dot{Y}	Transverse riser speed vector.

Lowercase letters.

a	Structure force over the fluid.
b	Mode associated gain.
c_1	Auxiliary constant 1.
c_2	Auxiliary constant 2.
e	Sine average amplitude.
f	Cosine average amplitude.
g	Apparent gravity.
h	Fluid force constant.
i	Imaginary unit.
k	Feedback gain.
l	Auxiliary variable.
m	Riser and fluid linear mass.
m_F	Fluid added linear mass.
m_I	Inertia coefficient.
m_S	Riser linear mass.
n	Number of discretization points.
o	Riser equilibrium position.
r	Tangential riser displacement.
s	Laplace variable.
t	Time.
u	Riser top external force.
\hat{u}	Riser top external force Laplace transform.
w	Apparent weight.
x	Horizontal axis.
y	System output.
\hat{y}	Laplace transform of the system output.
\hat{y}^P	Laplace transform of output part generated by P.
y_2	Delay system output.
z	Vertical axis.

Greek letters.

Θ	Bending.
Λ	Modified eigenvalue matrix.
Λ'	Reduced modified eigenvalue matrix.
Υ	Main riser displacement.
Υ_o	Reference trajectory.
Υ_R	Relative displacement.
Ω	Structure natural frequency.
α	Damping constant.
γ	Eigenvector real part.
ϵ	Delay.
ε	Van der Pol's equation parameter.
ζ	Auxiliary variable.
θ	Integration variable.
ϑ	Convergence time.
ι	Measure noise.
λ	Eigenvalue.
φ	Eigenvector imaginary part.
ϱ	Integration variable.
τ	Drag constant.
ϕ	Riser angle with the vertical.

Chapter 1

Introduction and background

The reentry operation consists in positioning the riser bottom end above the wellhead in order to connect it with the petroleum well. To reach this goal, it is necessary to move the riser bottom end to the wellhead as fast as possible, and to make it stop accurately above the wellhead. The main idea is to define a reference trajectory to move the riser bottom end from its initial position to the wellhead. Because of disturbances, a closed loop control is designed to make the structure bottom end track this trajectory.

Nowadays, reentry operations are made using a manual control. The interests of using an automatic control are to reduce the operation time and to extend the range of meteorological conditions within which the connection is possible. Nowadays, due to the severe weather conditions, a drilling ship or a FPSO (floating, production, storage and offloading unit) can wait several days until the manual reentry operation becomes possible. The final economic benefit of an active control is linked to the possible reduction of the global time necessary to drill an offshore well or to restart the production of a production well.

The riser is a structure with a low damping. The propagation of a mechanical wave from the top end to the bottom end induces large delays. These characteristics make manual control difficult, because a wrong control can easily make the riser oscillate, and it is quite difficult to manually reduce vibrations on a system involving large delay.

The dynamic behavior of offshore platforms has been largely studied. A

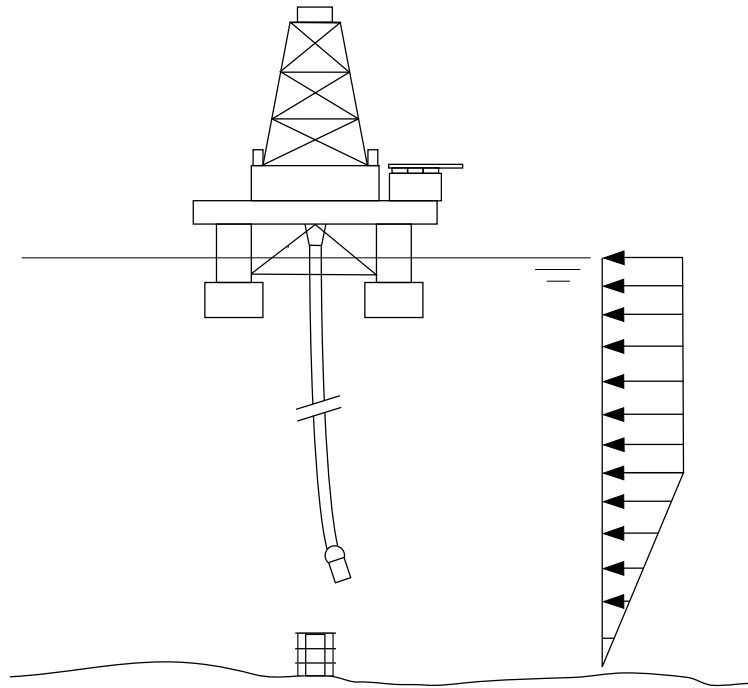


Figure 1.1: Platform during the reentry operation

model is presented in chapter 2. Some active control systems have been developed with different types of strategies. Two recent examples are a linear quadratic regulator (LQR) proposed by Yamamoto et al [44] and a linear parameter varying (LPV) proposed by Ioki et al [25]. However the precision of these methods and their ability to reduce the effect of the external disturbances remain limited. Chapter 3 presents two control systems.

The main strategy chosen to solve this problem is to define a reference trajectory that links the riser bottom end initial position to the wellhead, and then calculate the riser top end trajectory required to track this reference trajectory.

Two different approaches are proposed to calculate the top end trajectory in order to move the riser bottom end. The first one is presented in section 3.1. It is based on a reduced order model with a delay. This simple model comes from a modal reduction, the introduction of the delay improving the representation of the dynamic behavior of the structure.

The first step to obtain this reduced model is to spatially discretize the PDE

that defines the system behavior. The second step is a traditional modal reduction. The third and last step is the introduction of a delay that reduces the direct transfer introduced by the modal reduction.

The control system is based on this reduced model with a delay. It is used in the motion planning and in the tracking system. The stability of the closed loop system is proved by application of the simplified Nyquist criterion. The main advantages of this control system are the satisfactory performances, the robustness to external disturbances and the easy application for different kinds of flexible structures.

The second approach to design the open-loop control is presented in section 3.2 and uses the analytical solution of a PDE, that in several cases provides a good approximation of vertical structures dynamics. This motion planning is described in section 3.2.1.

Two different approaches are proposed for the closed loop. The first one is presented in section 3.2.2 and is based on a Lyapunov design that considers the mechanical energy of the system (dynamic and elastic). It gives good results in the undisturbed case as well as in presence of sea current. However it is inefficient in the case of waves.

The second feedback strategy in the case of the analytical motion planning is presented in section 3.2.3. It uses the analytical solution of the approximate system in the feedback loop and provides satisfactory results, not only in the cases where the Lyapunov control is efficient, but also in presence of waves. The stability of this control system is also proved with the use of the simplified Nyquist criterion.

Chapter 2

Modelling

In the offshore domain, riser is the usual term for any pipeline which links the platform to the seabed. As suggested by its name, this kind of pipeline usually serves to produce hydrocarbons from the undersea petroleum reservoirs. The most common form is a simple hollow cylinder.

In this chapter, we first present in section 2.1 a physical model of the riser, with the forces in the structure and the associated assumptions. Then, in section 2.2, we present a model for the hydrodynamic forces and the associated assumptions. The boundary conditions are presented in section 2.3. In section 2.4, two different methods are presented to discretize the complete model. Finally, section 2.4.3 summarizes the assumptions and presents the discrete model used along the sequence.

2.1 Structure forces

2.1.1 General case

The forces to be considered are depicted in figure 2.1. The forces over each point of the structure can be divided into internal and external forces. The internal forces for a riser are linked to the traction T and to the shearing force S , that are respectively locally parallel and locally perpendicular to the principal axis of the structure. The most important external forces are the

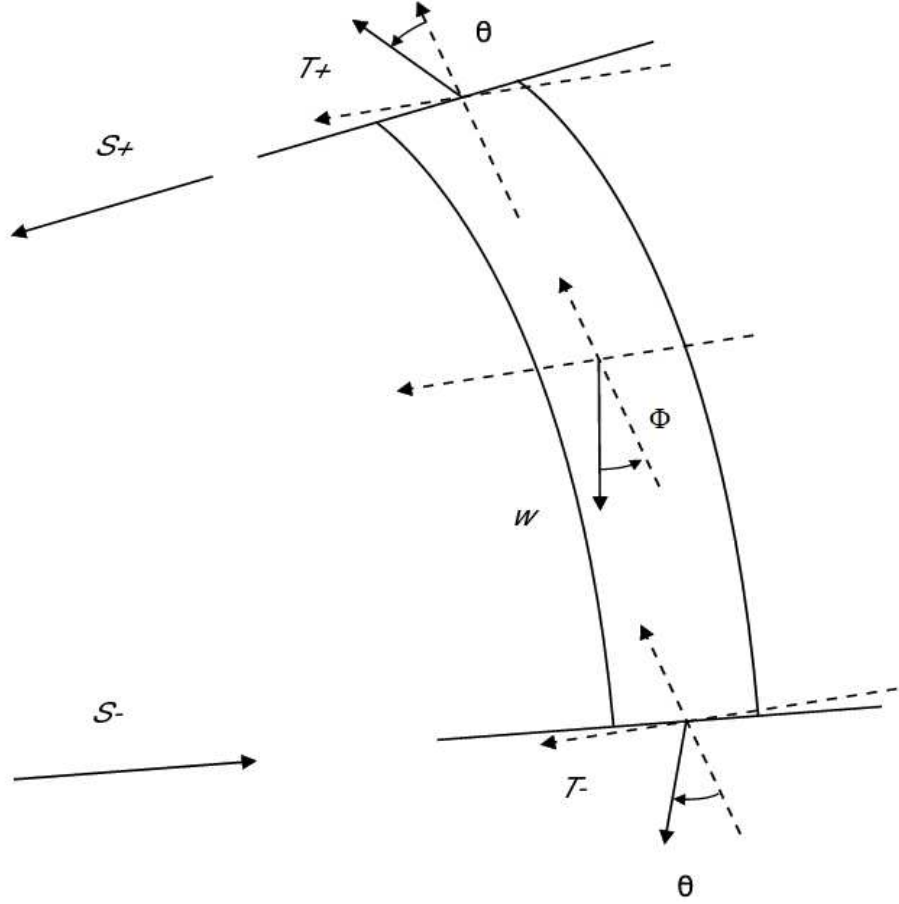


Figure 2.1: Forces schema

linear apparent weight w and the hydrodynamic forces, linked to the relative displacements of the structure and the fluid. For a better understanding, the riser dynamics and forces are described here in a curve coordinate system $o(z(\varsigma), x(\varsigma))$, where z is the vertical axis and x the horizontal axis. It is a parametric curve, function of ς , with the following characteristics: $\forall \varsigma, |\vec{\nabla} o| = 1$; $o(z(\varsigma), x(\varsigma))$ represents the riser equilibrium position in the (z, x) plan. The tangential riser displacements are represented by $\Xi(\varsigma, t)$ and the transverse displacements are defined by $\Upsilon(\varsigma, t)$.

Using Newton's inertia principle, it is possible to define the displacements in the cartesian directions $\Xi(\varsigma, t)$ and $\Upsilon(\varsigma, t)$ as functions of the forces represented in figure 2.1. We respectively define F_t and F_n as the tangential and normal hydrodynamic forces. θ and ϕ are respectively the bending and the

angle between the riser and the vertical axis z ; m_s is the riser linear mass. We have:

$$m_s \frac{\partial^2 \Xi}{\partial t^2} = \frac{T^+ \cos(\theta) - T^- \cos(\theta)}{-w \cos(\phi) + F_t(\varsigma, t)} - \frac{S^+ \sin(\theta) + S^- \sin(\theta)}{2}$$

$$m_s \frac{\partial^2 \Upsilon}{\partial t^2} = \frac{T^+ \sin(\theta) + T^- \sin(\theta)}{+w \sin(\phi) + F_n(\varsigma, t)} + \frac{S^+ \cos(\theta) - S^- \cos(\theta)}{2}$$

Considering $T^+ = T + \partial T / \partial \varsigma$, $T^- = T - \partial T / \partial \varsigma$, $S^+ = S + \partial S / \partial \varsigma$ and $S^- = S - \partial S / \partial \varsigma$ we can rewrite the first two equations into the following form:

$$m_s \frac{\partial^2 \Xi}{\partial t^2} = -S \sin(\theta) + \frac{\partial T}{\partial \varsigma} \cos(\theta) - w \cos(\phi) + F_t(\varsigma, t)$$

$$m_s \frac{\partial^2 \Upsilon}{\partial t^2} = T \sin(\theta) + \frac{\partial S}{\partial \varsigma} + w \sin(\phi) + F_n(\varsigma, t)$$

A third system equation comes from the Timoshenko beam equation. It describes the punctual relationship between the shearing force and the structure bending. This equation uses the constants E , J and A , that respectively denote the elastic modulus, the second moment of area and the surface riser section:

$$\frac{\partial \theta}{\partial \varsigma} \left(EJ \left(1 + \frac{T}{EA} \right)^{-3} \right) = -S$$

A fourth equation is based on the assumed linear elastic behavior of the structure, linked to the Hook's law, that correctly represents the behavior of ferrous materials in their elastic deformation domain:

$$\frac{\partial}{\partial \varsigma} \left(\frac{\partial \Xi}{\partial t} \right) = \frac{1}{EA} \frac{\partial T}{\partial t}$$

Using the time derivative of the ϕ definition we get the fifth equation:

$$\frac{\partial}{\partial \varsigma} \left(\frac{\partial \Upsilon}{\partial t} \right) = \frac{\partial \sin \phi}{\partial t}$$

The last equation comes from the definition of θ :

$$\frac{\partial \phi}{\partial \varsigma} = \theta$$

2.1.2 Small angle assumption

The risers can be considered as vertical structures ($\varsigma \mapsto (0, z)$, $\vec{\nabla}_o = (0, 1)$). Υ and Ξ are the displacements, respectively in the x and z directions. The offshore structures present small angles and small transversal displacements when compared to its length. This fact justifies that E and J can be considered constant and the following approximations: $\theta \rightarrow 0$, $\sin(\theta) \rightarrow \theta$, $\cos(\theta) \rightarrow 1$, and $w \rightarrow \partial T / \partial z$. This induces further approximations: $\phi \rightarrow 0$, $\sin(\phi) \rightarrow \phi$, and $\cos(\phi) \rightarrow 1$. Finally, under these assumptions, it is possible to rewrite the structure's equations as:

$$\left\{ \begin{array}{l} m_s \frac{\partial^2 \Xi}{\partial t^2} = \frac{\partial T}{\partial z} - \theta S - \frac{\partial T}{\partial z} + F_t(z, t) \\ m_s \frac{\partial^2 \Upsilon}{\partial t^2} = \frac{\partial S}{\partial z} + \theta T + \frac{\partial T}{\partial z} \phi + F_n(z, t) \\ EJ \frac{\partial \theta}{\partial z} \left(1 + \frac{T}{EA} \right)^{-3} = -S \\ \frac{\partial}{\partial z} \left(\frac{\partial \Xi}{\partial t} \right) = \frac{1}{EA} \frac{\partial T}{\partial t} \\ \frac{\partial}{\partial z} \left(\frac{\partial \Upsilon}{\partial t} \right) = \frac{\partial \phi}{\partial t} \\ \frac{\partial \phi}{\partial z} = \theta \end{array} \right. \quad (2.1)$$

The definition of vertical structures ($\varsigma \mapsto (0, z)$) gives $\phi = 0$ for $\Upsilon = 0$. So neither Υ nor ϕ have a constant term, and the EDP represented in the fifth equation of system 2.1 can be integrated in time to give

$$\phi = \frac{\partial \Upsilon}{\partial z} \quad (2.2)$$

According to the approximations, vertical and lateral displacements are independent; T does not depend on time t and is significantly smaller than EA . The third equation of system 2.1 can be rewritten without loss of accuracy as

$$S = -EJ \frac{\partial \theta}{\partial z} \quad (2.3)$$

This results assumes that the modified length of the riser, due to its apparent weight, is constant. In other words, the relative vertical displacements of the riser bottom end, in relation to the riser top end displacements, are considered as negligible. Applying equations 2.2 and 2.3 in the third equation of system 2.1, the equation of the transverse displacement becomes

$$m_s \frac{\partial^2 \Upsilon}{\partial t^2} = -EJ \frac{\partial^4 \Upsilon}{\partial z^4} + \frac{\partial}{\partial z} \left(T(z) \frac{\partial \Upsilon}{\partial z} \right) + F_n(z, t) \quad (2.4)$$

Equation 2.4 shows that a vertical slender structure with small transverse displacements can be analyzed (see [11, 31]) as a linearized Euler-Bernoulli beam with a constant section, under an axial traction plus external forces from the fluid. In this case, the transversal force associated to the beam model is represented by $-EJ(\partial^4 \Upsilon)/(\partial z^4)$. The transversal force associated to the traction is similar to the internal transversal force in a cable, and is represented by $\partial(T(z)(\partial \Upsilon/\partial z))/\partial z$. In some special cases, the difference between these two terms is so large that the structure behavior can be represented by only one of them. This is often the case for flexible risers, that are usually slender with small second moment of area J when compared to the riser length ($J = \pi r^4/4$ for a circular section of radius r).

2.2 Hydrodynamic forces

The hydrodynamic forces are defined in a general way by the Navier-Stokes equations, they are the unique external forces, except for the riser structure ends where external forces are present due to the boundary condition. In the case of reentry operation, the main hydrodynamic forces are in the plane including the riser bottom end and the wellhead. This force denoted $F_n(z, t)$ can be defined by the Morison's equation (valid for the actual Reynolds number of the flow around the structure):

$$F_n(z, t) = -m_F \frac{\partial^2 \Upsilon}{\partial t^2} - \mu \frac{\partial \Upsilon}{\partial t} \left| \frac{\partial \Upsilon}{\partial t} \right| \quad (2.5)$$

In this equation, μ is the drag constant and m_F is the fluid added mass. Denoting $m = m_S + m_F$, and considering the hydrodynamic force 2.5, equation 2.4 becomes

$$m \frac{\partial^2 \Upsilon}{\partial t^2} = -EJ \frac{\partial^4 \Upsilon}{\partial z^4} + \frac{\partial}{\partial z} \left(T(z) \frac{\partial \Upsilon}{\partial z} \right) - \mu \frac{\partial \Upsilon}{\partial t} \left| \frac{\partial \Upsilon}{\partial t} \right| \quad (2.6)$$

The drag term is linearized: $\frac{\mu}{m}|\frac{\partial \Upsilon}{\partial t}|$ is substituted by the constant τ , that is calculated as a function of μ/m and of the mean value of $\frac{\partial \Upsilon}{\partial t}$ along the structure. With this approximation the system becomes:

$$\frac{\partial^2 \Upsilon}{\partial t^2} = -\frac{EJ}{m} \frac{\partial^4 \Upsilon}{\partial z^4} + \frac{\partial}{\partial z} \left(\frac{T(z)}{m} \frac{\partial \Upsilon}{\partial z} \right) - \tau \frac{\partial \Upsilon}{\partial t} \quad (2.7)$$

2.3 Boundary conditions

The boundary conditions are defined by considering the physical fixation of the two extremities of the structure. The two kinds of fixation used in engineering are the fixed support and the rotary joint, as depicted in figure 2.2. The fixed support is used as default along this report. In this case, the

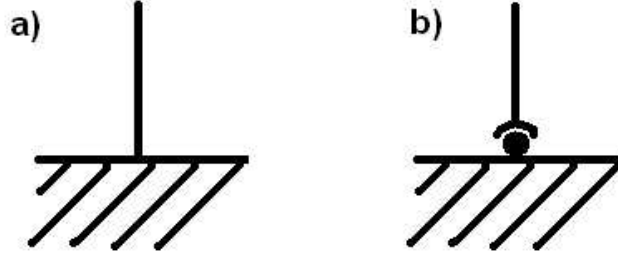


Figure 2.2: a) Fixed support b) Rotary joint

boundary conditions are $\Upsilon(L, t) = u(t)$, $\Upsilon(0, t) = 0$ (riser bottom end fixed), and $(\partial \Upsilon / \partial z)(L, t) = (\partial \Upsilon / \partial z)(0, t) = 0$ (rigidity condition at the fixation point). This boundary condition represents the external forces and moments applied by the supports to avoid the local displacement and rotation of the structure (for further information see [30]).

For a connected riser with rotary joints instead of fixed supports, the boundary conditions become: $\Upsilon(L, t) = u(t)$, $\Upsilon(0, t) = 0$, $(\partial^2 \Upsilon / \partial z^2)(L, t) = 0$ and $(\partial^2 \Upsilon / \partial z^2)(0, t) = 0$. This physically means that the rotary joint applies an external force over the structure to avoid its local displacement, however this kind of joint lets the structure free to turn around the fixation point.

The case of a riser with a disconnected bottom end with a punctual mass

m_a has the following boundaries conditions: $T_0 = m_a g$, $(\partial^2 \Upsilon / \partial z^2)(0, t) = 0$, and at $z = 0$ the cable term $\partial(mgz \partial Y / \partial z) / \partial z$ is replaced by $mg \partial Y / \partial z$.

2.4 Discretization of the physical model

The PDE presented in equation 2.7 does not have an analytical solution, so we propose two numerical methods, that can give an approximation of this solution. These methods discretize the transverse displacement function Υ and define Y as a vector of the structure displacement for N equidistant points along the structure.

2.4.1 Finite difference method

2.4.1.1 Numerical scheme

For the finite difference method, we denote L the structure length. The distance between two points, or between one riser extremity and its closest point, is defined by $l = L / (N + 1)$. The tension T is represented by $T = T_0 + mgz$, where T_0 is the tension on the riser bottom end and g the apparent gravity. The discrete derivatives of Y are calculated with the following recursive formula:

$$\frac{\partial^j Y_n}{\partial z^j} = \frac{1}{l} \left(\frac{\partial^{j-1} Y_{n+0.5}}{\partial z^{j-1}} - \frac{\partial^{j-1} Y_{n-0.5}}{\partial z^{j-1}} \right) \quad (2.8)$$

The values of Y are only available for $n \in N$, so in the special case of the first derivative at $n \in N$ it is not possible to use the values $Y_{n+0.5}$ and $Y_{n-0.5}$. Then the formula used is

$$\frac{\partial Y_n}{\partial z} = \frac{Y_{n+1} - Y_{n-1}}{2l} \quad (2.9)$$

Considering equation 2.7, the partial derivatives with respect to z at a point n (not an extremity) can be represented by

$$\begin{aligned} \frac{\partial^4 Y_n}{\partial z^4} &= \frac{Y_{n-2} - 4Y_{n-1} + 6Y_n - 4Y_{n+1} + Y_{n+2}}{l^4} \\ \frac{\partial}{\partial z} \left(T(z) \frac{\partial Y_n}{\partial z} \right) &= (T_0 + mgz) \frac{Y_{n-1} - 2Y_n + Y_{n+1}}{l^2} + mg \frac{-Y_{n-1} + Y_{n+1}}{2l} \end{aligned}$$

Observing that $z = nl$ at Y_n , equation 2.7 can be rewritten in a general way, for all the points not affected by the boundary conditions, as

$$\begin{aligned} \frac{d^2 Y_n}{dt^2} = & EJ \frac{-Y_{n-2} + 4Y_{n-1} - 6Y_n + 4Y_{n+1} - Y_{n+2}}{ml^4} \\ & + (T_0 + mgnl) \frac{Y_{n-1} - 2Y_n + Y_{n+1}}{ml^2} \\ & + g \frac{-Y_{n-1} + Y_{n+1}}{2l} - \tau \frac{dY_n}{dt} \end{aligned} \quad (2.10)$$

2.4.1.2 Boundary conditions

Considering $u(t)$ as the platform position, for a riser with both extremities connected to fixed supports (support used as default along this report), the boundary conditions are $\Upsilon(L, t) = u(t)$, $\Upsilon(0, t) = 0$ (riser bottom end fixed), and $(\partial\Upsilon/\partial z)(L, t) = (\partial\Upsilon/\partial z)(0, t) = 0$ (rigidity condition at the fixation point). Equation 2.7 can be redefined with these boundary conditions for the points $n = 1$ and $n = N$ as follows:

$$\begin{aligned} \frac{d^2 Y_1}{dt^2} = & EJ \frac{-6Y_1 + 4Y_2 - Y_3}{ml^4} + (T_0 + mgl) \frac{-2Y_1 + Y_2}{ml^2} \\ & + g \frac{Y_2}{2l} - \tau \frac{dY_1}{dt} \end{aligned}$$

$$\begin{aligned} \frac{d^2 Y_N}{dt^2} = & EJ \frac{-Y_{N-2} + 4Y_{N-1} - 6Y_N + 3u(t)}{ml^4} \\ & + (T_0 + mglN) \frac{Y_{N-1} - 2Y_N + u}{ml^2} \\ & + g \frac{-Y_{N-1} + u}{2l} - \tau \frac{dY_N}{dt} \end{aligned}$$

For a connected riser with rotary joints instead of fixed supports, the boundary conditions become $\Upsilon(L, t) = u(t)$, $\Upsilon(0, t) = 0$, $(\partial^2\Upsilon/\partial z^2)(L, t) = 0$ and $(\partial^2\Upsilon/\partial z^2)(0, t) = 0$. Equation 2.7 can be redefined for the points $n = 1$ and

$n = N$, now considering the rotary joints:

$$\frac{d^2 Y_1}{dt^2} = EJ \frac{-5Y_1 + 4Y_2 - Y_3}{ml^4} + \left(T_0 + \frac{mgl}{2} \right) \frac{-2Y_1 + Y_2}{ml^2} + g \frac{Y_2}{2l} - \tau \frac{dY_1}{dt}$$

$$\begin{aligned} \frac{d^2 Y_N}{dt^2} &= EJ \frac{-Y_{N-2} + 4Y_{N-1} - 5Y_N + 2u}{ml^4} \\ &\quad (T_0 + mglN) \frac{+Y_{N-1} - 2Y_N + u}{ml^2} \\ &\quad + g \frac{-Y_{N-1} + u}{2l} - \tau \frac{dY_N}{dt} \end{aligned}$$

The case of a riser with a disconnected bottom end and a punctual mass m_a should be analyzed considering $N + 1$ displacement points (Y_0 represents the riser bottom end displacement). In this case, the boundaries conditions are $T_0 = m_a g$, $(\partial^2 \Upsilon / \partial z^2)(0, t) = 0$, and at $z = 0$ the cable term $\partial(mgz \partial Y / \partial z) / \partial z$ is replaced by $mg \partial Y / \partial z$. The equation for Y_0 displacements is

$$\frac{d^2 Y_0}{dt^2} = EJ \frac{-Y_0 + 2Y_1 - Y_2}{m_a l^4} + g \frac{-Y_0 + Y_1}{l} \quad (2.11)$$

2.4.2 Finite element method

2.4.2.1 Numerical scheme

Discretization results similar to those of subsection 2.4.1 can be obtained using the finite element method (the fact that both approaches yield the same equations in this case is well known). This method divides the structure into N parts, and concentrates all the masses and forces of these parts on their gravity centers. The system becomes discrete in z , so the derivatives with

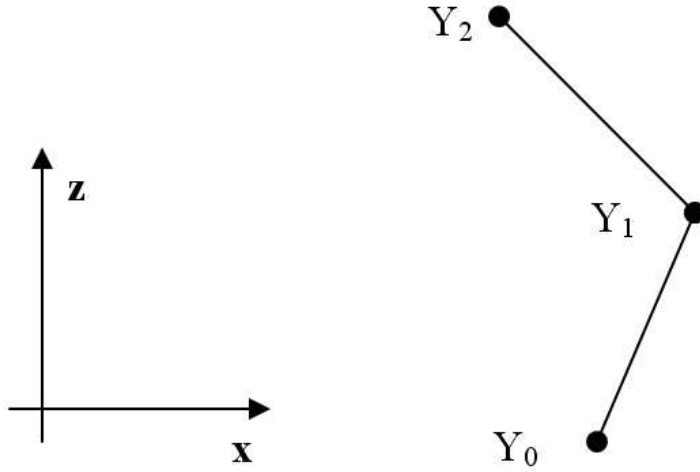


Figure 2.3: Discretization schema

respect to z can be calculated the same way than for equations 2.8 and 2.9.

$$\begin{aligned}
 & \frac{\partial^2 Y}{\partial t^2} \int_{nl-l/2}^{nl+l/2} mdz = \\
 & \int_{nl-l/2}^{nl+l/2} \left(-EJ \frac{\partial^4 Y}{\partial z^4} + \frac{\partial}{\partial z} \left(T(z) \frac{\partial Y}{\partial z} \right) - m\tau \frac{\partial Y}{\partial t} \right) dz \\
 & \frac{\partial^2 Y}{\partial t^2} ml = \\
 & \left[-EJ \frac{\partial^3 Y}{\partial z^3} + T(z) \frac{\partial Y}{\partial z} \right]_{nl-l/2}^{nl+l/2} + \int_{nl-l/2}^{nl+l/2} -m\tau \frac{\partial Y}{\partial t} dz
 \end{aligned}$$

Considering the beam term given by $-EJ \partial^4 Y / \partial z^4$, and the cable term given by $\partial(mgz \partial Y / \partial z) / \partial z$, both discretization schemes give equivalent results.

$$\begin{aligned} \left[-EJ \frac{\partial^3 Y}{\partial z^3} \right]_{nl-l/2}^{nl+l/2} &= -EJ \frac{+Y_{n-2} - 4Y_{n-1} + 6Y_n - 4Y_{n+1} + Y_{n+2}}{l^3} \\ \left[T(z) \frac{\partial Y}{\partial z} \right]_{nl-l/2}^{nl+l/2} &= \left(T_0 + mg \left(np + \frac{l}{2} \right) \right) \frac{Y_{n+1} - Y_n}{l} \\ &\quad - \left(T_0 + mg \left(np - \frac{l}{2} \right) \right) \frac{Y_n - Y_{n-1}}{l} \\ &= (T_0 + mgnl) \frac{+Y_{n-1} - 2Y_n + Y_{n+1}}{l} \\ &\quad + mg \frac{-Y_{n-1} + Y_{n+1}}{2} \end{aligned}$$

The finite element of first order approximates the transverse position of any element point by the position of center of mass of the element. So the hydrodynamic force can be defined as

$$\int_{nl-l/2}^{nl+l/2} -\tau \frac{\partial Y}{\partial t} dz = -ml\tau \frac{\partial Y}{\partial t}$$

In the case of the structures under study, the final model obtained by the finite element method of first order is exactly the same as the model obtained by the method of finite difference represented in equation 2.10.

$$\begin{aligned} ml \frac{d^2 Y_n}{dt^2} &= EJ \frac{-Y_{n-2} + 4Y_{n-1} - 6Y_n + 4Y_{n+1} - Y_{n+2}}{l^3} \\ &\quad + (T_0 + mgnl) \frac{Y_{n-1} - 2Y_n + Y_{n+1}}{l} \\ &\quad + mg \frac{-Y_{n-1} + Y_{n+1}}{2} - ml\tau \frac{dY_n}{dt} \end{aligned} \tag{2.12}$$

2.4.2.2 Boundary conditions

Considering $u(t)$ as the platform position, for a riser with both extremities connected to fixed supports (support used as default along this report), the

boundary conditions are $\Upsilon(L, t) = u(t)$, $\Upsilon(0, t) = 0$ (riser bottom end fixed), and $(\partial\Upsilon/\partial z)(L, t) = (\partial\Upsilon/\partial z)(0, t) = 0$ (rigidity condition at the fixation point). Equation 2.7 can be redefined with these boundary conditions for the points $n = 1$ and $n = N$ as follows:

$$\begin{aligned}
ml \frac{d^2 Y_1}{dt^2} &= EJ \frac{-6Y_1 + 4Y_2 - Y_3}{l^3} + (T_0 + mgl) \frac{-2Y_1 + Y_2}{l} \\
&\quad + mg \frac{Y_2}{2} - ml\tau \frac{dY_1}{dt} \\
ml \frac{d^2 Y_N}{dt^2} &= EJ \frac{-Y_{N-2} + 4Y_{N-1} - 6Y_N + 3u(t)}{l^4} \\
&\quad + (T_0 + mglN) \frac{Y_{N-1} - 2Y_N + u}{l^2} \\
&\quad + mg \frac{-Y_{N-1} + u}{2} - ml\tau \frac{dY_N}{dt}
\end{aligned}$$

For a connected riser with rotary joints instead of fixed supports, the boundary conditions become $\Upsilon(L, t) = u(t)$, $\Upsilon(0, t) = 0$, $(\partial^2\Upsilon/\partial z^2)(L, t) = 0$ and $(\partial^2\Upsilon/\partial z^2)(0, t) = 0$. Equation 2.7 can be redefined for the points $n = 1$ and $n = N$, now considering the rotary joints:

$$\begin{aligned}
ml \frac{d^2 Y_1}{dt^2} &= EJ \frac{-5Y_1 + 4Y_2 - Y_3}{l^3} + \left(T_0 + \frac{mgl}{2} \right) \frac{-2Y_1 + Y_2}{l} \\
&\quad + mg \frac{Y_2}{2} - ml\tau \frac{dY_1}{dt} U(l) \\
ml \frac{d^2 Y_N}{dt^2} &= EJ \frac{-Y_{N-2} + 4Y_{N-1} - 5Y_N + 2u}{l^3} \\
&\quad + (T_0 + mglN) \frac{+Y_{N-1} - 2Y_N + u}{l} \\
&\quad + mg \frac{-Y_{N-1} + u}{2} - ml\tau \frac{dY_N}{dt} U(Nl)
\end{aligned}$$

The case of a riser with a disconnected bottom end and a punctual mass m_a should be analyzed considering $N + 1$ displacement points (Y_0 represents the riser bottom end displacement). In this case, the boundaries conditions are $T_0 = m_a g$, $(\partial^2\Upsilon/\partial z^2)(0, t) = 0$, and at $z = 0$ the cable term

$\partial(mgz\partial Y/\partial z)/\partial z$ is replaced by $mg\partial Y/\partial z$. The equation for Y_0 displacements is

$$m_a l \frac{d^2 Y_0}{dt^2} = EJ \frac{-Y_0 + 2Y_1 - Y_2}{l^3} + m_a g (-Y_0 + Y_1) \quad (2.13)$$

2.4.3 Discrete model

The used continuous model is defined by equation 2.7. It is obtained with the assumptions of vertical structure, small angles displacements and linear drag.

$$\frac{\partial^2 \Upsilon}{\partial t^2} = -\frac{EJ}{m} \frac{\partial^4 \Upsilon}{\partial z^4} + \frac{\partial}{\partial z} \left(\frac{T(z)}{m} \frac{\partial \Upsilon}{\partial z} \right) - \tau \frac{\partial \Upsilon}{\partial t}$$

$$\Upsilon(L, t) = u(t) \quad \text{and} \quad \frac{\partial \Upsilon}{\partial z}(L, t) = 0$$

$$\frac{\partial^2 \Upsilon}{\partial z^2}(0, t) = 0 \quad \text{and} \quad \frac{\partial^3 \Upsilon}{\partial z^3}(0, t) = 0$$

The system obtained by one of the two methods of space discretization, for a structure with a top fixed support and a free bottom end, has a state X given by $X = (Y_1, \dots, Y_N, \dot{Y}_1, \dots, \dot{Y}_N)^T$. N is the number of discretization points used to discretize the system (normally about one hundred or more in the studied cases). The control u is defined as the riser top end displacement ($u = \Upsilon(L, t)$). This displacement is proportional to a force at the riser top end, giving:

$$\begin{cases} \dot{X} = AX + Bu, \text{ with } A = \begin{pmatrix} 0 & I \\ -K & -O \end{pmatrix} \\ y = CX \end{cases} \quad (2.14)$$

O is a diagonal matrix which form is $O = \tau I$, where I is an identity matrix. O contains the accelerations associated to the hydrodynamic damping. Vector B is the acceleration of the structure associated to the riser top end displacement, $B = (0, \dots, -EJ/(l^4 m), 3EJ/(l^4 m) + (T_0 + mgl(N + 0.5))/(l^2 m))^T$. The system output y is the displacement of the closest point to the riser bottom end $\Upsilon(0, t)$. The output equation can be expressed as $\Upsilon(0, t) = CX$ for a given row-matrix C with only one non-zero entry $C = (1, 0, \dots, 0)$. The stiffness matrix K is a symmetric matrix containing the structure internal accelerations according to the discretization scheme presented in sections 2.4.1 and 2.4.2. For instance, a restricted part of K writes

$$\begin{aligned}
K_{(N-3\dots N, N-3\dots N)} = & \begin{pmatrix} 6EJ/(l^4 m) + 2(T_0 + mgl(N-2))/(l^2 m) & & \\ -4EJ/(l^4 m) - (T_0 + mgl(N-1.5))/(l^2 m) & & \\ & EJ/(l^4 m) & \end{pmatrix} \\
& \begin{pmatrix} -4EJ/(l^4 m) - (T_0 + mgl(N-1.5))/(l^2 m) & & EJ/(l^4 m) \\ 6EJ/(l^4 m) + 2(T_0 + mgl(N-1))/(l^2 m) & -4EJ/(l^4 m) - (T_0 + mgl(N-0.5))/(l^2 m) & \\ -4EJ/(l^4 m) - (T_0 + mgl(N-0.5))/(l^2 m) & 6EJ/(l^4 m) + 2(T_0 + mglN)/(l^2 m) & \end{pmatrix}
\end{aligned}$$

Chapter 3

Control designs

In this chapter, we use the structure model, and its discretized form, both presented in section 2.4.3. The main strategy adopted in this chapter to design the control system can be divided into two main points:

- Define a convenient control model, that links the riser top end position $u = \Upsilon(L, t)$ to the position of the riser bottom end $y = \Upsilon(0, t)$.
- Use this control model to define reference trajectories for the system input and output, and to design closed loops to track the output reference.

The analytical solution of the continuous model is unknown and the inversion of the high order discrete model can not be robust, in particular because of numerical errors. In sections 3.1 and 3.2, two different solutions are proposed to define control models and associated control laws.

The first one is presented in 3.1. It is based on a reduced order model with a delay. This simple model comes from a modal reduction and correctly represents the dynamic behavior of the structure. The second approach to design the open-loop control is presented in 3.2 and uses the analytical solution of a PDE, that in several cases provides a good approximation of the system dynamics.

3.1 Control using the modal reduction

In this section, the high order discretized system of equations is approximated by a convenient control model, obtained by modal reduction, described in section 3.1.1, and by the introduction of a delay. In section 3.1.2, the inverted reduced model is used to directly calculate the input reference trajectory, and associated to a filter in the design of the feedback loop.

3.1.1 Modal reduction of the discrete model

3.1.1.1 Modal base

Infinite order physical models represented by PDEs are approximated by high order systems of Ordinary Differential Equations (ODE), as presented in sections 2.4.1 and 2.4.2. For these discretized models, it is very difficult to identify the influence of each state on the system output y , in response to variations of the input u . Changes of coordinates can be searched for, in order to clarify the picture. Such a change of coordinates is proposed by the modal base, that uses the system eigenvalues. For the transformed dynamics, it is possible to analyze the system output variations as a sum of influences due to distinct sets containing only one or two states (see [40, 20] for further information). However, using the eigenvalues matrix as the new state matrix implies the introduction of complex numbers. To avoid this, it is possible to use a block-diagonal matrix, for which each pair of complex conjugate eigenvalues is represented by a 2×2 sub-matrix. This coordinate change is usually called modal decomposition and is described in this section. We write the discrete model of the structure:

$$\begin{cases} \dot{X} &= AX + Bu, \text{ with } A = \begin{pmatrix} 0 & I \\ -K & -O \end{pmatrix} \\ y &= CX \end{cases} \quad (3.1)$$

The state vector X represents the positions and speeds of all the discretisation points, $u = \Upsilon(L, t)$ is the riser top end position and $y = \Upsilon(0, t)$ is the position of the riser bottom end. The first step for the modal decomposition of the state matrix A is to calculate the eigenvector matrix V , that is also a square $2N$ -dimensional matrix. It contains two kinds of columns (eigenvectors): one corresponding to negative real eigenvalues, with real entries, and the other,

pairwise, corresponding to complex conjugate eigenvalues λ_j and $\bar{\lambda}_j$, and containing complex conjugates values. The latter pairs of columns can be replaced by two columns, the first with the real part γ , and the other with the imaginary part φ . This leads to a new change of coordinates matrix \tilde{V} . In these coordinates, the dynamics of equation (3.1) with $A_M = \tilde{V}^{-1}A\tilde{V}$, $W = \tilde{V}^{-1}X$, $B_M = \tilde{V}^{-1}B$ and $C_M = C\tilde{V}$, writes

$$\begin{cases} \dot{W} &= A_M W + B_M u \\ y &= C_M W \end{cases} \quad (3.2)$$

where A_M has the same dimension of A , only real entries and the following form:

$$A_M = \begin{pmatrix} \lambda_1 & & & & & \\ & \ddots & & & & \\ & & Re(\lambda_j) & Im(\lambda_j) & & 0 \\ & & -Im(\lambda_j) & Re(\lambda_j) & & \\ & & & & \ddots & \\ 0 & & & & & \lambda_{2N} \end{pmatrix} \quad (3.3)$$

In this base, an under-damped mode of the structure is associated to a pair of complex conjugate eigenvalues $(\lambda_j, \bar{\lambda}_j)$ with negative real parts. Its dynamic behavior is given by

$$\begin{pmatrix} \dot{W}_j \\ \dot{W}_{j+1} \end{pmatrix} = \begin{pmatrix} Re(\lambda_j) & Im(\lambda_j) \\ -Im(\lambda_j) & Re(\lambda_j) \end{pmatrix} \begin{pmatrix} W_j \\ W_{j+1} \end{pmatrix} + \begin{pmatrix} B_{M_j} \\ B_{M_{j+1}} \end{pmatrix} u \quad (3.4)$$

The dynamic behavior of an over-damped mode of the structure is associated to two real eigenvalues. It is represented in the following form:

$$\begin{pmatrix} \dot{W}_j \\ \dot{W}_{j+1} \end{pmatrix} = \begin{pmatrix} \lambda_j & 0 \\ 0 & \lambda_{j+1} \end{pmatrix} \begin{pmatrix} W_j \\ W_{j+1} \end{pmatrix} + \begin{pmatrix} B_{M_j} \\ B_{M_{j+1}} \end{pmatrix} u$$

Rewriting the dynamical system into this coordinate system makes the sub-systems independent between them. So, it is possible to analyze the dynamic response of each sub-system separately. In the case of offshore structures, a specific excitation produces a system response largely dominated by a group of sub-matrices. A possible reduced order model is made of this group of sub-matrices as state matrix. The choice of this group and the replacement of the other part of the state matrix is different for each kind of system. Two different cases are detailed in sections 3.1.1.3 and 7.1.

3.1.1.2 Modal base: numerical example

Consider the equation 7.1 in the case of an adimensional model of a vertical soft cable (strong influence of the hydrodynamic drag). The input is considered as the cable top end and the free structure bottom end is the output:

$$\dot{X} = \begin{pmatrix} 0 & 0 & 1 & 0 \\ 0 & 0 & 0 & 1 \\ -1 & 1 & -2 & 0 \\ 1 & -3 & 0 & -2 \end{pmatrix} + \begin{pmatrix} 0 \\ 0 \\ 0 \\ 2 \end{pmatrix} \Upsilon(L, t) \quad (3.5)$$

For sake of simplicity, only two discrete points are considered. The eigenvalues of the state matrix are $-1 \pm 1.55i, -0.36$ and -1.64 . The eigenvector matrix is

$$V = \begin{pmatrix} -0.0986 - 0.1532i & -0.0986 + 0.1532i & -0.8703 & -0.4802 \\ 0.2380 + 0.3698i & 0.2380 - 0.3698i & -0.3605 & -0.1989 \\ 0.3366 & 0.3366 & 0.3102 & 0.7893 \\ -0.8125 & -0.8125 & 0.1285 & 0.3269 \end{pmatrix}$$

and the matrix \tilde{V} and A_M have the following form:

$$\tilde{V} = \begin{pmatrix} -0.0986 & 0.1532 & -0.8703 & -0.4802 \\ 0.2380 & -0.3698 & -0.3605 & -0.1989 \\ 0.3366 & 0 & 0.3102 & 0.7893 \\ -0.8125 & 0 & 0.1285 & 0.3269 \end{pmatrix}$$

$$A_M = \begin{pmatrix} -1 & -1.5538 & 0 & 0 \\ 1.5538 & -1 & 0 & 0 \\ 0 & 0 & -0.3564 & 0 \\ 0 & 0 & 0 & -1.6436 \end{pmatrix}$$

Equation 3.6 writes in this case

$$\dot{W} = \begin{pmatrix} -1 & -1.55 & 0 & 0 \\ 1.55 & -1 & 0 & 0 \\ 0 & 0 & -0.37 & 0 \\ 0 & 0 & 0 & -1.64 \end{pmatrix} W + \begin{pmatrix} -2.10 \\ -1.35 \\ -0.63 \\ 1.14 \end{pmatrix} \Upsilon(L, t) \quad (3.6)$$

$$\Upsilon(0, t) = (-0.098 \quad 0.153 \quad -0.870 \quad -0.480) W$$

In this example, three groups of independent equations can be isolated. The first is associated to the complex conjugate eigenvalues and the 2×2 sub-matrix. The two others groups are associated to real eigenvalues.

3.1.1.3 Modal reduction

The main objective of the reentry operation is to move the riser to a specific horizontal position and to stop it at this position. Consider the system represented in its modal base by

$$\begin{cases} \dot{W} &= A_M W + B_M u \\ y &= C_M W \end{cases} \quad (3.7)$$

The suggested modal reduction consists in only keeping the modes associated to the largest static gains between the input $u = \Upsilon(L, t)$ and the output $y = \Upsilon(0, t)$, to represent the major part of the slow-frequencies behavior of system 3.1. These modes are captured in a low order system as in Sabri's work [33]. The matrix A'_M and the vectors B'_M , C'_M and W' are the small part of the original system that approximates the dynamic behavior of the structure associated to the chosen eigenvalues

$$\begin{cases} \dot{W}' &= A'_M W' + B'_M u \\ y &= C'_M W' + D'_M u \end{cases} \quad (3.8)$$

The classical modal reduction represented in equation 3.8 (see Benner [4] for further information) replaces all the others modes by a direct transfer D'_M . Equation 3.9 represents this direct transfer. Its value is the static gain of the removed part of the system, so that the reduction conserves the static gain:

$$D'_M = C'_M A'^{-1}_M B'_M - C_M A^{-1}_M B_M \quad (3.9)$$

Identified model In the case of the reentry operation, the conventional modal reduction represented in equation 3.8 is not adapted, because of the direct transfer D'_M : this direct transfer gives to the model a high frequency behavior, which is not at all in accordance with the structure behavior as, normally, the structure does not present such a large direct transfer.

The solution proposed by Sabri in [33] is to keep the matrix A'_M and to use an identification procedure, from sinusoidal input excitation on the real system. This identification considers $D = 0$, and defines the values for B_I and C_I to best fit the real structure response by the following reduced model

$$\begin{cases} \dot{W}_I &= A'_M W_I + B_I u \\ y &= C_I W_I \end{cases} \quad (3.10)$$

The main limitations of this strategy are the cost of on field identification, the problems of accuracy associated to the measurement, and the fact that slender vertical structures behavior is better represented when a pure delay is used in the reduced order model.

Reduced model with a delay As discussed in the previous section, the conventional modal reduction is not adapted to describe the structure behavior. In order to improve accuracy of the reduced model, the proposed solution is to determine the equivalent model with a delay ϵ that best represents the dynamic behavior of the high order model 3.7

$$\begin{cases} \dot{W}_D &= A'_M W_D + B_D u(t - \epsilon) \\ y &= C'_M W_D + D_D u(t - \epsilon) \end{cases} \quad (3.11)$$

Proposition 1 Consider a step input at time t' . For $t \geq t' + \epsilon$, providing that vectors B_D and D_D in 3.11 satisfy

$$\begin{aligned} B_D &= A'_M (e^{\epsilon A'_M} - I) A'^{-1}_M B'_M + B'_M \\ D_D &= C'_M (e^{\epsilon A'_M} - I) A'^{-1}_M B'_M + D'_M \end{aligned} \quad (3.12)$$

the output of system 3.11 is equal to the output of system 3.8. For $t < t' + \epsilon$, the output of system 3.11 keeps its initial value.

Proof The ϵ input delay guarantees that system 3.11 keeps its initial state until $t = t' + \epsilon$. Assume that for $t \geq t' + \epsilon$, the two systems have the same output. As the systems inputs $u(t)$ and $u(t - \epsilon)$ are constant for $t \geq t'$, if there exists $T \geq t' + \epsilon$ such that $\dot{W}_D(T) = \dot{W}'(T)$ and $C'_M W_D(T) + D_D u(T - \epsilon) = C'_M W'(T) + D'_M u(T)$, then, for all $t \geq t' + \epsilon$, $C'_M W_D(t) + D_D u(t - \epsilon) = C'_M W'(t) + D'_M u(t)$. Considering $T = t' + \epsilon$, the following expressions hold:

$$B_D u(t') = (A'_M (e^{\epsilon A'_M} - I) A'^{-1}_M B'_M + B'_M) u(t' + \epsilon)$$

$$D_D u(t') = (C'_M (e^{\epsilon A'_M} - I) A'^{-1}_M B'_M + D'_M) u(t' + \epsilon)$$

from which expressions of B_D and D_D are derived, as for all $t \geq t' + \epsilon$, $u(t - \epsilon) = u(t)$. ■

The delay ϵ can be chosen to reduce D_D . Actually, the delay ϵ is chosen in such a way that

- the direct transfer is small but different from zero;
- the sign of the time derivative of the output at $t + \epsilon$ is equal to the sign of the input variation. Otherwise stated, subject to an input step, the reduced system does not exhibit any inverse response.

The first condition tells that the reduced system is non strictly causal, which permits the realization of its inverse. The second condition induces that the zeroes of the reduced system are stable, guaranteing the stability of the inverse system.

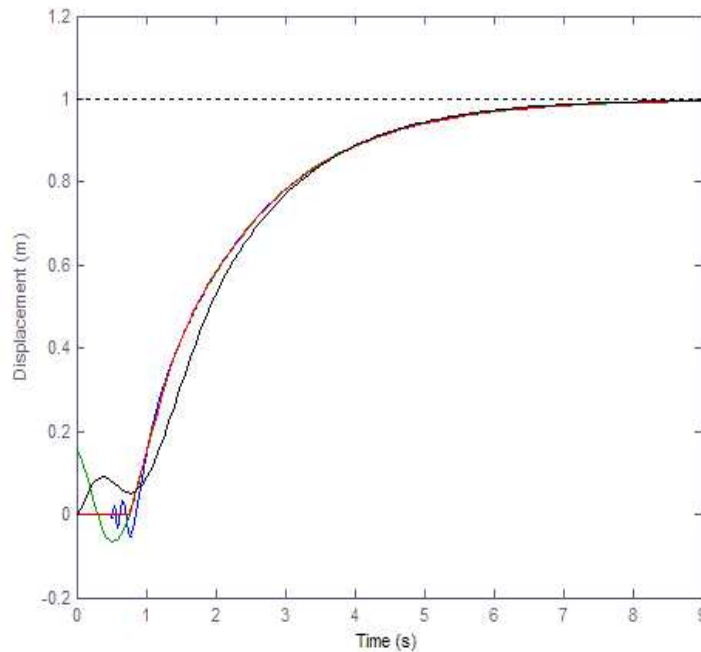


Figure 3.1: Dynamic response of the different models

In figure 3.1, the reduced models are compared using the complete model of a the reduced scale system used by Sabri [33]. The complete system response is represented in blue, the response of the reduced models 3.8, 3.10 and 3.11 are respectively presented in green, black and red. On the blue curve, non stable zeroes generate the initial oscillations. Figure 3.2 is a zoom on the

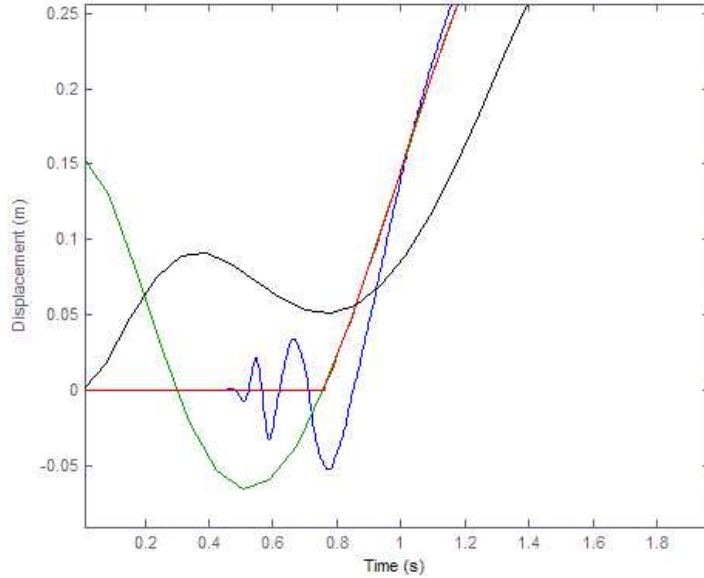


Figure 3.2: Dynamic response of the different models (zoom)

initial part of the step responses. The complete model is a 80^{th} order system and the reduced models are 4^{th} orders systems, that represent a reduction of 95% of the system order. However this drastic reduction does not imply a large loss of precision.

3.1.2 Control system

This subsection presents the control strategy based upon the reduced model 3.11. In the Laplace domain, the transfer function for this model is denoted $G(s) = e^{-\epsilon s}(C'_M(sI - A'_M)^{-1}B_D + D_D)$. The open loop control u_o can be calculated using the system inverse $G(s)^{-1}$ and the bottom reference trajectory y_o ($u_o = G(s)^{-1}y_o$).

Proposition 2 *Applied on system 3.11, the control law*

$$u(s) = \frac{-kG(s)^{-1}e^{-\epsilon s}}{s}(y(s) - y_o(s)) + u_0(s) \quad (3.13)$$

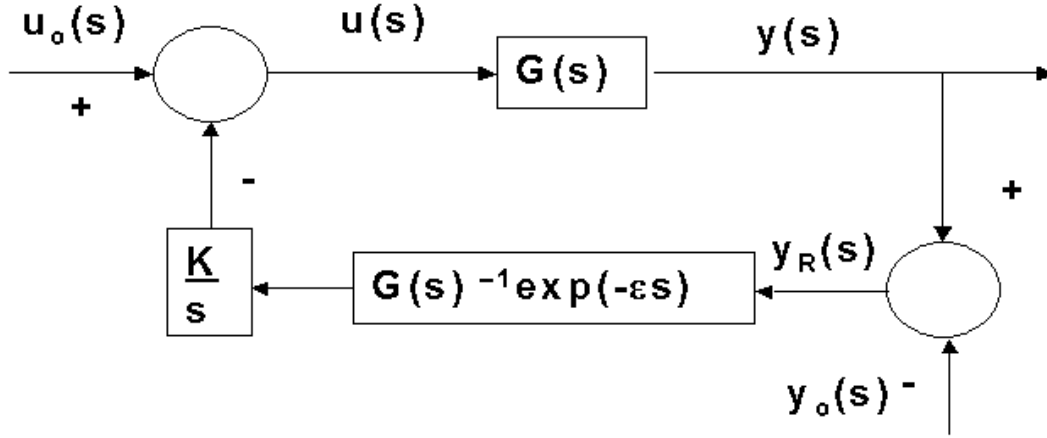


Figure 3.3: Block diagram of the tracking system

stabilizes system 3.11 around any trajectory y_o if $k < \pi/(2\epsilon)$.

Proof As the transfer function $G(s)$ does not have unstable zeros or poles, the closed loop does not induce any cancellation between unstable zeros and poles. Thus the stability of this feedback law can be analyzed by the simplified Nyquist criterion. Denote $M(s)$ the open loop transfer function between $y_o(s)$ and $y(s)$, $M(s) = k \exp(-\epsilon s)/s$. Rewriting $\exp(-\epsilon s)$ into its trigonometric form and replacing $s = i\omega$:

$$M(i\omega) = \frac{k(\cos(\epsilon\omega) - i \sin(\epsilon\omega))}{i\omega} \quad (3.14)$$

Considering $k > 0$, the most negative real value of equation 3.14 occurs for $\omega = \omega_0 = \pi/(2\epsilon)$. For this value, $M(\omega_0) = -k/\omega_0$. A sufficient condition for the closed loop stability is $M(\omega_0) > -1$, which leads to $k < \pi/(2\epsilon)$. ■

In practice, a value of k much smaller than $k < \pi/(2\epsilon)$ is used, to provide robustness. Typically, $k = \pi/(16\epsilon)$. The diagram of this tracking system is presented in figure 3.3. The same principle is used in the sequel (section 3.2.3). The main difference between the tracking systems comes from the inverted model that is used. In this section, the inverted model comes from a reduced order system, and in section 3.2.3 the inverted system comes from the analytical solution of a simplified model.

For this feedback design, the inverted system $G(s)^{-1}$ is associated to an integrator k/s . This integrator is used as a filter to attenuate high frequencies

brought by the inversion process.

Proposition 3 *Applied on system 3.11, the control law 3.13 rejects low frequencies disturbances.*

Proof The closed loop transfer function between the disturbance $P(s)$ and the system output $y(s)$ is

$$\frac{y(s)}{P(s)} = \frac{s}{s + ke^{-\epsilon s}} \quad (3.15)$$

Replacing $s = i\omega$, The transfer function 3.15 gives the associated system gain to each frequency ω .

$$\frac{y(i\omega)}{P(i\omega)} = \frac{i\omega}{i\omega + ke^{-\epsilon i\omega}}$$

For low frequencies disturbances ($\omega \rightarrow 0$), the influence of the disturbances over the system output goes to zero ($|y(i\omega)/P(i\omega)| \rightarrow 0$). ■

The delay is added in the controller to insure its causality. Results are illustrated in figure 3.4. We respectively have in blue, red and green, the reference trajectory, the open loop and the closed loop response for a system with external disturbances. Even if the system is stable, the disturbances generate errors on the system trajectory. The tracking system is able to reduce the system error in the case of disturbances with periods larger than the system delay.

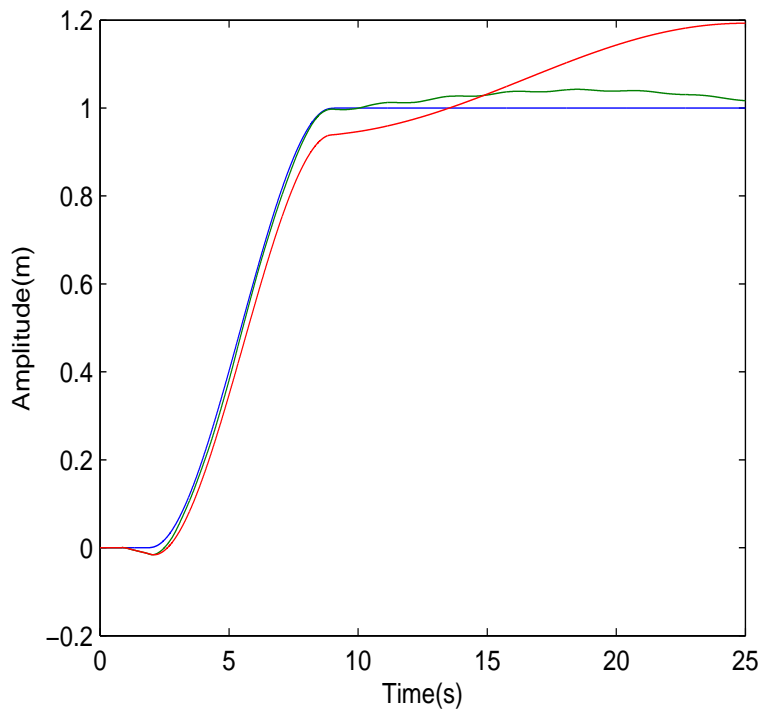


Figure 3.4: Closed loop system output

3.2 Analytical reentry control

This chapter presents a control strategy based on an approximated solution of a PDE, valid for flexible structures with low damping (see Fortaleza et al in [15] and [16]). The corresponding model turns out to be differentially flat [12], a property directly used in the control design, providing an extension to previous works of Petit and Rouchon [34], Thull et al [41]. The presented solution permits to calculate the reference trajectory for the riser top position, from a pre-defined reference trajectory for the riser bottom end position. This solution avoids the errors introduced in the model by the spatial discretization.

Two controllers are proposed to ensure that the trajectories are tracked. The first one is based on a Lyapunov function. It provides an efficient solution in the undisturbed case and, with slight modifications, in presence of sea current. The second one is directly based on the system analytical solution and provides a larger application range that also includes the systems disturbed by waves.

3.2.1 Motion planning

As presented in chapter 2, we can consider a structure with small transverse displacements (see [11, 31]) as a linearized Euler-Bernoulli beam with a constant section, under an axial traction plus external forces from the fluid:

$$\frac{\partial^2 \Upsilon}{\partial t^2} = -\frac{EJ}{m} \frac{\partial^4 \Upsilon}{\partial z^4} + \frac{\partial}{\partial z} \left(\frac{T(z)}{m} \frac{\partial \Upsilon}{\partial z} \right) - \tau \frac{\partial \Upsilon}{\partial t}$$

The tension for a disconnected riser without an added mass is a linear function of its weight ($T = (m_s - \rho S)z$), where ρ represents the water density and S the transverse section surface. The constant term $(m_s - \rho S)/m$ can be replaced by an effective gravity g , so we can rewrite equation 2.7 as

$$\frac{\partial^2 \Upsilon}{\partial t^2} = -\frac{EJ}{m} \frac{\partial^4 \Upsilon}{\partial z^4} + \frac{\partial}{\partial z} \left(gz \frac{\partial \Upsilon}{\partial z} \right) - \tau \frac{\partial \Upsilon}{\partial t} \quad (3.16)$$

Extremely long vertical structures with small angles displacements or small Young modulus E share the particular characteristic that $EJ \partial^4 \Upsilon / \partial z^4 \ll$

$\partial(T(\partial\Upsilon)/\partial z)/\partial z$. So equation 3.16 can be reduced to the Bernoulli's traditional cable equation, completed with a damping factor:

$$\frac{\partial^2 \Upsilon}{\partial t^2}(z, t) = \frac{\partial}{\partial z} \left(gz \frac{\partial \Upsilon}{\partial z}(z, t) \right) - \tau \frac{\partial \Upsilon}{\partial t}(z, t) \quad (3.17)$$

Proposition 4 *The damping factor τ can be developed in Taylor series around zero, to get an approximate solution of 3.17. This solution links the trajectory of the structure bottom end to the trajectory of any other point of the structure. In particular, it can be used to link the bottom trajectory to the top trajectory. For a development up to order 2 in τ , this solution is given by*

$$\begin{aligned} \Upsilon(z, t) = & \frac{1}{2\pi} \int_{-\pi}^{\pi} \left(\Upsilon(0, t - 2\sqrt{\frac{z}{g}} \sin \theta) \right. \\ & \left. (1 - \tau \sqrt{\frac{z}{g}} \sin \theta + \tau^2 \frac{z \sin^2 \theta}{g}) \right. \\ & \left. + \frac{\tau^2}{2} \int_0^t \Upsilon(0, \varrho - 2\sqrt{\frac{z}{g}} \sin \theta) \sqrt{\frac{z}{g}} \sin \theta d\varrho \dots \right) d\theta \end{aligned} \quad (3.18)$$

Proof First the change of coordinates $l = 2\sqrt{z/g}$ transforms equation 3.17 into

$$-l \frac{\partial^2 \Upsilon}{\partial t^2}(l, t) - \tau l \frac{\partial \Upsilon}{\partial t}(l, t) + \frac{\partial \Upsilon}{\partial l}(l, t) + l \frac{\partial^2 \Upsilon}{\partial l^2}(l, t) = 0 \quad (3.19)$$

Using a t -Laplace transform and considering the cable stopped at $t = 0$, equation 3.19 can be rewritten, with $\hat{\Upsilon}$ the Laplace transform of Υ , as:

$$-ls^2 \hat{\Upsilon}(l, s) - \tau ls \hat{\Upsilon}(l, s) + \frac{\partial \hat{\Upsilon}}{\partial l}(l, s) + l \frac{\partial^2 \hat{\Upsilon}}{\partial l^2}(l, s) = 0 \quad (3.20)$$

Consider the second change of coordinates $\zeta = il\sqrt{s(s+\tau)}$. It transforms (3.20) into a well-known Bessel equation of the first kind:

$$\zeta \hat{\Upsilon}(\zeta, s) + \frac{\partial \hat{\Upsilon}}{\partial \zeta}(\zeta, s) + \zeta \frac{\partial^2 \hat{\Upsilon}}{\partial \zeta^2}(\zeta, s) = 0 \quad (3.21)$$

The solution $\hat{\Upsilon}(z, s)$ has the following form:

$$\hat{\Upsilon}(z, s) = c_1 J_0(2i\sqrt{s(s+\tau)}\sqrt{z/g}) + c_2 Y_0(2i\sqrt{s(s+\tau)}\sqrt{z/g})$$

where J_0 and Y_0 are respectively the Bessel functions of first and second kinds [1]. Sought after solutions are finite for $z = 0$, so these solutions must be such that $c_2 = 0$.

$$\widehat{\Upsilon}(z, s) = \widehat{\Upsilon}(0, s) J_0(2i\sqrt{s(s+\tau)}\sqrt{z/g}) \quad (3.22)$$

Another way to define $\widehat{\Upsilon}(z, s)$ is:

$$\widehat{\Upsilon}(z, s) = \frac{1}{2\pi} \int_{-\pi}^{\pi} \exp(-2\sqrt{s(s+\tau)}\sqrt{z/g} \sin \theta) \widehat{\Upsilon}(0, s) d\theta \quad (3.23)$$

The term $\exp(-2\sqrt{s(s+\tau)}\sqrt{z/g} \sin \theta)$ in equation 3.23 can be expanded into a Taylor series around $\tau = 0$:

$$\begin{aligned} \exp(-2\sqrt{s(s+\tau)}\sqrt{z/g} \sin \theta) &= \left(\exp(-2\sqrt{s(s+\tau)}\sqrt{z/g} \sin \theta) \right)_{\tau=0} \\ &+ \tau \left(\frac{\partial(\exp(-2\sqrt{s(s+\tau)}\sqrt{z/g} \sin \theta))}{\partial \tau} \right)_{\tau=0} \\ &+ \tau^2 \left(\frac{\partial^2(\exp(-2\sqrt{s(s+\tau)}\sqrt{z/g} \sin \theta))}{\partial \tau^2} \right)_{\tau=0} \dots \end{aligned}$$

The terms of the series can be rewritten into the following form:

$$\begin{aligned} \left(\exp(-2\sqrt{s(s+\tau)}\sqrt{z/g} \sin \theta) \right)_{\tau=0} &= \exp(-2\sqrt{s^2}\sqrt{z/g} \sin \theta) \\ \left(\frac{\partial(\exp(-2\sqrt{s(s+\tau)}\sqrt{z/g} \sin \theta))}{\partial \tau} \right)_{\tau=0} &= - \exp(-2\sqrt{s^2}\sqrt{z/g} \sin \theta) \\ &\quad \sqrt{z/g} \sin \theta \\ \left(\frac{\partial^2(\exp(-2\sqrt{s(s+\tau)}\sqrt{z/g} \sin \theta))}{\partial \tau^2} \right)_{\tau=0} &= \exp(-2\sqrt{s^2}\sqrt{z/g} \sin \theta) \\ &\quad \left(\frac{z \sin^2 \theta}{g} + \sqrt{z/g} \frac{\sin \theta}{s} \right) \end{aligned} \quad (3.24)$$

Using the Taylor series, the transfer function between $\widehat{\Upsilon}(0, s)$ and $\widehat{\Upsilon}(z, s)$ can be represented in the Laplace domain by

$$\begin{aligned} \widehat{\Upsilon}(z, s) &= \frac{1}{2\pi} \int_{-\pi}^{\pi} \widehat{\Upsilon}(0, s) \exp(-2\sqrt{s^2}\sqrt{z/g} \sin \theta) \\ &\quad \left(1 - \tau \sqrt{\frac{z}{g}} \sin \theta + \tau^2 \left(\frac{z \sin^2 \theta}{g} + \sqrt{\frac{z}{g}} \frac{\sin \theta}{2s} \right) \right) + \dots d\theta \end{aligned} \quad (3.25)$$

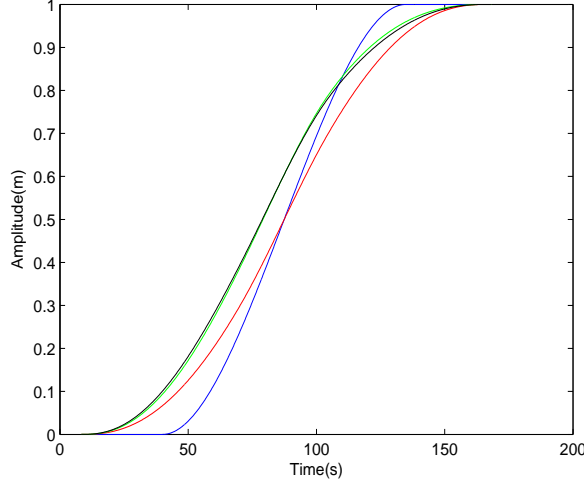


Figure 3.5: System input

Inverse Laplace transforms are easily found for the terms of the series. They can be analyzed as delays and associated to a reference trajectory $\Upsilon(0, t)$ as

$$\begin{aligned} \Upsilon(z, t) = & \frac{1}{2\pi} \int_{-\pi}^{\pi} \left(\Upsilon(0, t - 2\sqrt{\frac{z}{g}} \sin \theta) \right. \\ & \left. (1 - \tau \sqrt{\frac{z}{g}} \sin \theta + \tau^2 \frac{z \sin^2 \theta}{g}) \right. \\ & \left. + \frac{\tau^2}{2} \int_0^t \Upsilon(0, \varrho - 2\sqrt{\frac{z}{g}} \sin \theta) \sqrt{\frac{z}{g}} \sin \theta d\varrho \dots \right) d\theta \end{aligned}$$

■

The open loop solution is found by numerically integrating equation 3.18, to define the control trajectory $\Upsilon_o(L, t)$, where L is the riser length. A numerical example shows that the accuracy is increased when the number of terms in the series increases. Figure 3.5 shows the reference trajectory of $\Upsilon(0, t)$ in blue and the lines in red, green and black respectively show the trajectories of $\Upsilon(L, t)$ using the terms of the series up to the first one, the second one and third one (order 2 in τ). Looking at equation 3.18, we observe that the smaller τ is, the faster the series converges to the exact trajectory.

Figure 3.6 shows in blue the reference trajectory of $\Upsilon(0, t)$ and the output trajectories, using the input trajectories calculated with series up to the first, second and third term (respectively in red, dark blue and green).

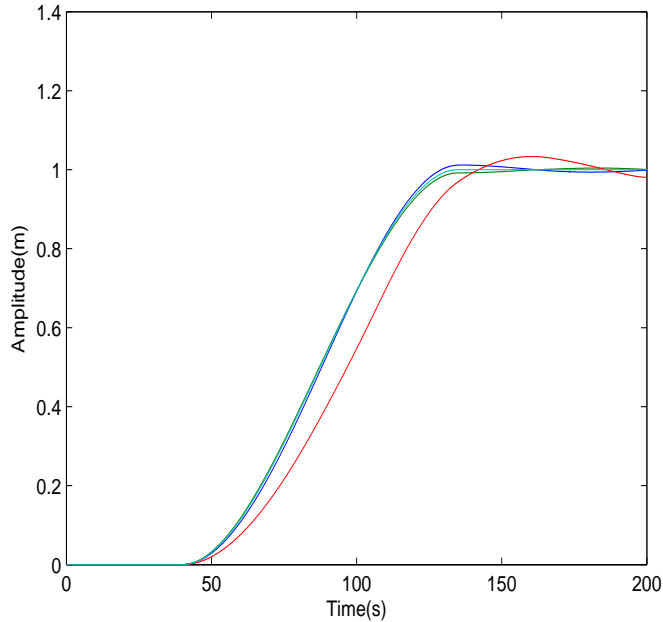


Figure 3.6: System output

One way to estimate the validity of the approximations in the real operation conditions is to simulate a typical case of reentry. The considered discrete system for this numerical simulation comes from the use of the finite element method on the equation (2.4), for a vertical 2 km long steel riser with external diameter = 0.55 m, internal diameter = 0.5 m and a fixed support at the top. These are typical values for a drilling riser in deep water. In figure 3.7, the hydrodynamic force is represented by equation (2.5). The example in Figure 3.7 shows that the approximations made have a small effect on the open loop system response.

3.2.2 Lyapunov design

This section presents a strategy that uses a Lyapunov function to design a tracking system in order to ensure the stability and reduce the system error, defined as the difference between the real position of the structure and the reference trajectory.

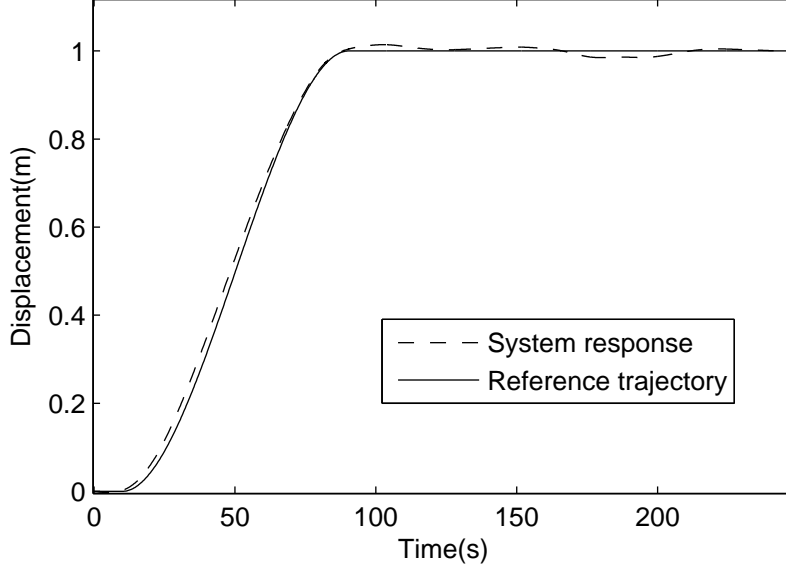


Figure 3.7: Undisturbed case. Reference trajectory and system response.

3.2.2.1 Undisturbed case

We consider the relative displacement Υ_R around the reference trajectory Υ_o : $\Upsilon_R = \Upsilon - \Upsilon_o$. The objective is to define a tracking system to enforce the convergence of Υ_R to zero.

Proposition 5 *Applied on system given by the equation 3.17, the control law*

$$\Upsilon(L, t) = \Upsilon_o(L, t) - k \int_0^t \left(g \frac{\partial \Upsilon_R}{\partial z}(L, v) + \frac{\Upsilon_R(L, v)}{\vartheta^2} \right) dv \quad (3.26)$$

can be used to asymptotically track any bottom reference $\Upsilon_o(0, t)$. In equation 3.26, k is the controller gain, ϑ a tuning parameter, and $\Upsilon_o(L, t)$ a top reference trajectory, computed from the specified bottom reference trajectory $\Upsilon_o(0, t)$ from equation 3.18.

Proof Consider the system given by 3.17. Following the idea proposed by Thull et al [41], a candidate Lyapunov function H , based on the system

energy associated to Υ_R , is given by

$$H = \frac{L\Upsilon_R^2(L, t)}{2\vartheta^2} + \frac{1}{2} \int_0^L \left(z \left(\frac{\partial \Upsilon_R}{\partial z} \right)^2 + \left(\frac{\partial \Upsilon_R}{\partial t} \right)^2 \right) dz \quad (3.27)$$

Parameter ϑ represents the convergence time and determines the energy associated to the relative displacement of the structure top. Using equation (3.17), the time derivative of H is computed as follows:

$$\begin{aligned} \frac{dH}{dt} &= \frac{L\Upsilon_R(L, t)}{\vartheta^2} \frac{\partial \Upsilon_R}{\partial t}(L, t) + \int_0^L \left(z \frac{\partial \Upsilon_R}{\partial z} \frac{\partial^2 \Upsilon_R}{\partial z \partial t} \right) dz \\ &+ \int_0^L \left(\frac{\partial \Upsilon_R}{\partial t} \left(\frac{\partial}{\partial z} \left(gz \frac{\partial \Upsilon}{\partial z} \right) - \tau \frac{\partial \Upsilon}{\partial t} \right) \right) dz \end{aligned} \quad (3.28)$$

After integration by parts, it comes

$$\frac{dH}{dt} = L \frac{\partial \Upsilon_R}{\partial t}(L, t) \left(g \frac{\partial \Upsilon_R}{\partial z}(L, t) + \frac{\Upsilon_R(L, t)}{\vartheta^2} \right) - \tau \int_0^L \left(\frac{\partial \Upsilon_R}{\partial t} \right)^2 dz$$

A proposed control law is

$$\frac{\partial \Upsilon_R}{\partial t}(L, t) = -k \left(g \frac{\partial \Upsilon_R}{\partial z}(L, t) + \frac{\Upsilon_R(L, t)}{\vartheta^2} \right) \quad (3.29)$$

With this law, $dH/dt \leq 0$, so the system converges to the largest invariant set contained in $dH/dt = 0$.

$$dH/dt = -kL \left(g \frac{\partial \Upsilon_R}{\partial z}(L, t) + \frac{\Upsilon_R(L, t)}{\vartheta^2} \right)^2 - \tau \int_0^L \left(\frac{\partial \Upsilon_R}{\partial t} \right)^2 dz$$

This set is such that

$$\int_0^L \left(\frac{\partial \Upsilon_R}{\partial t} \right)^2 dz = 0 \quad \text{and} \quad \frac{\partial}{\partial z} \left(gz \frac{\partial \Upsilon}{\partial z} \right) = 0$$

This first relation implies $\partial \Upsilon_R / \partial t(z, t) = 0$ for all z and all t , so the solution of the second relation is $\Upsilon_R(z) = c \ln(z)$, where c is an arbitrary constant. At rest, the balance of the external forces is given, at the top, by the sum of F_t , accounting for the horizontal part of the tension at the top of the structure, and F_p , the resultant of the disturbances. By definition, F_t is proportional to $\partial \Upsilon_R / \partial z(L, t)$. In this undisturbed case, $F_p = 0$, so $F_t = 0$ and $\partial \Upsilon_R / \partial z(L, t) = 0$, which leads to $\Upsilon_R(L, t) = 0$. The unique possible solution for $\Upsilon_R(z) = c \ln(z)$ considering $\Upsilon_R(L) = (\partial \Upsilon_R) / (\partial z)(L) = 0$ is $c = 0$. That proves the convergence of Υ_R to zero for all z , and in particular gives $\Upsilon_R(0, t) = \Upsilon_R(L, t) = 0$: the re-entry operation is successful. ■

3.2.2.2 Disturbances

In practical cases, the structure has two main kinds of disturbances, that change the flow speed: waves and marine currents. The waves have their energy concentrated on the initial meters of the depth. They normally have two main frequencies, the faster around 50 mHz and the other around 10 mHz. The marine currents have their energy distributed more uniformly, with smooth time variations. The effect of the marine currents generates an offset that slowly changes. The changes of the flow speed due to these disturbances are represented by the function $U(z, t)$, that, with respect to the undisturbed case given by 2.5, induces the following changes in the hydrodynamic forces (m_I is a constant usually called the inertia coefficient):

$$F(z, t) = -m_F \frac{\partial^2 \Upsilon}{\partial t^2} + \mu \left(U(z, t) - \frac{\partial \Upsilon}{\partial t} \right) \left| U(z, t) - \frac{\partial \Upsilon}{\partial t} \right| + m_I \frac{\partial U}{\partial t} \quad (3.30)$$

During the re-entry operation, the marine current can be assumed constant and generates a static deformation of the structure $\bar{\Upsilon}(z)$. If the assumption of small angles in the vertical direction holds, $\bar{\Upsilon}(z)$ can be defined by

$$-\frac{\partial}{\partial z} \left(gz \frac{\partial \bar{\Upsilon}}{\partial z}(z) \right) = \frac{\mu}{m} U(z) |U(z)|$$

with the boundary condition $\bar{\Upsilon}(L) = 0$. In these conditions, when the control law used in the undisturbed case is applied, it is easily proved that the system is stabilized at an equilibrium point given by $\Upsilon(z, t) = \bar{\Upsilon}(z) - g\vartheta^2 \partial \bar{\Upsilon} / \partial z(L)$. To avoid this bias at the bottom end, we propose the following solution. Before applying the control law:

- Estimate the current distance from the bottom end to the wellhead. From this estimation, choose a reference trajectory for the bottom end, and compute the top reference trajectory as in the undisturbed case.
- Estimate the current angle at the top ($\partial \bar{\Upsilon} / \partial z(L)$).

The definition of $\Upsilon_R(z, t)$ is modified into $\Upsilon_R(z, t) = \Upsilon(z, t) - \Upsilon_o(z, t) - \bar{\Upsilon}(z)$. So, the computation of the control law obeys equation 3.26, exactly like in the undisturbed case. Indeed, the only difference lies in the use of the estimation $\partial \bar{\Upsilon} / \partial z(L)$. Simulation of closed loop is presented in Figure 3.8.

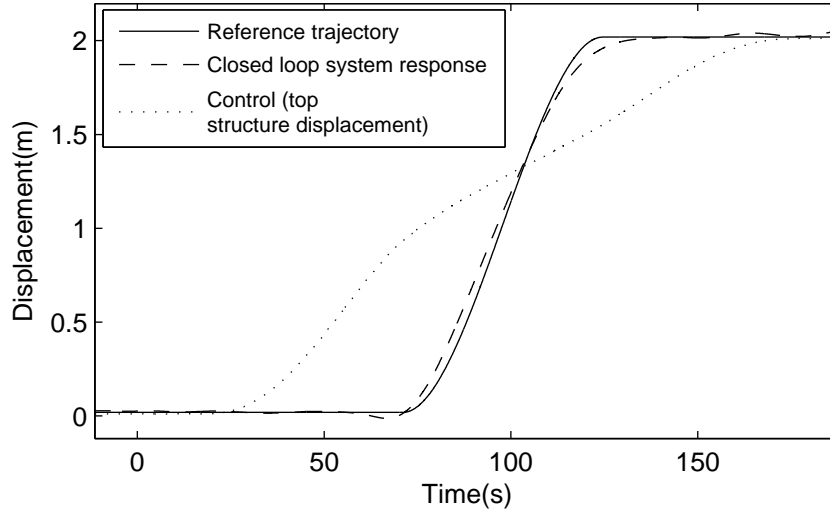


Figure 3.8: Structure under constant disturbance due to the current.

The considered discrete system for these numerical simulations (Figures 3.8 and 3.10) comes from the discretization of equation (2.4), for a vertical 2 km long steel riser with a fixed support at the top external diameter = 0.55 m, internal diameter = 0.5 m. These are typical values for a drilling riser in deep water. The hydrodynamic force is represented by equation (3.30). In the case of sea current, the flow U is considered uniform. In the case of waves, the flow has two different parts: close to the surface the flow is considered as a linear combination of two sinusoidal functions with different frequencies; for the other part of the riser the flow is considered as equal to zero.

In the case of waves, the structure deformation linked to the disturbance is not constant. We miss a formal approach for a Lyapunov function, that could guide us to an efficient closed loop control in this case. For all the simulated situations, the control approach derived from a Lyapunov function does not provide good results in case of sea current plus waves.

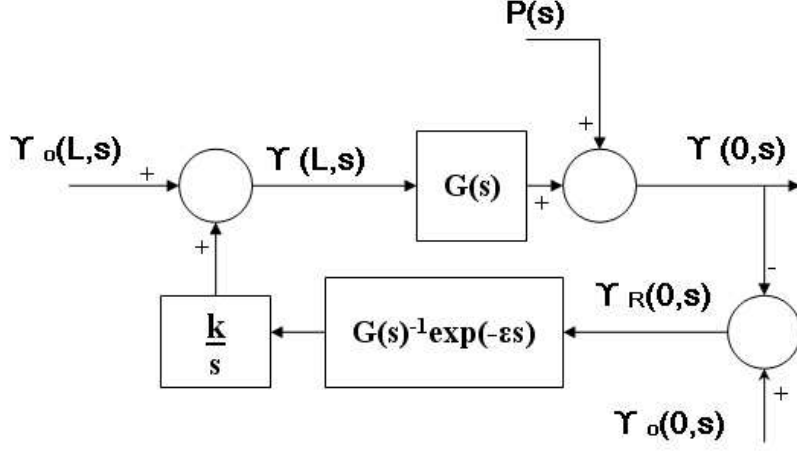


Figure 3.9: Block diagram of the tracking system.

3.2.3 Inverse model control

There are different alternatives to reduce the effects of disturbances. One of them is to use the system inversion to define a tracking system, a second one is to choose an open loop trajectory, that reduces the disturbances influence on the system output. The proposed approach consists in combining these two aspects using a tracking system with the inverted model defined by equation 3.18. Regarding equation 2.5, it is possible to observe that an artificial increase of the structure speed $\partial\Upsilon/\partial t$ implies a larger system damping, that reduces the relative effect of the flow speed changes. So, an open loop trajectory, that is fast enough to increase the damping during a given period of time, can reduce the effect of waves. Figure 3.9 presents the block diagram of the tracking system. The transfer function $G(s)$ between the riser top $\Upsilon(L, s)$ and the riser bottom end $\Upsilon(0, s)$ is represented by

$$G(s) = \frac{2\pi}{\int_{-\pi}^{\pi} \exp(-2\sqrt{s^2}\sqrt{z/g} \sin \theta)}$$

Denote Υ_o is the reference trajectories and Υ is the real riser position.

Proposition 6 *Applied on system given by equation 3.17, the control law*

$$\Upsilon(L, s) = \frac{-kG(s)^{-1}e^{-\epsilon s}}{s}(\Upsilon(0, s) - \Upsilon_o(0, s)) + \Upsilon_o(L, s) \quad (3.31)$$

stabilizes system 3.17 around any trajectory $\Upsilon_o(0, s)$ if $k < \pi/(2\epsilon)$.

Proof As the transfer function $G(s)$ does not have unstable zeros or poles, the closed loop does not induce any cancellation between unstable zeros and poles. In fact, the Bessel function of first order J_0 just have real zeros (see Ismail and Muldoon [24] for further information). So, the poles of $G(s)$ only lie in the region $Re(s) < 0$. The stability of this feedback law can be analyzed by the simplified Nyquist criterion. Denote $M(s)$ the open loop transfer function between $y_o(s)$ and $y(s)$, $M(s) = k \exp(-\epsilon s)/s$. Rewriting $\exp(-\epsilon s)$ into its trigonometric form and replacing $s = i\omega$:

$$M(i\omega) = \frac{k(\cos(\epsilon\omega) - i \sin(\epsilon\omega))}{i\omega} \quad (3.32)$$

Considering $k > 0$, the most negative real value of equation 3.32 occurs for $\omega = \omega_0 = \pi/(2\epsilon)$. For this value, $M(\omega_0) = -k/\omega_0$. A sufficient condition for the closed loop stability is $M(\omega_0) > -1$, which leads to $k < \pi/(2\epsilon)$. ■

In practise, a value of k much smaller than $k < \pi/(2\epsilon)$ is used, to provide robustness. Typically, $k = \pi/(16\epsilon)$. $G(s)$ has a maximum delay equal to $\epsilon = 2\sqrt{L/g}$ (see equation 3.18), so its inverse $G(s)^{-1}$ is associated to the same delay to insure causality. The delay of the control estimation is an important problem for the high frequencies, however for the low frequencies this delay is negligible.

Proposition 7 *Applied on system given by equation 3.17, the control law given by equation 3.31 rejects low frequencies disturbances.*

Proof The closed loop transfer function between the disturbance $P(s)$ and the system output $\Upsilon(0, s)$ is

$$\frac{y(s)}{P(s)} = \frac{s}{s + ke^{-\epsilon s}} \quad (3.33)$$

Replacing $s = i\omega$, The transfer function 3.33 gives the associated system gain to each frequency ω .

$$\frac{y(i\omega)}{P(i\omega)} = \frac{i\omega}{i\omega + ke^{-\epsilon i\omega}}$$

For low frequencies disturbances ($\omega \rightarrow 0$), the influence of the disturbances over the system output goes to zero ($|y(i\omega)/P(i\omega)| \rightarrow 0$). ■

Figure 3.10 gives an example of what can be obtained with this approach for the control of a structure with waves and sea current disturbances. The use of the tracking system associated to the motion planning stabilizes the riser bottom end at its target during a certain time (region close to $t = 1000$ s in the figure). During this time the connection of the riser bottom end to the wellhead is possible.

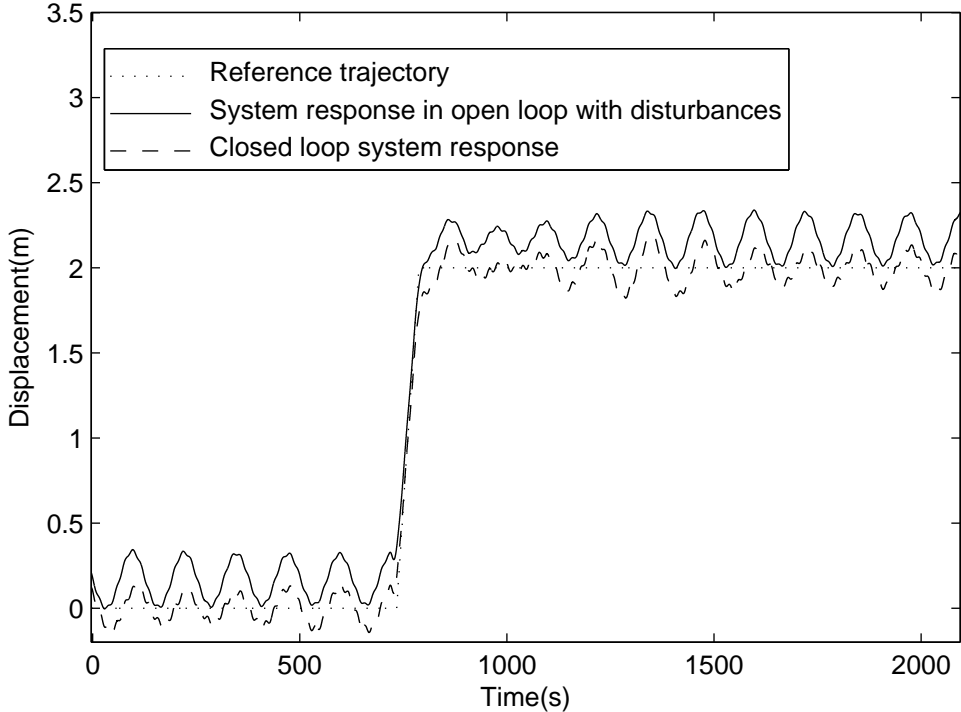


Figure 3.10: Structure under disturbances due to waves and sea current.

The shape of the reference trajectory is such that the reference speed is kept large almost until the end of the bottom end displacement (but indeed this reference trajectory is chosen smooth enough to be followed on the nominal model with no modeling errors and no disturbances). This avoids the increase of the disturbances before the structure has reached its target.

A problem with this kind of trajectory is that, for a given disturbance, a maximum speed must be used, during a large enough period for the disturbances to be attenuated. This turns out to require a minimum initial distance

between the bottom end of the structure and the wellhead. The choice of this maximum speed is constrained by the following considerations, that are difficult to quantify in advance and does not prevent the constraints of the actuators:

- if the speed is too large, the small angles assumption does not hold, and more terms are required in the expansion of the damping term;
- if the acceleration is too large, the beam effect is no more negligible.

Chapter 4

Conclusion for the reentry control part

In this part, the fundamental characteristics of long offshore structures have been described. Simplified structure models have been presented, that are adapted to the practical control problem associated to the reentry operation. For each model presented in this part, a dedicated control law has been designed. The choice of the model and the control strategy are not only linked to the system to be controlled, but also to the disturbances.

The reentry operation is used to displace the riser bottom end to the wellhead and stabilize it. The proposed solutions achieve the reentry. In both proposed control systems, the required time to achieve the operation depends on the initial distance between the wellhead and the riser bottom end. The assumption that the riser presents small deformation angles limits the maximum displacement speed that can be applied.

The reduced model associated to a delay is obtained from the modal analysis presented in chapter 3.1. It is used to model the infinite order system, which does not seem to have an analytical solution. The interest is to avoid the use of high orders state models that are sources of numerical problems and so can not be efficiently used in the design of feedback controls. The closed loop uses the inverted reduced system, however a delay must be added for causality. The results with this technique are satisfactory. They favorably compare with classical internal model controls, not described in this document. The largest advantage of this technique lies in the possibility to easily apply it to

a large group of offshore structures subject to different kinds of disturbances.

The other proposed solution is presented in chapter 3.2. It consists in a two steps procedure: first approximate the structure by the model of a cable with a linear damping; then transpose the analytical solution from the Laplace domain to the time domain thanks to a series expansion. The final result is a function that has as input the bottom reference trajectory and as output the top trajectory necessary to produce the bottom end displacement. This motion planning is presented in section 3.2.1. Two different closed loop controls are proposed in sections 3.2.2 and 3.2.3. The first one is based on a Lyapunov function and proposes a less conventional solution. It uses the top structure angle as a measured input and the structure top position as control output. This closed loop gives satisfactory results, in the cases of undisturbed systems and systems submerged in a constant flow. However, we still miss a strategy to take into account non stationary disturbances in a Lyapunov design.

The other way to design the feedback control is to rely on the PDE solution, that was used to define the open loop control. Provided the addition of a delay, it is possible to use it in the feedback control. The association of the closed and open loop control based on the analytical solution is presented in section 3.2.3. This complete control system has very interesting performances, not only in the undisturbed case or systems submerged in a constant flow, but also in the presence of waves. The possibility to compensate for the waves effects, and so to ensure the reentry operation under difficult weather conditions, is the most important result of this part.

Part II

VIV control

Main Nomenclature

Capital letters.

A	State matrix.
B	Input matrix.
E	Elastic modulus.
F	Hydrodynamic force.
F_{VIV}	Vortex shedding force.
I	Identity matrix.
J	Second moment of area.
K	Stiffness matrix.
L	Observer state vector.
O	Damping matrix.
P	Vortex shedding acceleration vector.
P_m	Vortex shedding acceleration vector of modal base.
Q	Fluid variable.
R	Surface riser section.
S	Shearing force.
T	Tension.
U	Flow speed.
V	Eigenvector matrix.
\tilde{V}	Modified eigenvector matrix.
X	Structure state vector.

Y	Transverse riser displacement vector.
\dot{Y}	Transverse riser speed vector.

Lowercase letters.

a	Structure force over the fluid.
b	Mode associated gain.
c_1	Auxiliary constant 1.
c_2	Auxiliary constant 2.
e	Sine average amplitude.
f	Cosine average amplitude.
g	Apparent gravity.
h	Fluid force constant.
i	Imaginary unit.
m	Riser and fluid linear mass.
m_F	Fluid added linear mass.
m_I	Inertia coefficient.
m_S	Riser linear mass.
n	Number of discretization points.
s	Laplace variable.
t	Time.
u	Riser top external force.
\hat{u}	Riser top external force Laplace transform.
w	Apparent weight.
x	Horizontal axis.
y	System output.
\hat{y}	Laplace transform of the system output.
\hat{y}^P	Laplace transform of output part generated by P.
z	Vertical axis.

Greek letters.

- Υ Riser displacement, transverse to the flow.
- Ω Structure natural frequency.
- γ Eigenvector real part.
- ε Van der Pol's equation parameter.
- ζ Auxiliary variable.
- ι Transfer function constant.
- κ Filter gain.
- λ Eigenvalue.
- φ Eigenvector imaginary part.
- ϱ Integration variable.
- σ Limit cycle frequency.
- τ Drag constant.
- ω Vortex shedding natural frequency.

Chapter 5

VIV background

5.1 Vortex Induced Vibrations

In regions with large sea currents, a known source of mechanical fatigue is the vibration generated by an alternating vortex shedding that periodically produces lift forces on the structure. These vibrations are usually called vortex induced vibrations (VIV). The slender structures in a flow, like mooring cables, catenary and vertical risers, are the most affected by this phenomenon. The mechanical fatigue generated by the VIV can be the cause of a mechanical failure of the structure. A mechanical failure in a riser represents a stop of the well production that can spend weeks, because the tools and heavy machines required for the riser replacement are not present on a FPSO. Usually this operation is only made by a dedicated installation vessel. The exploration and production of new petroleum fields each time deeper makes the VIV a more frequent problem, because of the larger sea currents present in these regions, and the fact that the structures are each time more flexible, because of the increase of the structure ratio length per diameter.

This kind of vibrations along offshore flexible structures is an important research domain, however some characteristics of the VIV are nowadays well known (see [5], [10] and [43]):

- The VIV normally have their largest displacements in a perpendicular direction to the flow and the structure axis.

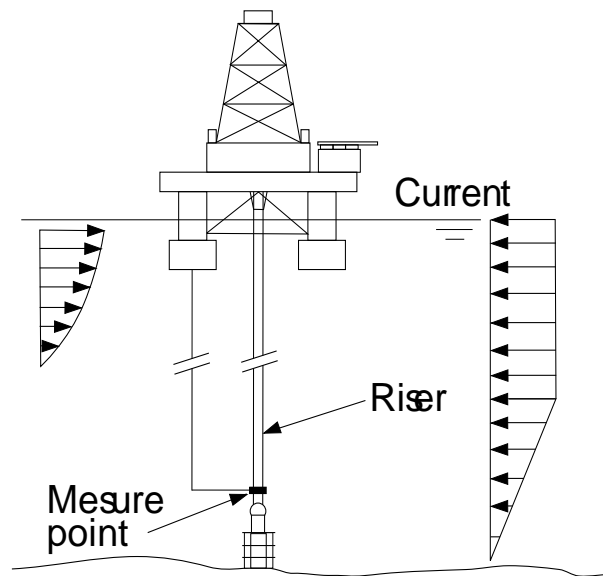


Figure 5.1: System under analysis

- For a fixed cylinder, the frequency of the vortex shedding is a function of the cylinder diameter and the sea current speed. This frequency is considered as the natural frequency of the vortex shedding.
- For a flexible structure, the frequency of the vortex shedding and consequently the generated vibration can be different from the vortex shedding natural frequency. In this case, there is a phenomenon of lock-in, that makes the structure oscillates at its natural frequency that is the closest to the natural frequency of the vortex shedding.
- VIV have large amplitudes only when associated to low damped modes of the structure.
- The vortex shedding is a hydrodynamic phenomenon, that has a local effect over the structure and the fluid around it, however this effect is propagated by the structure and generates a synchronism of the vortex shedding along all the regions with a similar vortex shedding frequency.

These characteristics of VIV give essential information about this phenomenon. This information is used in the design of the control system presented in section 5.4 and chapter 7.

5.2 Passive VIV limitation

Nowadays, the proposed solutions to reduce VIV are always associated to mechanical devices, that are put around the riser to change its hydrodynamic behavior. They can be divided into two main groups represented in figure 5.2:

- The first group is designed to reduce the turbulence around the riser, and consequently the forces associated to the vortex shedding (see [6] for further explanations). Normally they are free to rotate around the riser and have an external profile that looks like a symmetric aircraft wing.
- The second group of mechanical devices for VIV suppression are designed to reduce the synchronism of the vortex shedding (solution exemplified by Vaz in [42]). These structures are basically straps or small objects, that are fixed in a helicoidal way along the structure.

The most usual problems linked to this kind of solutions are the restricted range of sea currents for which some of these systems are effective, the increase of the drag force over the structure, and the problems of reliability.

In figure 5.2, **a)** is an example of a mechanical device that is designed to reduce VIV by the reduction of the flow turbulence. It is important to observe that each part of this device is supposed to be free to turn around the riser following the changes of the sea current. Figure 5.2 **b)** represents a mechanical device that tries to reduce the VIV by the reduction of the vortex shedding synchronism. The fact that this device does not have mobile parts increases its reliability, however its performance can be reduced along the time, because of the marine environment. For instance, marine growth can stick on the structure and change the hydrodynamic profile.

The increase of the drag force is related to the increase of the structure transverse section and its new profile. This consequently increases the mechanical fatigue. In certain cases, the mechanical fatigue generated by this drag increase can be larger than the reduction of the mechanical fatigue associated to the VIV reduction.

These devices are positioned over the riser, where maintenance is almost impossible and very expensive when it is possible. So, the reliability is essential

for these devices, because they must resist to the environment and be efficient along all the service life of the riser without maintenance.

5.3 Vibration control

The term vibration control is largely applied nowadays to define a precise group of control systems. For this group of systems, the main (or unique) objective of the active control is the reduction of the effect of external disturbances over the controlled system. The three classical ways to solve this kind of problems are the control systems that act as cancel devices, isolators or dampers.

The principle of a cancellation system is to put a control system in parallel to the source of disturbances. This control system is designed in such a way that its output is in phase opposition to the disturbances. This configuration makes the sum of the control and disturbance signals close to zero, so the global excitation of the system is reduced. The most known application is in the field of acoustic noise as proposed by Adachi and Sano in [2]. Another practical example is given in figure 5.3. It represents a building with an anti-earthquake system. The building displacement x_1 is given by the following equation

$$\ddot{x}_1 = -kx_1 - \alpha\dot{x}_1 + kx_2 + \alpha\dot{x}_2 + u \quad (5.1)$$

where u is the force applied by the active control, k and α are respectively the elastic and damping constants. x_2 is the ground displacement generated by the earthquake. In this case, a cancellation system can be defined by $u = -kx_2 - \alpha\dot{x}_2$. This control system cancels the earthquake effect, so the building displacement becomes independent from the ground displacement.

The second kind of vibration control system is the isolator. The principle of an isolator is to put a control system in series between the disturbance source and the controlled system. This control system is designed in such a way that its response for the disturbance excitation is close to zero. This strategy is largely used in domains where the disturbance just has high frequencies and the link between the controlled system and the disturbance source is necessary to support the weight of one of the parts. This principle is used for washing machines, or anti-earthquakes devices for buildings and bridges for instance. This kind of technology is well described by El-Sinawi in [9].

In the case of an anti-earthquake device as the one represented in figure 5.3 and equation 5.1, the transfer function between the ground displacement x_2 and the building displacement x_1 is given by

$$\frac{x_1(s)}{x_2(s)} = \frac{\alpha s + k}{s^2 + \alpha s + k} \quad (5.2)$$

The earthquakes are disturbances with large frequencies. The isolator system can be a passive device, that reduces the values for k and α , thus the gain of the transfer function 5.2 for high frequencies.

The third kind of vibration control is the damper. It is designed to dissipate the maximum of kinetic energy from the system to reduce the vibration amplitudes. They can be passive, active or semi-active, although they are characterized by the application of a force with a sign opposite to the local speed at the force application point. An interesting explanation about the calculus of the optimal force amplitude is proposed by Inman in [23].

Just to exemplify the usual limitation of collocated sensor and actuator, we consider a horizontal cable with two masses. We define the transversal displacements of these two masses as x_1 and x_2 , and consider the measure y equal to x_1 and the control u as a force applied at the same point (see figure 5.4). The system can be written as

$$\begin{cases} \ddot{x}_1 = -2x_1 + x_2 + u(y) \\ \ddot{x}_2 = x_1 - 2x_2 \\ y = x_1 \end{cases}$$

For $u = 0$, this system is marginally stable, in other words any external disturbance makes the system continually oscillate. In the case of a linear damping ($u = -\alpha\dot{x}_1$) the system is stable for any positive α , however for $\alpha \rightarrow \infty$ the system becomes marginal stable again. Equation 5.3 represents the system dynamics for $\alpha \rightarrow \infty$. This system shows the limitation of a collocated control, because of the influence of the feedback control over the measure of the disturbance. In this case a too large damping coefficient reduce the x_1 amplitudes and the possibility for the control system to accurately measure the vibration introduced by the disturbance.

$$\begin{cases} \ddot{x}_2 = -2x_2 \\ y = 0 \end{cases} \quad (5.3)$$

Even with this limitation, the linear dampers are largely used in all engineering fields because of their robustness, reliability and simple design. However, in the case of VIV, the vibrations are distributed all along the structure, so the bias of the feedback control over the measured signal represents a key problem for the efficiency of such controllers.

5.4 Active VIV limitation

Instead of trying to reduce vibrations by changing the behavior of the flow around the structure, the technology proposed in the present work is a system that uses an active vibration control, acting on the structure top end in order to change the dynamic behavior of the structure. The fact that displacements at the structure top end can reduce VIV has been observed by Vandiver [37]. The present technique focuses on this aspect, and proposes a preliminary control strategy to minimize VIV of slender structures. The objective is to design a control system that reduces the VIV, while requiring the smallest external force at the riser top end (minimum energy requirement).

We present in chapter 6 the wake model used to model the alternating lift force. The limit cycle, that results from the action of such a force over a rigid cylinder fixed by a spring, is also studied.

In chapter 7, a modal analysis is proposed, that emphasizes some specific aspects of the slender structures undergoing VIV: linear behavior of the structure for small lateral displacements, convergence of the vibration frequencies to one or some natural frequencies of the structure, synchronism and modal behavior of the structure.

A control strategy is proposed to reduce the vibrations along the riser, and thus minimize the fatigue of the structure. The effect of hydrodynamic forces over the structure is attenuated by the active control. This control induces a change in the structure modal behavior, thus reducing the VIV.

For control design, the idea is to consider the displacements of the structure

points as the sum of two displacements. The first displacement accounts for the result of movements at the structure's top. The structure is described by a linear PDE model, under the assumption of small displacements (small angles). It gives a relationship between the control u (force applied at the structure's top) and the controlled output y (displacement of a structure point located near the structure's bottom end). The second displacement is due to nonlinear effects (non linear part of the hydrodynamic forces plus the vortex shedding). This nonlinear force is considered as a disturbance in the control design.

The relationship between u and y that is provided by the linear partial differential equation is still too complicated for control design. We rely upon the fact that structures with low damping undergoing VIV behave like oscillators (oscillating at frequencies corresponding to the structure resonant modes). We then approximate the input-output relationship between u and y by a second order transfer function, corresponding to the most excited mode. It is derived from a modal analysis, done on a spatially discretized model of the structure.

The control law derived from this transfer function is tested in two different ways: the first one is presented in section 7.4. It uses numerical simulations of a complete model, that couples the lift forces and the structure displacement to test the control system. The second one is a reduced scale system, that is presented in chapter 8. This reduced scale system is a flexible structure, that has its natural frequencies close to the natural frequencies of the vortex shedding.

This control system can be viewed as a damping system, with an important difference when compared to traditional systems, as the measure point is away from the force application point. This physical distance between measure and force application point avoids the measurement problem discussed in section 5.3.

Not collocating actuator and sensor avoids the disturbance measurement problem, however this introduces other problems. In this configuration, the design of the best damping system is much more complicated and its performance is totally dependent of the model precision. That is why the control system for structure undergoing VIV only acts upon the main frequency of the vibration, as the characteristics of those frequencies permits some assumptions about the dynamic behavior of the structure, that are used in the control system design.

The proposed control system has rather good experimental and numerical simulation results. It reduces the displacement and speed of 35% all along the structure, noticing that the control simply implies a punctual force that generates a displacement of the riser top end (of about 10% of the maximum punctual displacement). The final result concerning the mechanical fatigue of the structure is a reduction of more than 70% of the mechanical fatigue associated to the VIV.

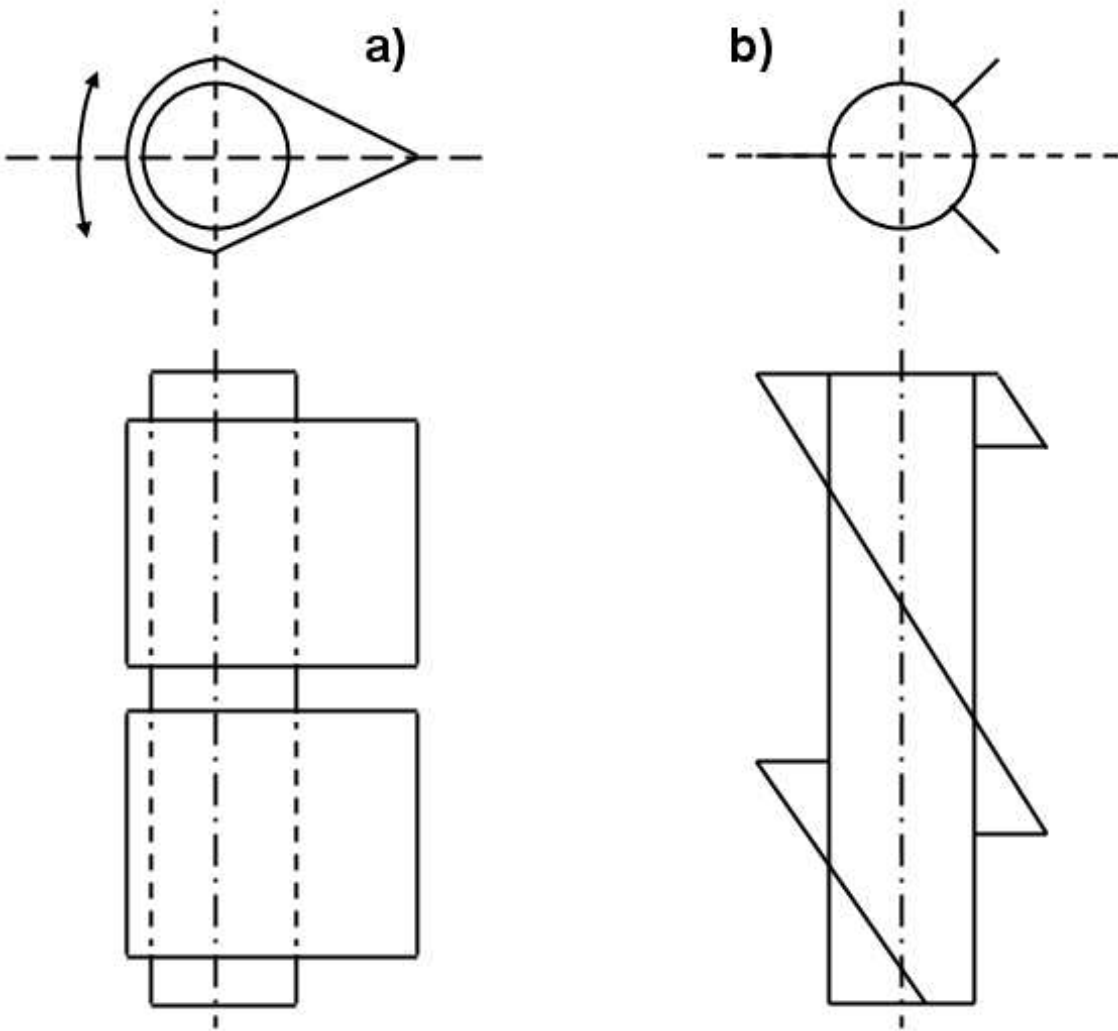


Figure 5.2: Transversal section and lateral view of devices to suppress VIV

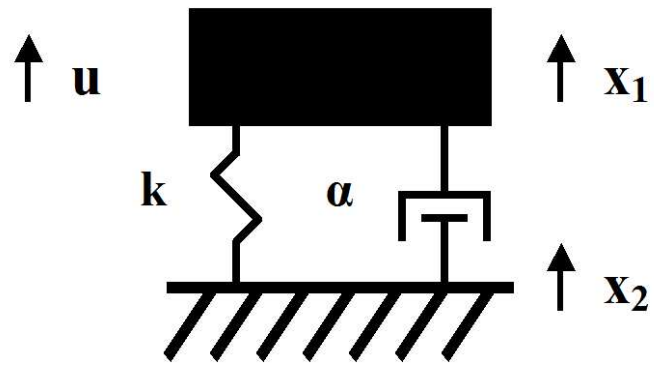


Figure 5.3: Simplified model of building undergoing an earthquake

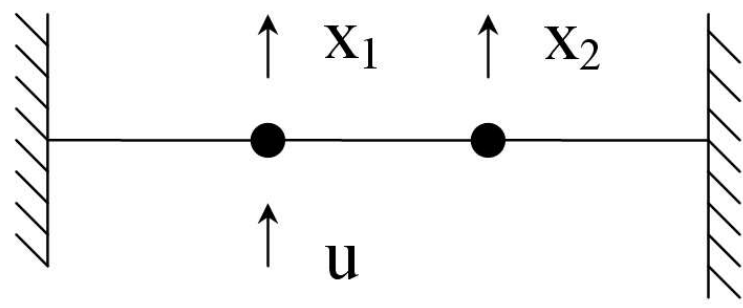


Figure 5.4: Tensioned cable

Chapter 6

Wake model

This chapter first recalls in section 6.1 the phenomenological model developed by Facchinetti [10] for the structures undergoing vortex induced vibrations. This model is used for all the simulations reported in this part of the thesis. The remaining sections of this chapter are devoted to qualitative studies of a simplified version of this model, that deals with a rigid structure fixed by strings.

In section 6.2, a first harmonic study suggests possible limit cycles. The amplitude and frequency of these cycles are studied quantitatively. The two remaining sections are dedicated to the stability of these limit cycles:

- in section 6.3, we show that, for a given range of values for the natural frequencies of the structure and the vortex shedding, the study of the limit cycle can be achieved, following the lines given by Guckenheimer and Holmes [19] for the study of the Van der Pol equation. Namely, a rotation group is proposed, governing the high frequency part of the dynamics. An averaging method is applied to derive the slow dynamics. Its (numerical) study shows that the limit cycles are stable.
- in section 6.4, an attempt is also made to use the averaging method. However, in this case, it is difficult to distinguish between fast and slow dynamics: using the averaging method is not fully justified. Yet, the numerical solutions that follow its application, indicating stability for the limit cycle, lead to results that kindly agree with those of both the first harmonic study and the simulations.

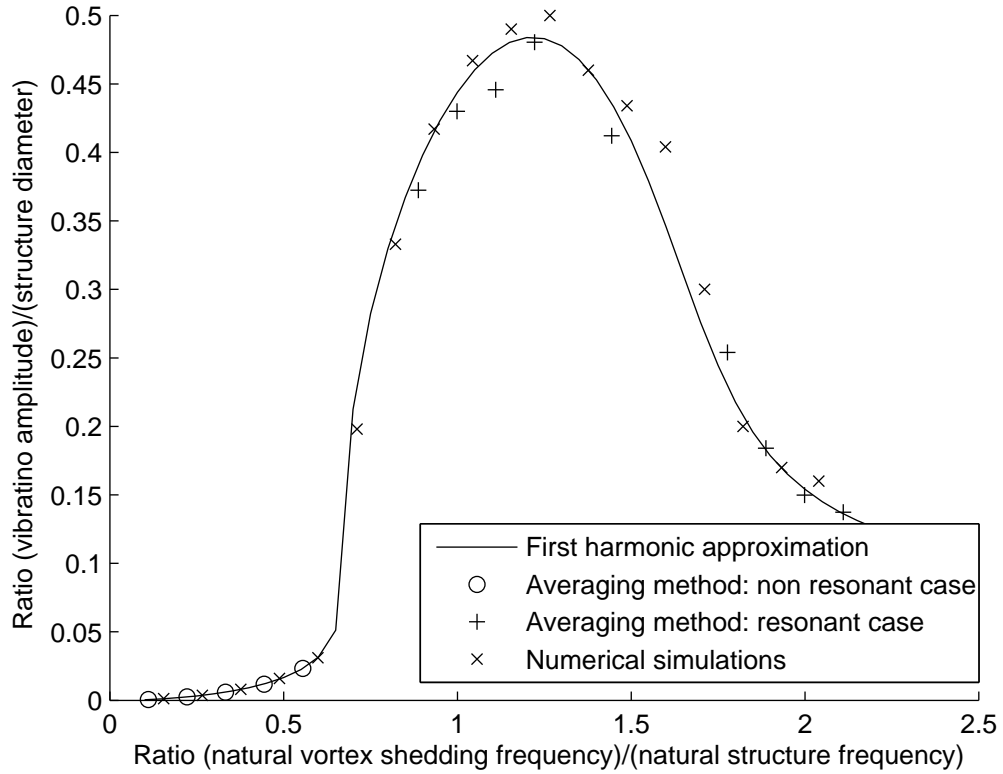


Figure 6.1: VIV amplitudes for different vortex shedding frequencies

Figures 6.1 and 6.2 compare the results from non dimensional model. They compare the first harmonic approximation to the stable limit cycles obtained with the two different averaging methods. Are also plotted on these curves values for the amplitude and frequency, that are estimated on plots resulting from numerical simulations. In these figures the natural frequency of the vortex shedding is normalized with respect to the structure natural frequency ($\omega U/\Omega$). It is possible to distinguish between small amplitudes (referred to as non-resonant cases) and large amplitudes (referred to as resonant cases).

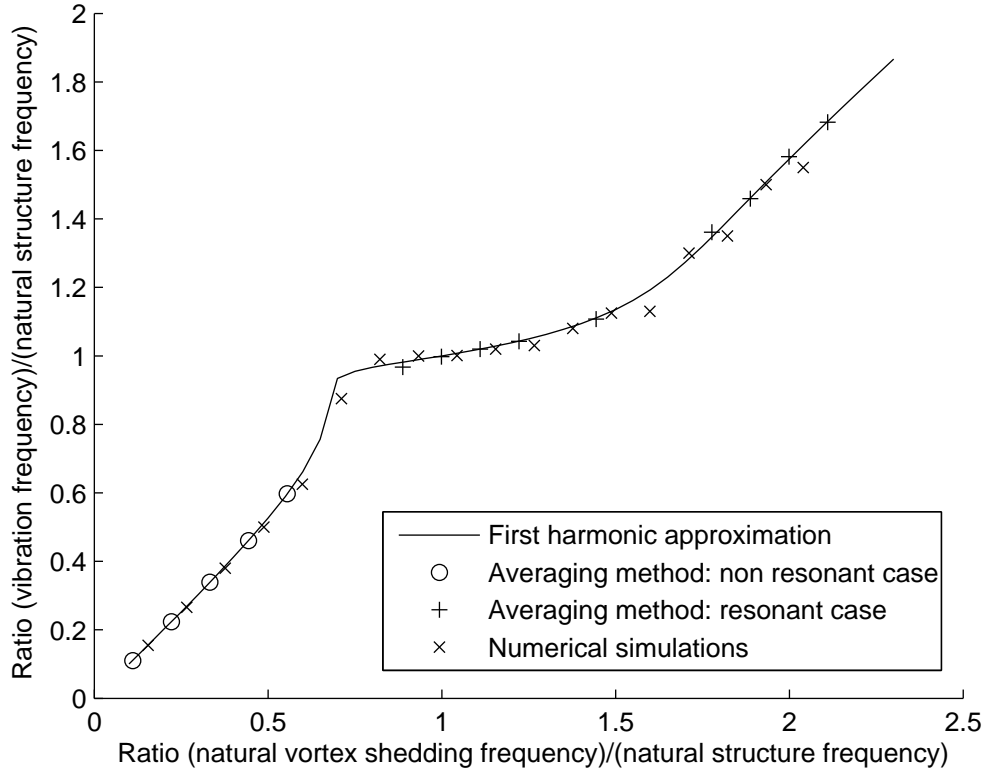


Figure 6.2: VIV frequencies for different vortex shedding frequencies

6.1 Phenomenological model

Several models have been designed to describe the forces associated to a relative movement between a solid and a fluid (see Larsen [27] for further information). A common fact for all these models is a nonlinear damping ratio that always increases with the speed of the relative movement. This nonlinear effect causes a kinetic energy concentration around some frequencies. The displacements associated to one frequency increase the average speed of the structure and so the damping ratio of the structure. In other words, the fact that one frequency is excited helps to damp the movement at other frequencies.

Our interest is to use a wake model that is complicated enough to represent the main aspects of VIV (frequency concentration of the movement, phase

lock between the structure and the vortex shedding at the natural frequencies of the structure), but kept simple enough for numerical simulations to be tractable. The model chosen to represent the nonlinear fluid forces is the wake oscillator model described by Facchinetti [10], and compared to direct numerical simulations of Navier-Stokes equations in [38].

This phenomenological model considers the structure undergoing VIV as a vertical structure with small angles displacements, thus it defines the structure as the Euler-bernoulli beam under traction:

$$m \frac{\partial^2 \Upsilon}{\partial t^2} = -EJ \frac{\partial^4 \Upsilon}{\partial z^4} + \frac{\partial}{\partial z} \left(T(z) \frac{\partial \Upsilon}{\partial z} \right) + F_n(z, t)$$

where E and J are respectively the elastic modulus and the second moment of area; Υ represents the structure displacement transverse to its main axis and to the flow. The hydrodynamic forces are defined in a general way by the Navier-Stokes equations. In the case of VIV the main vibrations are in the transverse plane to the sea current $U(z)$. This force denoted $F_n(z, t)$ is approximated by a linear part inspired by the Morison's equation and a non linear part represented by $F_{VIV}(z, t)$:

$$F_n(z, t) = F_{VIV}(z, t) - m_F \frac{\partial^2 \Upsilon}{\partial t^2} - \tau \frac{\partial \Upsilon}{\partial t} U(z)$$

Considering τ as the drag constant, m_F as the linear fluid added mass and m_s the structure linear mass, we denote the total linear mass of the structure as $m = m_s + m_F$. The association of the structures forces and the hydrodynamic loads defines the system behavior on the main direction of VIV as

$$m \frac{\partial^2 \Upsilon}{\partial t^2} = -EJ \frac{\partial^4 \Upsilon}{\partial z^4} + \frac{\partial}{\partial z} \left(T(z) \frac{\partial \Upsilon}{\partial z} \right) - \tau \frac{\partial \Upsilon}{\partial t} U(z) + F_{VIV}(z, t) \quad (6.1)$$

The two first terms of the left hand side represent the conservative forces of the structure. The VIV present a constant amplitude when the energy introduced by the lift force associated to F_{VIV} is equal to the energy taken by the drag force $-\tau(\partial \Upsilon / \partial t)U(z)$.

This model represents a phenomenological approach to describe the wake dynamics. It uses the historical Van der Pol equation (see subsection 6.3) to describe the non linear part of the fluid dynamics, instead of using Navier-Stokes equations for direct simulation. Q represent the fluid state, $\omega U(z)$ the natural frequency of the vortex shedding, while a , ϵ and h are phenomeno-

logical constants:

$$\begin{cases} F_{VIV} = hU(z)^2Q \\ \frac{\partial^2 Q}{\partial t^2} = -\varepsilon U(z)(Q^2 - 1)\frac{\partial Q}{\partial t} - (\omega U(z))^2Q + a\frac{\partial^2 \Upsilon}{\partial t^2} \end{cases} \quad (6.2)$$

We replace equation 6.2 in equation 6.1 to obtain the complete system model:

$$\begin{cases} m\frac{\partial^2 \Upsilon}{\partial t^2} = -EJ\frac{\partial^4 \Upsilon}{\partial z^4} + \frac{\partial}{\partial z} \left(T(z)\frac{\partial \Upsilon}{\partial z} \right) - \tau U(z)\frac{\partial \Upsilon}{\partial t} + hU(z)^2Q \\ \frac{\partial^2 Q}{\partial t^2} = -\varepsilon U(z)(Q^2 - 1)\frac{\partial Q}{\partial t} - (\omega U(z))^2Q + a\frac{\partial^2 \Upsilon}{\partial t^2} \end{cases} \quad (6.3)$$

Figure 6.3 presents a numerical simulation of this model in the case of a flexible structure.

6.2 First harmonic approximation

This section presents the study made on the first harmonic behavior of a structure undergoing VIV. The approach is used to describe the limit cycle characteristics of a unitary mass ($m = 1$) rigid cylinder, submerged in a flow and fixed by a spring. We identify the first harmonic of a possible oscillating solution for the system (frequency and amplitude of the limit cycle). The stability of this solution, so the limit cycle existence is analyzed in sections 6.3 and 6.4. The rigid cylinder assumption gives $\partial^4 \Upsilon / \partial z^4 = \partial(T\partial \Upsilon / \partial z) / \partial z = 0$, and the unique natural pulsation Ω is the square root of the spring constant. System 6.3 simplifies into:

$$\begin{cases} \frac{d^2 \Upsilon}{dt^2} = -\Omega^2 \Upsilon - \tau U \frac{d\Upsilon}{dt} + hU^2Q \\ \frac{d^2 Q}{dt^2} = -\varepsilon U(Q^2 - 1)\frac{dQ}{dt} - (\omega U)^2Q + a\frac{d^2 \Upsilon}{dt^2} \end{cases} \quad (6.4)$$

The first equation describes a linear system with input Q . Q is linearly linked to Υ , so we search for a first harmonic behavior, where $[\Upsilon, \dot{\Upsilon}]$ also oscillate on a cycle at the same frequency than Q (see Slotine [36]). The first harmonic behavior of variables Υ and Q are defined as:

$$\begin{cases} Q = \rho \sin(\sigma t) \\ \Upsilon = e \sin(\sigma t) + f \cos(\sigma t) \end{cases} \quad (6.5)$$

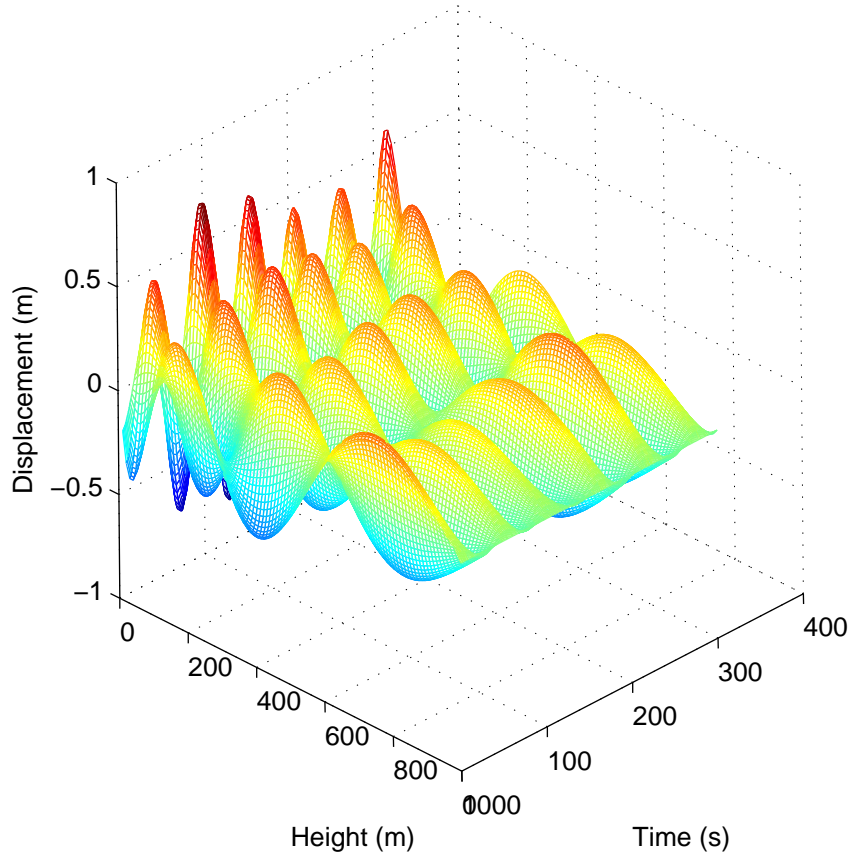


Figure 6.3: Flexible structure undergoing VIV

Using these definitions, it is possible to rewrite the first equation of system 6.4 as:

$$\begin{aligned} -\sigma^2(e \sin(\sigma t) + f \cos(\sigma t)) &= -\Omega^2(e \sin(\sigma t) + f \cos(\sigma t)) \\ -\tau U \sigma (e \cos(\sigma t) - f \sin(\sigma t)) + h U^2 \rho \sin(\sigma t) & \end{aligned} \quad (6.6)$$

So, separating the terms of equation (6.6) in relation to sine and cosine, we get the following equations:

$$\begin{cases} e\sigma^2 - e\Omega^2 + f\tau U\sigma + hU^2\rho = 0 \\ f\sigma^2 - f\Omega^2 - e\tau U\sigma = 0 \end{cases}$$

The two coefficients e and f can be expressed as functions of ρ and σ . In other words the first harmonic behavior of the structure is defined with respect to

the fluid behavior.

$$\begin{cases} e = \frac{-\rho h U^2 (\sigma^2 - \Omega^2)}{(\sigma^2 - \Omega^2)^2 + \tau^2 U^2 \sigma^2} \\ f = \frac{-\rho h \tau U^3 \sigma}{(\sigma^2 - \Omega^2)^2 + \tau^2 U^2 \sigma^2} \end{cases} \quad (6.7)$$

Inserting (6.5) in the second equation of system (6.4) gives

$$\begin{aligned} -\sigma^2 \rho \sin(\sigma t) = & -(\omega U)^2 \rho \sin(\sigma t) + \\ \varepsilon U (1 - \rho^2 \sin(\sigma t)^2) \sigma \rho \cos(\sigma t) - & a \sigma^2 (e \sin(\sigma t) + f \cos(\sigma t)) \end{aligned} \quad (6.8)$$

Only the first harmonic component of the nonlinear dynamic of Q is considered to determine the low frequency behavior of the system. The high frequency component of equation 6.8 is reduced to its average value:

$$\begin{aligned} \sin(\sigma t)^2 \cos(\sigma t) &= \frac{1}{4} (\cos(\sigma t) - \cos(3\sigma t)) \\ \int_0^{\frac{2\pi}{\sigma}} \cos(3\sigma t) dt &= 0 \\ \sin(\sigma t)^2 \cos(\sigma t) &\sim \frac{1}{4} \cos(\sigma t) \end{aligned}$$

With this first harmonic approximation of the nonlinearities, we can rewrite equation 6.8 the following way:

$$\begin{aligned} -\sigma^2 \rho \sin(\sigma t) = & -(\omega U)^2 \rho \sin(\sigma t) + \\ \varepsilon U (1 - \rho^2/4) \sigma \rho \cos(\sigma t) - & a \sigma^2 (e \sin(\sigma t) + f \cos(\sigma t)) \end{aligned}$$

This approximation permits to compute Q first harmonic frequency and amplitude, thanks to the two equations defined by the sine and cosine parts:

$$\begin{cases} \sigma^2 - (\omega U)^2 + \frac{ahU^2(\sigma^2 - \Omega^2)\sigma^2}{(\sigma^2 - \Omega^2)^2 + \tau^2 U^2 \sigma^2} = 0 \\ \varepsilon U (1 - \frac{\rho^2}{4}) + \frac{ahU^3 \tau \sigma^2}{(\sigma^2 - \Omega^2)^2 + \tau^2 U^2 \sigma^2} = 0 \end{cases} \quad (6.9)$$

For example, if we consider the case where $\omega U = \Omega$, the first harmonic parameters are defined as:

$$\begin{cases} \sigma = \Omega \\ \rho = 2\sqrt{1 + \frac{ah}{\varepsilon\tau}} \end{cases}$$

$$\begin{cases} Q = 2\sqrt{1 + \frac{ah}{\varepsilon\tau}} \sin(\Omega t) \\ \Upsilon = -2\sqrt{1 + \frac{ah}{\varepsilon\tau} \frac{h}{\tau}} \cos(\Omega t) \end{cases}$$

The interesting point of this analysis is the description of a resonant effect when ω is close to Ω . This effect largely increases the Υ and Q amplitudes, as in these cases $ahU\sigma^2/((\sigma^2 - \Omega^2)^2 + \tau^2U^2\sigma^2) > 1$, so $\sigma \simeq \Omega$. This behavior kindly fits the practical experiments related by [5, 18, 37]. In the sequel, section 7.1 proposes to analyze a flexible structure vibrating in one of its natural frequencies as a single mode structure. This reduction justifies why these flexible structures have a similar resonant behavior than the one described in this section.

The numerical solution of equation (6.9) shows that, varying the flow speed U , we can observe two different types of limit cycles. For ωU close to Ω we have large amplitudes ρ and $\sigma \simeq \Omega$, meaning that the system oscillates at a frequency close to the natural frequency of the structure. The second kind of limit cycle is present when Ω and ωU are not close. In this case the system oscillates with small amplitudes ρ and $\sigma \simeq \omega U$ meaning that in this case the system oscillates at a frequency close to the natural frequency of the vortex shedding. These two kinds of limit cycles and their different aspects are studied in sections 6.3 and 6.4.

6.3 VIV limit cycle: non resonant case

The objective of this section is to study the stability of limit cycles of equation (6.4), suggested in section 6.2, in the cases where the natural frequency of the structure is not close to the natural frequency of the vortex shedding. The proposed analysis is based on the averaging method. This method attempts to define a part of the system that defines a fast periodic response, then analyzes the influence of the slow part of the system on this periodic response.

Approach We consider a general approach to apply the averaging method for all dynamic systems that can be written as

$$\dot{X} = AX + \varepsilon A'(X) \tag{6.10}$$

where X represents the system state, \dot{X} its derivative with respect to time t , the matrix A has different and purely imaginary eigenvalues. The function $\varepsilon A'$ represents the remaining part of the system, including the nonlinear part. It is assumed to be small compared to the linear part linked to A , this being underlined by the real parameter ε ($0 < \varepsilon \ll 1$)

Let $\Gamma(t)$ be a linear change of coordinates, and denote Z the transformed vector, $X = \Gamma(t)Z$. Equation (6.10) is transformed into:

$$\left(\dot{\Gamma} - A\Gamma\right) Z + \Gamma\dot{Z} = \varepsilon A'(\Gamma Z) \quad (6.11)$$

Therefore, if we set $\dot{\Gamma} = A\Gamma$, or $\Gamma(t) = e^{tA}\Gamma_0$, where Γ_0 is an invertible arbitrary matrix, equation (6.11) admits the following slow representation:

$$\dot{Z} = \varepsilon\Gamma(t)^{-1}A'(\Gamma(t)Z) \quad (6.12)$$

The fact that all eigenvalues of A are purely imaginary and different gives to Γ the form of rotation matrix periodic in time. This fact permits to analyze the effects of A' over this oscillating solution.

Example of the Van der Pol equation First, we propose to apply this technique on a simple example, and consider the system defined by the historical Van der Pol equation, that is characterized by a nonlinear damping, positive for small amplitudes and negative for the large ones (see Guckenheimer and Holmes [19]):

$$\begin{pmatrix} \dot{X}_1 \\ \dot{X}_2 \end{pmatrix} = \begin{pmatrix} 0 & 1 \\ -k^2 & 0 \end{pmatrix} \begin{pmatrix} X_1 \\ X_2 \end{pmatrix} + \varepsilon \begin{pmatrix} 0 & 0 \\ 0 & -(X_1^2 - 1)X_2 \end{pmatrix} \quad (6.13)$$

The matrix of coordinate change Γ is given by $\dot{\Gamma} = \begin{pmatrix} 0 & 1 \\ -k^2 & 0 \end{pmatrix} \Gamma$, or

$$\Gamma = \begin{pmatrix} \cos(kt) & \frac{1}{k} \sin(kt) \\ -k \sin(kt) & \cos(kt) \end{pmatrix} \Gamma_0$$

Without loss of generality, we can choose Γ_0 as

$$\Gamma_0 = \begin{pmatrix} 1 & 0 \\ 0 & -k \end{pmatrix}$$

So the proposed change of coordinate is

$$\begin{pmatrix} X_1 \\ X_2 \end{pmatrix} = \begin{pmatrix} \cos(kt) & -\sin(kt) \\ -k \sin(kt) & -k \cos(kt) \end{pmatrix} \begin{pmatrix} Z_1 \\ Z_2 \end{pmatrix}$$

and its inverse is

$$\begin{pmatrix} Z_1 \\ Z_2 \end{pmatrix} = \begin{pmatrix} \cos(kt) & -\frac{1}{k} \sin(kt) \\ -\sin(kt) & -\frac{1}{k} \cos(kt) \end{pmatrix} \begin{pmatrix} X_1 \\ X_2 \end{pmatrix}$$

then, equation (6.12) reads

$$\left\{ \begin{array}{l} \dot{Z}_1 = \varepsilon(4kZ_1 - kZ_1^3 - kZ_1Z_2^2 - 4kZ_1 \cos(2kt) \\ \quad + 4kZ_1Z_2^2 \cos(2kt) + kZ_1^3 \cos(4kt) - 3kZ_1Z_2^2 \cos(4kt) \\ \quad + 4kZ_2 \sin(2kt) + 2kZ_1^2Z_2 \sin(2kt) - 2kZ_2^3 \sin(2kt) \\ \quad - 3kZ_1^2Z_2 \sin(4kt) + kZ_2^3 \sin(4kt))/8k \\ \dot{Z}_2 = \varepsilon(4kZ_2 - kZ_1^2Z_2 - kZ_2^3 + 4kZ_2 \cos(2kt) \\ \quad - 4kZ_1^2Z_2 \cos(2kt) - 3kZ_1^2Z_2 \cos(4kt) + kZ_2^3 \cos(4kt) \\ \quad + 4kZ_1 \sin(2kt) - 2kZ_1^3 \sin(2kt) + 2kZ_1Z_2^2 \sin(2kt) \\ \quad - kZ_1^3 \sin(4kt) + 3kZ_1Z_2^2 \sin(4kt))/8k \end{array} \right. \quad (6.14)$$

The fact that $\varepsilon A'$ is considered small permits to consider that its effect is slow, when compared to the system's period. So observing the system (6.14), we can replace the terms by their averages over one period $([t, t + 2\pi/k])$ and represent the average dynamic of the system as

$$\begin{pmatrix} \dot{Z}_1 \\ \dot{Z}_2 \end{pmatrix} = \frac{\varepsilon}{2} \begin{pmatrix} Z_1(1 - \frac{1}{4}(Z_1^2 + Z_2^2)) \\ Z_2(1 - \frac{1}{4}(Z_1^2 + Z_2^2)) \end{pmatrix}$$

Rewriting this system with the polar coordinates $R = Z_1^2 + Z_2^2$ and $\sin \theta = \frac{Z_1}{R}$ we get:

$$\left\{ \begin{array}{l} \dot{R} = \frac{\varepsilon R}{2} \left(1 - \frac{R^2}{4}\right) \\ \dot{\theta} = 0 \end{array} \right.$$

The first equation has two equilibrium points: one unstable at $R = 0$ and the other one, stable at $R = 2$. This second equilibrium point corresponds to an attractive limit cycle with an average radius equal to 2. The second equation means that the angle between the rotation matrix and the system state is constant and defined by the initial condition θ_0 .

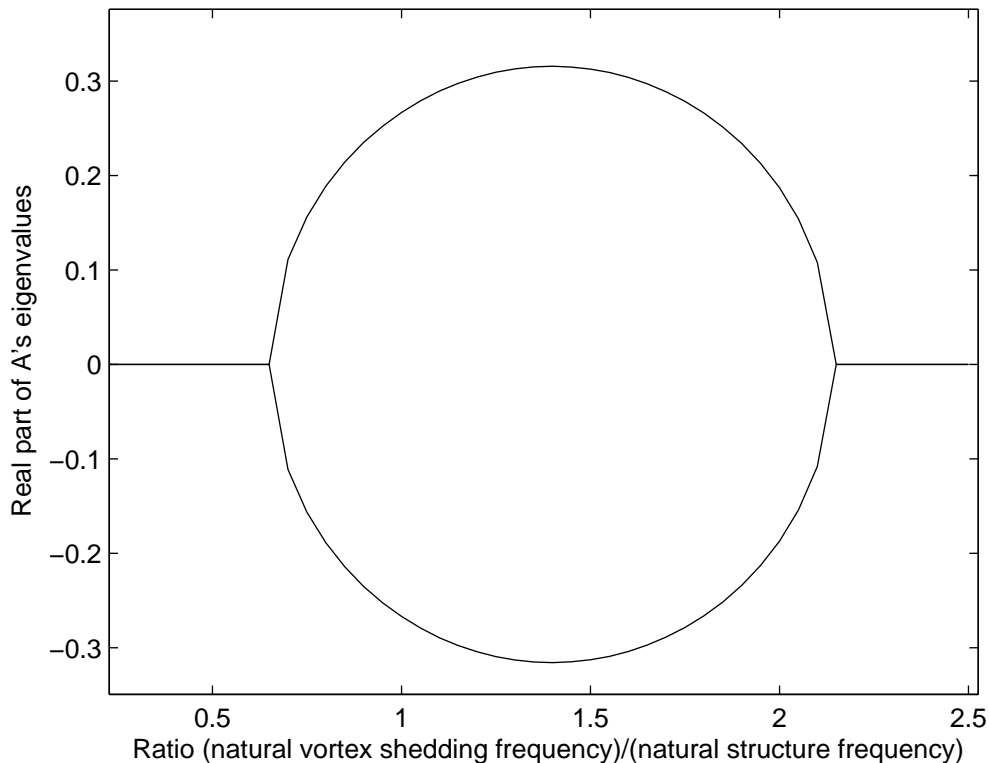


Figure 6.4: Real part of matrix A eigenvalues. Zero values are associated to the non-resonant case.

Application to the VIV system The lines applied on the Van der Pol equation can be followed to analyze the behavior of a structure undergoing vortex induced vibrations in the cases where the eigenvalues of the matrix with large parameters A are all purely imaginary and different. This condition is satisfied for small values of U (in fact small values of τU and ϵU), see figure 6.4 for abscissa around 0.5. In these cases the terms τU and ϵU can be considered as small parameters.

Considering the system (6.4), we use the first equation to determine the fluid variable Q as a function of the structure position Υ and its derivatives:

$$Q = \frac{1}{hU^2}(\ddot{\Upsilon} + \tau U \dot{\Upsilon} + \Omega^2 \Upsilon)$$

Thus, the system represented by (6.4) is written as the fourth order differ-

ential equation

$$\begin{aligned} & \Upsilon^{(4)} + \tau U \Upsilon^{(3)} + (\Omega^2 + \omega^2 U^2 - hU^2 a) \ddot{\Upsilon} + \omega^2 U^3 \tau \dot{\Upsilon} + \omega^2 U^2 \Omega^2 \Upsilon \\ & = \varepsilon U \left(1 - \frac{1}{h^2 U^4} (\ddot{\Upsilon} + \tau U \dot{\Upsilon} + \Omega^2 \Upsilon)^2 \right) \left(\Upsilon^{(3)} + \tau U \ddot{\Upsilon} + \Omega^2 \dot{\Upsilon} \right) \end{aligned} \quad (6.15)$$

We consider that Ω is not close to ωU . Then the roots of the biquadratic characteristic polynomial $s^4 + (U^2(ah - \omega^2) - \Omega^2)s^2 + \omega^2 U^2 \Omega^2 = 0$ of matrix A are purely imaginary and different. As described before, we can define the matrices A and Γ as

$$A = \begin{pmatrix} 0 & 1 & 0 & 0 \\ 0 & 0 & 1 & 0 \\ 0 & 0 & 0 & 1 \\ -\omega^2 U^2 \Omega^2 & 0 & U^2(ah - \omega^2) - \Omega^2 & 0 \end{pmatrix}$$

$$\Gamma = \begin{pmatrix} \cos(\sigma_1 t) & -\sin(\sigma_1 t) & \cos(\sigma_2 t) & -\sin(\sigma_2 t) \\ -\sigma_1 \sin(\sigma_1 t) & -\sigma_1 \cos(\sigma_1 t) & -\sigma_2 \sin(\sigma_2 t) & -\sigma_2 \cos(\sigma_2 t) \\ -\sigma_1^2 \cos(\sigma_1 t) & \sigma_1^2 \sin(\sigma_1 t) & -\sigma_2^2 \cos(\sigma_2 t) & \sigma_2^2 \sin(\sigma_2 t) \\ \sigma_1^3 \sin(\sigma_1 t) & \sigma_1^3 \cos(\sigma_1 t) & \sigma_2^3 \sin(\sigma_2 t) & \sigma_2^3 \cos(\sigma_2 t) \end{pmatrix}$$

where $\pm\sigma_1 i$ and $\pm\sigma_2 i$ are the roots of the characteristic polynomial. The dynamics of Z can be expressed as $\dot{Z} = \dot{\Gamma}^{-1} Z + \Gamma^{-1} \dot{X}$, where Γ^{-1} is given by

$$\Gamma^{-1} = \frac{1}{\sigma_1^2 - \sigma_2^2} \begin{pmatrix} -\sigma_2^2 \cos(\sigma_1 t) & \sigma_2^2 \sin(\sigma_1 t)/\sigma_1 & -\cos(\sigma_1 t) & \sin(\sigma_1 t)/\sigma_1 \\ \sigma_2^2 \sin(\sigma_1 t) & \sigma_2^2 \cos(\sigma_1 t)/\sigma_1 & \sin(\sigma_1 t) & \cos(\sigma_1 t)/\sigma_1 \\ \sigma_1^2 \cos(\sigma_2 t) & -\sigma_1^2 \sin(\sigma_2 t)/\sigma_2 & \cos(\sigma_2 t) & -\sin(\sigma_2 t)/\sigma_2 \\ -\sigma_1^2 \sin(\sigma_2 t) & -\sigma_1^2 \cos(\sigma_2 t)/\sigma_2 & -\sin(\sigma_2 t) & -\cos(\sigma_2 t)/\sigma_2 \end{pmatrix}$$

Substituting into equation 6.12 and applying the averaging method, we ob-

tain the slow average dynamics of Z :

$$\left\{ \begin{aligned}
\dot{Z}_1 &= \frac{-\varepsilon}{8\sigma_1(\sigma_1^2 - \sigma_2^2)h^2U^3} (Z_1(4\sigma_1h^2U^4(\Omega^2 - \sigma_1^2) + 4\sigma_1\tau h^2\omega^2U^4 \\
&\quad (\sigma_1^2 - U^2)/\varepsilon) - 4\sigma_1^2h^2\omega^2U^5\tau Z_2 + (Z_1(\sigma_1^7 - 3\sigma_1^5\Omega^2 + 3\sigma_1^3\Omega^4 \\
&\quad - \sigma_1\Omega^6 + \sigma_1^5\tau^2U^2 - \sigma_1^3\Omega^2\tau^2U^2) + Z_2(+\sigma_1^6\tau U - 2\sigma_1^4\Omega^2\tau U \\
&\quad + \sigma_1^2\Omega^4\tau U + \sigma_1^4\tau^3U^3))(Z_1^2 + Z_2^2) + (Z_1(2\sigma_1^3\sigma_2^4 - 4\sigma_1^3\sigma_2^2\Omega^2 - 2\sigma_1\sigma_2^4\Omega^2 \\
&\quad + 2\sigma_1^3\Omega^4 + 4\sigma_1\sigma_2^2\Omega^4 - 2\sigma_1\Omega^6 + 2\sigma_1^3\sigma_2^2\tau^2U^2 - 2\sigma_1\sigma_2^2\Omega^2\tau^2U^2) \\
&\quad + Z_2(2\sigma_1^2\sigma_2^4\tau U - 4\sigma_1^2\sigma_2^2\Omega^2\tau U + 2\sigma_1^2\Omega^4\tau U + 2\sigma_1^2\sigma_2^2\tau^3U^3))(Z_3^2 + Z_4^2)) \\
\dot{Z}_2 &= \frac{-\varepsilon}{8\sigma_1(\sigma_1^2 - \sigma_2^2)h^2U^3} (Z_2(4\sigma_1h^2U^4(\Omega^2 - \sigma_1^2) + 4\sigma_1\tau h^2\omega^2U^4 \\
&\quad (\sigma_1^2 - U^2)/\varepsilon) + 4\sigma_1^2h^2\omega^2U^5\tau Z_1 + (Z_1(-\sigma_1^6\tau U + 2\sigma_1^4\Omega^2\tau U \\
&\quad - \sigma_1^2\Omega^4\tau U - \sigma_1^4\tau^3U^3) + Z_2(\sigma_1^7 - 3\sigma_1^5\Omega^2 + 3\sigma_1^3\Omega^4 - \sigma_1\Omega^6 + \sigma_1^5\tau^2U^2 \\
&\quad - \sigma_1^3\Omega^2\tau^2U^2))(Z_1^2 + Z_2^2) + (Z_1(-2\sigma_1^2\sigma_2^4\tau U + 4\sigma_1^2\sigma_2^2\Omega^2\tau U - 2\sigma_1^2\Omega^4\tau U \\
&\quad - 2\sigma_1^2\sigma_2^2\tau^3U^3) + Z_2(2\sigma_1^3\sigma_2^4 - 4\sigma_1^3\sigma_2^2\Omega^2 - 2\sigma_1\sigma_2^4\Omega^2 + 2\sigma_1^3\Omega^4 \\
&\quad + 4\sigma_1\sigma_2^2\Omega^4 - 2\sigma_1\Omega^6 + 2\sigma_1^3\sigma_2^2\tau^2U^2 - 2\sigma_1\sigma_2^2\Omega^2\tau^2U^2))(Z_3^2 + Z_4^2)) \\
\dot{Z}_3 &= \frac{\varepsilon}{8\sigma_2(\sigma_2^2 - \sigma_1^2)h^2U^3} (+Z_3(4\sigma_2h^2U^4(\Omega^2 - \sigma_2^2) + 4\sigma_2\tau h^2\omega^2U^4 \\
&\quad (\sigma_2^2 - U^2)/\varepsilon) - 4\sigma_2^2h^2\omega^2U^5\tau Z_4 + (Z_3(\sigma_2^7 - 3\sigma_2^5\Omega^2 + 3\sigma_2^3\Omega^4 - \sigma_2\Omega^6 \\
&\quad + \sigma_2^5\tau^2U^2 - \sigma_2^3\Omega^2\tau^2U^2) + Z_4(+\sigma_2^6\tau U - 2\sigma_2^4\Omega^2\tau U + \sigma_2^2\Omega^4\tau U \\
&\quad + \sigma_2^4\tau^3U^3))(Z_3^2 + Z_4^2) + (Z_3(2\sigma_2^3\sigma_1^4 - 4\sigma_2^3\sigma_1^2\Omega^2 - 2\sigma_2\sigma_1^4\Omega^2 + 2\sigma_2^3\Omega^4 \\
&\quad + 4\sigma_2\sigma_1^2\Omega^4 - 2\sigma_2\Omega^6 + 2\sigma_2^3\sigma_1^2\tau^2U^2 - 2\sigma_2\sigma_1^2\Omega^2\tau^2U^2) \\
&\quad + Z_4(2\sigma_2^2\sigma_1^4\tau U - 4\sigma_2^2\sigma_1^2\Omega^2\tau U + 2\sigma_2^2\Omega^4\tau U + 2\sigma_2^2\sigma_1^2\tau^3U^3))(Z_1^2 + Z_2^2)) \\
\dot{Z}_4 &= \frac{\varepsilon}{8\sigma_2(\sigma_2^2 - \sigma_1^2)h^2U^3} (+Z_4(4\sigma_2h^2U^4(\Omega^2 - \sigma_2^2) + 4\sigma_2\tau h^2\omega^2U^4 \\
&\quad (\sigma_2^2 - U^2)/\varepsilon) + 4\sigma_2^2h^2\omega^2U^5\tau Z_3 + (Z_3(-\sigma_2^6\tau U + 2\sigma_2^4\Omega^2\tau U \\
&\quad - \sigma_2^2\Omega^4\tau U - \sigma_2^4\tau^3U^3) + Z_4(\sigma_2^7 - 3\sigma_2^5\Omega^2 + 3\sigma_2^3\Omega^4 - \sigma_2\Omega^6 + \sigma_2^5\tau^2U^2 \\
&\quad - \sigma_2^3\Omega^2\tau^2U^2))(Z_3^2 + Z_4^2) + (Z_3(-2\sigma_2^2\sigma_1^4\tau U + 4\sigma_2^2\sigma_1^2\Omega^2\tau U - 2\sigma_2^2\Omega^4\tau U \\
&\quad - 2\sigma_2^2\sigma_1^2\tau^3U^3) + Z_4(2\sigma_2^3\sigma_1^4 - 4\sigma_2^3\sigma_1^2\Omega^2 - 2\sigma_2\sigma_1^4\Omega^2 + 2\sigma_2^3\Omega^4 \\
&\quad + 4\sigma_2\sigma_1^2\Omega^4 - 2\sigma_2\Omega^6 + 2\sigma_2^3\sigma_1^2\tau^2U^2 - 2\sigma_2\sigma_1^2\Omega^2\tau^2U^2))(Z_1^2 + Z_2^2))
\end{aligned} \right. \tag{6.16}$$

Applying the second change of coordinates given by $R_1^2 = Z_1^2 + Z_2^2$, $R_2^2 =$

$Z_3^2 + Z_4^2$, $\sin \theta_1 = Z_1/R_1$ and $\sin \theta_2 = Z_3/R_2$, we get

$$\left\{ \begin{array}{l} \dot{R}_1 = \frac{-\varepsilon R_1}{8(\sigma_1^2 - \sigma_2^2)h^2U^3}((\sigma_1^2 - \Omega^2)(-4h^2U^4 + (\sigma_1^2 - \Omega^2)^2 \\ + \sigma_1^2\tau^2U^2)R_1^2 + 2((\sigma_2^2 - \Omega^2)^2 + \sigma_2^2\tau^2U^2)R_2^2) \\ - 4\tau h\omega^2U^2(U^2 - \sigma_1^2)/\varepsilon \\ \\ \dot{R}_2 = \frac{\varepsilon R_2}{8(\sigma_1^2 - \sigma_2^2)h^2U^3}((\sigma_2^2 - \Omega^2)(-4h^2U^4 + 2((\sigma_1^2 - \Omega^2)^2 \\ + \sigma_1^2\tau^2U^2)R_1^2 + ((\sigma_2^2 - \Omega^2)^2 + \sigma_2^2\tau^2U^2)R_2^2) \\ - 4\tau h\omega^2U^4(U^2 - \sigma_2^2)/\varepsilon \\ \\ \dot{\theta}_1 = \frac{-\varepsilon}{8(\sigma_1^2 - \sigma_2^2)h^2U^2}(-4\sigma_1h^2\omega^2U^4\tau + (\sigma_1^5\tau - 2\sigma_1^3\Omega^2\tau \\ + \sigma_1\Omega^4\tau + \sigma_1^3\tau^3U^2)R_1^2 + (2\sigma_1\sigma_2^4\tau - 4\sigma_1\sigma_2^2\Omega^2\tau \\ + 2\sigma_1\Omega^4\tau + 2\sigma_1\sigma_2^2\tau^3U^2)R_2^2) \\ \\ \dot{\theta}_2 = \frac{\varepsilon}{8(\sigma_1^2 - \sigma_2^2)h^2U^2}(-4\sigma_2h^2\omega^2U^4\tau + (\sigma_2^5\tau - 2\sigma_2^3\Omega^2\tau \\ + \sigma_2\Omega^4\tau + \sigma_2^3\tau^3U^2)R_2^2 + (2\sigma_2\sigma_1^4\tau - 4\sigma_2\sigma_1^2\Omega^2\tau \\ + 2\sigma_2\Omega^4\tau + 2\sigma_2\sigma_1^2\tau^3U^2)R_1^2) \end{array} \right. \quad (6.17)$$

For R_1 and R_2 at an equilibrium point, $\dot{\theta}_1$ and $\dot{\theta}_2$ are constant. This means that the system oscillates with a constant frequency. Analyzing the first two equations that define the behavior of R_1 and R_2 , it is possible to observe that this system has 4 different equilibrium points $[\bar{R}_1, \bar{R}_2]$. The study of the stability of the system around these points is made using the linearized system defined by $\dot{R} = A_R R$ in the regions close to these points.

$$A_R = \frac{\varepsilon}{8(c_1^2 - c_2^2)h^2U^3} \left(\begin{array}{cc} 4\tau h^2\omega^2U^4(U^2 - \sigma_1^2)/\varepsilon & -4((\sigma_2^2 - \Omega^2)^2 + \sigma_2^2\tau^2U^2) \\ +(\sigma_1^2 - \Omega^2)(4h^2U^4) & (\sigma_1^2 - \Omega^2)\bar{R}_1\bar{R}_2 \\ -3((\sigma_1^2 - \Omega^2)^2 + \sigma_1^2\tau^2U^2)\bar{R}_1^2 & \\ -2((\sigma_2^2 - \Omega^2)^2 + \sigma_2^2\tau^2U^2)\bar{R}_2^2 & \\ \\ 4((\sigma_1^2 - \Omega^2)^2 + \sigma_2^2\tau^2U^2) & -4\tau h^2\omega^2U^4(U^2 - \sigma_2^2)/\varepsilon \\ (\sigma_2^2 - \Omega^2)\bar{R}_1\bar{R}_2 & -(\sigma_2^2 - \Omega^2)(4h^2U^4) \\ & -3((\sigma_2^2 - \Omega^2)^2 + \sigma_2^2\tau^2U^2)\bar{R}_2^2 \\ & -2((\sigma_1^2 - \Omega^2)^2 + \sigma_1^2\tau^2U^2)\bar{R}_1^2 \end{array} \right) \quad (6.18)$$

First of all, we consider the origin ($\bar{R}_1 = \bar{R}_2 = 0$):

$$A_R = \frac{U}{2(\sigma_1^2 - \sigma_2^2)} \begin{pmatrix} \varepsilon(\sigma_1^2 - \Omega^2) - \tau\omega^2(\sigma_1^2 - U^2) & 0 \\ 0 & -\varepsilon(\sigma_2^2 - \Omega^2) + \tau\omega^2(\sigma_2^2 - U^2) \end{pmatrix}$$

In this case, A_R always has at least one unstable eigenvalue whatever the value of τ is. This fact represents the instability of the system at the origin.

The second and the third equilibrium points to be analyzed are $\bar{R}_1 = 0$, $\bar{R}_2 = 2\sqrt{\frac{h^2U^4(\sigma_2^2 - \Omega^2) - \tau h^2\omega^2U^4(\sigma_2^2 - U^2)/\varepsilon}{(\sigma_2^2 - \Omega^2)((\sigma_2^2 - \Omega^2)^2 + \sigma_2^2\tau^2U^2)}}$ and $\bar{R}_1 = 2\sqrt{\frac{h^2U^4(\sigma_1^2 - \Omega^2) - \tau\omega^2h^2U^4(\sigma_1^2 - U^2)/\varepsilon}{(\sigma_1^2 - \Omega^2)((\sigma_1^2 - \Omega^2)^2 + \sigma_1^2\tau^2U^2)}}$, $\bar{R}_2 = 0$. Considering the first of these two points the state matrix A_R becomes

$$A_R = \frac{U}{2(\sigma_1^2 - \sigma_2^2)} \begin{pmatrix} -\varepsilon(\sigma_1^2 - \Omega^2) - \tau\omega^2(\sigma_1^2 - U^2) & 0 \\ +2\tau\omega^2(\sigma_2^2 - U^2) & \\ (\sigma_1^2 - \Omega^2)/(\sigma_2^2 - \Omega^2) & \\ 0 & 2(\varepsilon(\sigma_2^2 - \Omega^2) - \tau\omega^2(\sigma_2^2 - U^2)) \end{pmatrix} \quad (6.19)$$

Considering the second of these two equilibrium points, we get the following state matrix A_R :

$$A_R = \frac{U}{2(\sigma_1^2 - \sigma_2^2)} \begin{pmatrix} -2(\varepsilon(\sigma_1^2 - \Omega^2) + \tau\omega^2(\sigma_1^2 - U^2)) & 0 \\ 0 & \varepsilon(\sigma_2^2 - \Omega^2) + \tau\omega^2(\sigma_2^2 - U^2) \\ & -2\tau\omega^2(\sigma_1^2 - U^2) \\ & (\sigma_2^2 - \Omega^2)/(\sigma_1^2 - \Omega^2) \end{pmatrix} \quad (6.20)$$

For any pair of ωU and Ω there is a τ_0 such that for $\tau \geq \tau_0$, either (6.19) or (6.20) has both eigenvalues strictly negative. That means for $\tau \geq \tau_0$ there is a limit cycle that is stable and attractive. This limit cycle corresponds to

the solution calculated by the first harmonic method. The equilibrium point for which $\bar{R}_1 \neq 0$ and $\bar{R}_2 \neq 0$ can not be analyzed by this method. In this case, the periodic function defined by the composition of these two different sines has a too long period and the assumption that we can separate the system into two different time scales and apply the averaging method does not hold any more. However, in the analyzed region, the first harmonic method suggests just one limit cycle and this limit cycle is represented by the equilibrium points previously analyzed.

The numerical simulations correspond in frequency and amplitude to the limit cycle described by this analysis. Figure 6.5 represents a typical non dimensional behavior associated to this kind of limit cycle:

- Extremely small structure displacement.
- Phase shift between the wake variable Q and the structure displacement of 0° or 180° .
- The system oscillates at the natural frequency (ωU) of the wake variable.

6.4 VIV limit cycle: resonant case

The objective of this section is to study the stability of a limit cycle suggested in section 6.2, in the particular cases where the structure natural frequency Ω is close to the natural frequency of the vortex shedding ωU . The rigid cylinder assumption gives $\partial^4 \Upsilon / \partial z^4 = \partial(T \partial \Upsilon / \partial z) / \partial z = 0$, and the unique natural pulsation Ω is the square root of the spring constant. The system can be written as

$$\begin{cases} \ddot{\Upsilon} &= -\Omega^2 \Upsilon - \tau U \dot{\Upsilon} + h U^2 Q \\ \ddot{Q} &= -\varepsilon U (Q^2 - 1) \dot{Q} - (\omega U)^2 Q + a \ddot{\Upsilon} \end{cases} \quad (6.21)$$

It is important to note that the specific limit cycle studied in this section corresponds to cases where Ω and ωU are close to each other. So we can define the limit cycle frequency σ such $|\sigma^2 - \Omega^2| \ll 1$ and $|\sigma^2 - (\omega U)^2| \ll 1$.

To use the averaging method, we suggest the following change of coordinates:

$$\left\{ \begin{array}{l} H_1 = \Upsilon \sin(\sigma t) + \frac{\dot{\Upsilon}}{\sigma} \cos(\sigma t) \\ H_2 = \Upsilon \cos(\sigma t) - \frac{\dot{\Upsilon}}{\sigma} \sin(\sigma t) \\ Z_1 = Q \cos(\sigma t) - \frac{\dot{Q}}{\sigma} \sin(\sigma t) \\ Z_2 = -Q \sin(\sigma t) - \frac{\dot{Q}}{\sigma} \cos(\sigma t) \end{array} \right. \quad (6.22)$$

The detailed computations are given in appendix A. This change of coordinates defines new dynamics, for which the averaging method is applied. On the averaged dynamics, the following change of coordinates is applied

$$\left\{ \begin{array}{l} R_H^2 = H_1^2 + H_2^2 \\ R_Z^2 = Z_1^2 + Z_2^2 \\ \sin \theta_H = H_1/R_H \\ \sin \theta_Z = Z_1/R_Z \end{array} \right. \quad (6.23)$$

We are left with the stability study of the equilibria for the following system:

$$\left\{ \begin{array}{l} \dot{R}_H = \frac{U}{2\sigma} (-\tau\sigma R_H + hUR_Z \cos(\theta_Z - \theta_H)) \\ \dot{R}_Z = \frac{1}{2\sigma} \left(-\varepsilon U\sigma \left(\frac{R_Z^2}{4} - 1 \right) R_Z + aR_H(\Omega^2 \cos(\theta_Z - \theta_H) - \tau U\sigma \sin(\theta_Z - \theta_H)) \right) \\ \dot{\theta}_H = \frac{1}{2\sigma} (-\Omega^2 + \sigma^2 + hU^2 \sin(\theta_Z - \theta_H) R_Z/R_H) \\ \dot{\theta}_Z = \frac{1}{2\sigma} \left(-(\omega U)^2 + \sigma^2 + hU^2 a + a(-\Omega^2 \sin(\theta_Z - \theta_H) - \tau U\sigma \cos(\theta_Z - \theta_H)) R_H/R_Z \right) \end{array} \right. \quad (6.24)$$

The equilibria of (6.24) are numerically computed. For values of $\omega U \simeq \Omega$, the tangent approximation around these equilibria indicates stable limit cycles. These equilibria correspond in frequency and amplitude to the limit cycles described in 6.2 and observed in numerical simulations, with this parameter set. Figure 6.6 represents a typical behavior of this kind of limit cycle:

- Amplified structure displacement.
- Delay of 90° between the wake variable Q and the structure displacement.
- The system oscillates at the natural frequency of the structure.

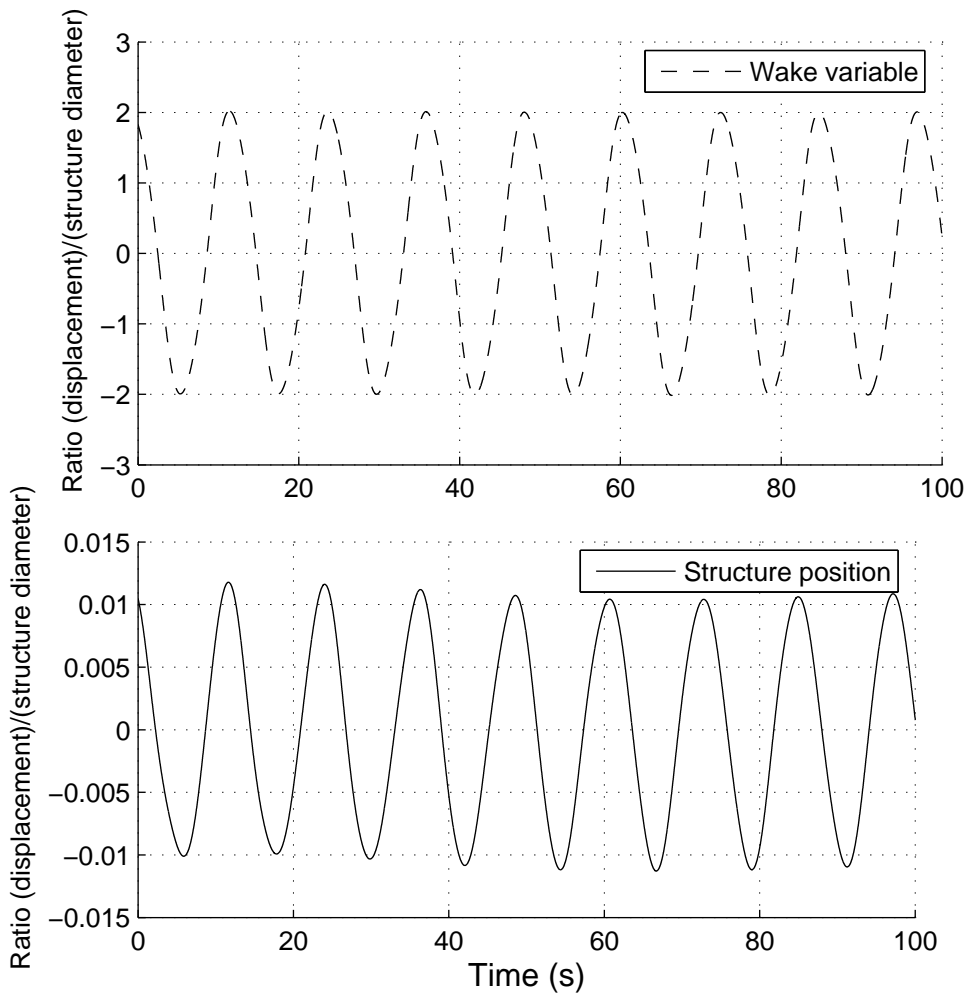


Figure 6.5: Rigid cylinder undergoing vortex induced vibration in a non resonant case: structure displacement Y (continuous line), wake variable Q (dashed line)

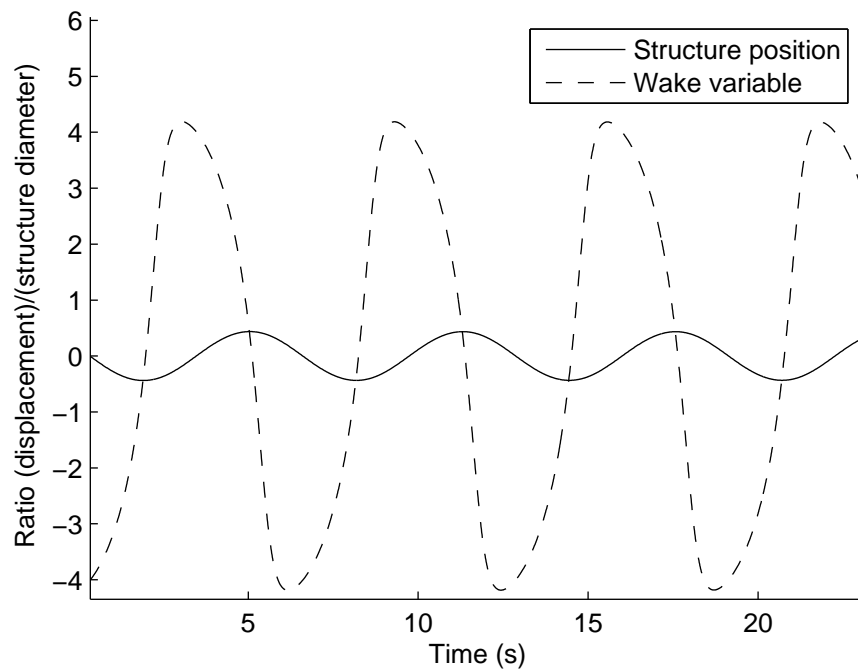


Figure 6.6: Rigid cylinder undergoing vortex induced vibration in a resonant case: Structure displacement Υ (continuous line), wake variable Q (dashed line)

Chapter 7

VIV control

This chapter proposes a control system to reduce the mechanical fatigue associated to the VIV. The riser top end is the unique part of the riser that is non-submerged and easily accessible, as the remaining part of the structure is underwater and more difficult to access. So the proposed idea is to introduce an active control using actuators at the riser top end, because of the ease of installation and maintenance in this non-submerged part, and the less aggressive environment for the actuators. A vibration sensor is required, and is the unique submerged part of the control system. Note that some of the new risers are already equipped with a sensor to measure the angle between the riser bottom end and the wellhead; this sensor can be used to calculate the vibration of the structure close to the wellhead.

The phenomenological model presented in section 6.1 is used to model the structure undergoing VIV. This model gives to the structure a behavior in amplitude and frequency that fits real measurements, in the sense that the average radius of the the limit cycle, as well as its associated oscillation period, are correctly represented. A more detailed picture of the interaction between the structure and the hydrodynamic forces would be much more complicated to accurately model. This discards the design of observers or control laws that are based upon accurate estimations of the hydrodynamic forces.

The chosen approach is to attenuate the vibration associated to the most excited frequency. It uses a control only based on the structure behavior at this frequency. This choice for the control design benefits from the fact

that VIV frequencies are low damped and that the vortex shedding along the structure amplifies small displacement at this frequency. These two features help the force applied at the riser top end to propagate along the structure, so a small force amplitude is required to modify the whole structure behavior.

Physically, the actuators system consists in a device or a group of devices able to apply a force over the riser top end. This force should be in the same direction than the main vibrations. In practical cases, the direction of the sea current can change, as well as the main direction of the vibrations. So the actuators must be able to apply a force in any direction that is included in the plane perpendicular to the riser top end. An example is given by an hydraulic piston over a kind of rotatory table, with its rotation axis coinciding with the riser axis. Another example of actuators is a group of pistons in two perpendicular directions in the plan defined by the axis of the riser top end. Further details of these technologies are presented by Fortaleza et al in [13].

7.1 VIV modal analysis

The considered model comes from the spatial discretization of equation (6.3) in N points, with a distance l between two points. Y_j represents the structure transversal displacement at point j . The state vector is given by $X = (Y_1, \dots, Y_N, \dot{Y}_1, \dots, \dot{Y}_N)^T$. The control u is defined as a force at the riser top end, giving:

$$\begin{cases} \dot{X} &= AX + Bu + P, \text{ with } A = \begin{pmatrix} 0 & I \\ -K & -O \end{pmatrix} \\ y &= CX \end{cases}$$

P represents the system disturbances generated by the nonlinear behavior of the vortex shedding. O is a diagonal matrix that writes $O = \tau I$, where I is the N -dimensional identity matrix. O contains the accelerations associated to the hydrodynamic damping. Vector B is the acceleration of the structure associated to the riser's top end displacement, $B = (0.., 1/(ml))^T$. The system output y is the displacement of the discretization point closest to the riser bottom end $\Upsilon(0, t)$. The output equation can be expressed as $y = CX$ for a given row-matrix C with only one non-zero entry $C = (1, 0.., 0)$. The

expressed by

$$\lim_{\text{Re}(\lambda_j) \rightarrow 0} \left| \frac{b_j(1 + i|\lambda_j|\iota_j)}{((\lambda_j + \bar{\lambda}_j)|\lambda_j|)} i \right| = \infty$$

The excited mode has an amplitude that tends toward infinity, thus it has a larger amplitude than the finite sum of the bounded amplitudes of the others modes. So, the structure dynamics can be approximated by the dynamics of the corresponding excited mode:

$$\frac{y(i|\lambda_j|)}{u(i|\lambda_j|)} = \frac{b_j(\iota_j i|\lambda_j| + 1)}{2\text{Re}(\lambda_j)|\lambda_j|} i \quad (7.2)$$

As $\iota_j \ll 1$, the transfer function for $s = i|\lambda_j|$ tends toward a purely imaginary number. Thus the displacements tend to become orthogonal (phase = $\pm 90^\circ$) to the force that generates them. ■

This is a key aspect to understand the behavior of a structure undergoing VIV, because VIV only have large amplitudes when they are associated to these resonant frequencies. To illustrate this point, figure 7.1 compares the Bode diagram of a 200th order system and the Bode diagram of a second order model that only represents one system mode.

After modal reduction, once a single mode that corresponds to pulsation $|\lambda_j|$ has been kept, the relation between the top end external force $u(i|\lambda_j|)$ and the displacement $y(i|\lambda_j|)$ of another point of the structure, taken as the output, is simply given by equation (7.2).

In the case of a force that has the same frequency than a natural mode, for all the points in phase with the force application point ($b_j > 0$), the phase between the displacements of these points and the force is -90° ; for the others points ($b_j < 0$), the phase shift is 90° . This property allows to determine the required phase relation between a measured vibration and the top riser force, in order to generate a vibration in phase opposition.

7.2 Control system

The idea is to generate a vibration in phase opposition ($\pm 180^\circ$) to the VIV, in order to neutralize them (see Fortaleza et al in [14]). The control strategy uses some system information: VIV have large amplitudes only for the natural frequencies of the structure [5], and for these frequencies, the modal analysis

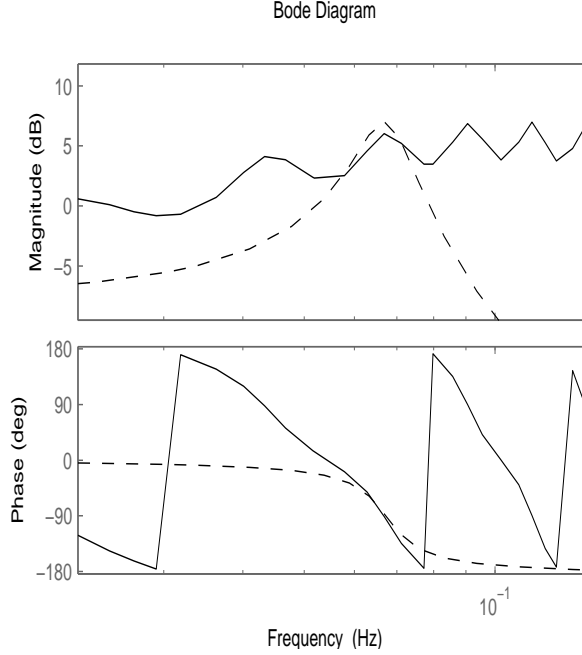


Figure 7.1: Bode diagrams of the structure (continuous line) and the single mode model

shows that structure displacements are orthogonal ($\pm 90^\circ$) to the forces that generate them. So, it is sufficient to add a $\pm 90^\circ$ shift to generate a vibration in phase opposition.

Proposition 9 *Using a top force with a phase shift of $\pm 90^\circ$ with respect to the measured vibration can reduce VIV.*

Proof The relation (7.2) can be rewritten, considering $\iota_j = 0$ and including the main component of the vortex shedding disturbance $y^P(i|\lambda_j|)$, as

$$y(i|\lambda_j|) = \frac{b_j}{2\text{Re}(\lambda_j)|\lambda_j|} iu(i|\lambda_j|) + y^P(i|\lambda_j|) \quad (7.3)$$

The external force at the riser top end is such that ($\pm 90^\circ$ shift) $u(i|\lambda_j|) = -i\kappa y(i|\lambda_j|)$, where κ has the same sign of b_j . Thus the equation (7.3) becomes

$$y(i|\lambda_j|) = \frac{b_j\kappa}{2\text{Re}(\lambda_j)|\lambda_j|} y(i|\lambda_j|) + y^P(i|\lambda_j|) \quad (7.4)$$

Equation (7.4) gives a relationship between the vortex shedding excitation and the structure vibration:

$$y(i|\lambda_j|) = y^P(i|\lambda_j|) \left(1 - \frac{b_j \kappa}{2 \operatorname{Re}(\lambda_j) |\lambda_j|} \right)^{-1} \quad (7.5)$$

According to equation (7.5), as $b_j \kappa > 0$ and $\operatorname{Re}(\lambda_j) < 0$, the influence of an unmodified disturbance y^P on y is reduced at the resonance frequency. ■

However, the following limits of this approach must be noticed:

- According to simulations and experimental results, the gain κ must be kept sufficiently small. Otherwise, movements at the structure's top end become too large, regarding the assumptions made in the control design: the structure behavior cannot be reduced to the behavior of a simple oscillator anymore. For instance, for large κ , the structure can suffer from large vibrations, due to a lock in with vortex shedding at another natural frequency.
- It is well known that disturbance y^P increases when the amplitude of y is reduced, i.e. when the control is applied. However the analysis presented in chapter 6 and the modal analysis presented in section 7.1 suggest that, if κ is chosen small enough for the original frequency of VIV (open loop frequency) to remain unchanged (no switch to another structure mode), the control law works. The control system can be analyzed as an artificial damping increase, that reduces the amplitude of the limit cycle generated by the vortex shedding. Yet, as it can be seen, for example in figures 7.3 and 7.4, the control can slightly increase the mean amplitude of the vibrations for some specific points of the structure, those close to the excited mode nodes. As these regions have small displacements, the impact of their vibrations over the mechanical fatigue remains negligible.

The control system is made of two physical parts: an actuator to impose horizontal forces at the riser top end, and two sensors, one close to the riser top end, and the other close to the riser bottom end. The system starts in a VIV detection mode. In this mode, the system measures the vibrations at the two points, detects their amplitudes and the phase shift between them. Once the vibration amplitude crosses a specified threshold, a control law is generated, considering the main frequency of the VIV and the phase shift between the displacement at the bottom measure point and the

force application point. This part identifies if b_j is positive or negative, thus it defines the sign of κ . This control law is designed with three features:

- A bandpass effect, that makes the control system only react to the dynamics of the main frequency excited by the vortex shedding. This condition avoids the control system to generate vibrations in other frequencies.
- A phase shifter, to generate a force at the same frequency, but in phase opposition to the VIV.
- A gain κ , between the measured vibration and the force to be applied. The value of this gain can be increased on-line, through an adaption law, as long as the VIV frequency does not change.

Linear filter These features can be implemented through the following linear control law:

$$\frac{\hat{u}(s)}{\hat{y}(s)} = \frac{2\kappa\alpha s}{s^2 + 2\alpha s + |\lambda_j|^2} \times \frac{\pm(|\lambda_j| - s)}{|\lambda_j| + s} \quad (7.6)$$

Notice that, as the vibrations are perpendicular to the current, the reference position at rest always corresponds to $y = 0$. That is why no reference appears in equation (7.6). This transfer function combines two terms in series. The first term is a second order bandpass. It filters the signal, in order to keep just a narrow frequency band around the excited natural frequency. It also defines the gain between the measured signal and the top riser external force. The second term is a phase shifter, that gives $\pm 90^\circ$ depending on the sign of b_j , identified during the VIV detection mode.

The width of the frequency band is based on the precision of the main frequency estimation. In the transfer function represented in equation (7.6), the bandwidth is related to the damping constant α . Replacing $s = i|\lambda_j|$ in equation (7.6), it is readily verified that this transfer function satisfies the condition $\hat{u}(i|\lambda_j|) = -i\kappa\hat{y}(i|\lambda_j|)$.

Observer Dedicated observers provide another way to calculate the control output with an orthogonal phase ($\pm 90^\circ$). This is a two steps approach. First, an observer, especially designed to observe periodic disturbances at

the vibration known main frequency (that corresponds to $|\lambda_j|$), decomposes the vibration into two terms (sine and cosine). Then the control is computed, considering the adaptive gain κ and the orthogonal direction ($\pm 90^\circ$). The chosen observer is in the spirit of the work of Chauvin [7]. The signal to be observed being $y(t) = L_1 \sin(|\lambda_j|t) + L_2 \cos(|\lambda_j|t)$, with $L = (L_1, L_2)^T$, the observation \hat{y} of y , computed from the estimated gains \hat{L}_1 and \hat{L}_2 , with $\hat{L} = (\hat{L}_1, \hat{L}_2)^T$, is obtained by

$$\begin{cases} \frac{d\hat{L}_1}{dt} = \alpha \sin(|\lambda_j|t)(y - \hat{y}) \\ \frac{d\hat{L}_2}{dt} = \alpha \cos(|\lambda_j|t)(y - \hat{y}) \\ \hat{y} = \hat{L}_1 \sin(|\lambda_j|t) + \hat{L}_2 \cos(|\lambda_j|t) \end{cases} \quad (7.7)$$

α is a tuning parameter, proportional to the width of the frequency band. The larger α , the larger the influence of the frequencies close to $|\lambda_j|$ over L . The control is computed considering the adaptive gain κ and the orthogonal direction $\pm 90^\circ$. For example, considering an orthogonal direction of -90° , the riser top end displacement can be computed as:

$$u(t) = \kappa \begin{pmatrix} -\cos(|\lambda_j|t) \\ \sin(|\lambda_j|t) \end{pmatrix} L(t) \quad (7.8)$$

L represents the first terms of an estimated Fourier series. This method is advantageous in cases where the system does not have a constant discretization period. In these cases, the fact that the discretization period is not constant makes variable the width of the frequency band, however it does not change the main observed frequency $|\lambda_j|$.

7.3 Mechanical fatigue

The accurate estimation of the mechanical fatigue of offshore structures remains a research domain. However, an estimation of this mechanical fatigue can be done, based on the intensity of the maximum structure stress over a cycle, and on the number of cycles that the structure material can support.



Figure 7.2: Typical example of Wöhler curve

Normally a Wöhler curve is defined for each material. This is an experimental curve that relates the maximum stress over a cycle and the number of cycles that the material can support. Figure 7.2 represents a typical example of Wöhler curve.

The mechanical structures are designed to be on the right hand side of the curve, thus they support a large number of stress cycles. In this region a small change on the system stress represents a large change on the number of cycles supported by the structure.

For a given frequency, the stress generated by the VIV is proportional to the structure displacement. However the direct effect of a VIV reduction over the reduction of the associated mechanical fatigue depends on other structure parameters and on the effect of the other fatigue sources (drag force, waves, etc). A safe assumption is to consider that the mechanical fatigue in those cases is reduced by a factor of $(\Upsilon_c/\Upsilon_o)^3$, where Υ_c is the system closed loop response and Υ_o the system open loop response. For the numerical simulations presented in section 7.4, the control system provides

a fatigue reduction of more than 70%. That is a rather good result for a controller that only uses small displacements at the riser top.

7.4 Numerical simulations

Equation (6.3) is discretized using the finite element method. The simulated structure is a steel vertical riser held by rotary joints at both ends. The tension at the riser bottom end is taken equal to zero. Geometric dimensions and other constants used to simulate the system are presented in table 7.1.

Table 7.1: Structure dimensions and constants.

Type	Value	Unit
Height	10^3	m
External Diameter	.2	m
Internal Diameter	.18	m
Elastic Modulus	2.1×10^{11}	Pa
Steel Density	7.8×10^3	kg/m ³
Water Density	10^3	kg/m ³

Two different cases are simulated. The first case represents the structure totally immersed, with a constant flow along the structure. The considered flow speed is 0.1 m/s. The second case represents a marine current that is constant with respect to time, but linearly increases from the sea bed ($z = 0$ m) to the surface, its speed is represented in m/s as $U(z) = 0.05 + 0.00005z$.

These two different profiles of sea current excite the same mode. The interest of this choice is to show that the structure cross displacement has a form mainly defined by the structure and its most excited mode j , and that the sea current profile is important to define the amplitude envelope. Note that the structure behavior is much more complex than the one used for the control design. However simulations show that the vibration control suitably reduces the vibration envelope. The structure envelope is close to the modal envelope defined by the associated eigenvectors $(V_j, \bar{V}_j)^T$.

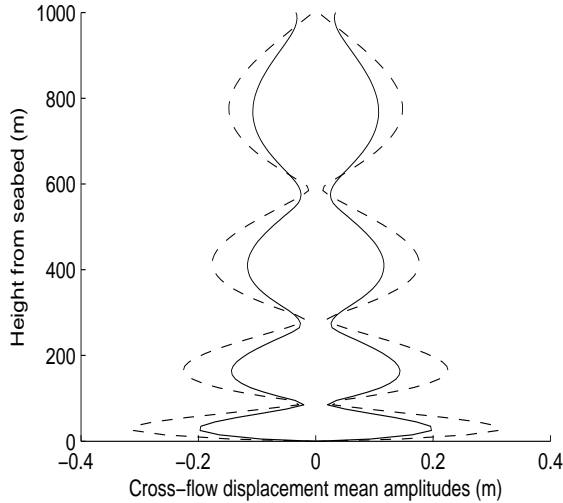


Figure 7.3: Cross-flow displacement for a constant sea current: open loop (dashed line) closed loop (continuous line)

In figures 7.3 to 7.10, the vibrations are compared, considering the following four aspects: cross-flow displacements, speeds, highest punctual displacement and its Fourier transform. The interest is to compare the vibration intensity and to observe the impact of the feedback control along the structure and on the other structure modes. The cross-flow displacements presented in figures 7.3 and 7.4 present a displacement reduction of 35% at the critical points. It is interesting to observe a small amplitude amplification in the minimum displacement regions. This phenomenon happens because of the non linear damping. A vibration reduction in the main frequency increases the lift forces, and consequently increases the vibrations associated to other modes.

The cross-flow speeds presented in figures 7.5 and 7.6 show an average speed decrease of almost 35%, the same rate as for the displacement reduction. This point shows that the structure under active control keeps the same relation between displacement and speed, and it happens because the structure continues to oscillate with the same natural main frequencies than in open loop. The results are interesting, noticing that the control simply implies a punctual force that generates a displacement of the riser top end about 10% of the maximum punctual displacement, and a reduction of the mechanical fatigue associated to the VIV up to 70%.

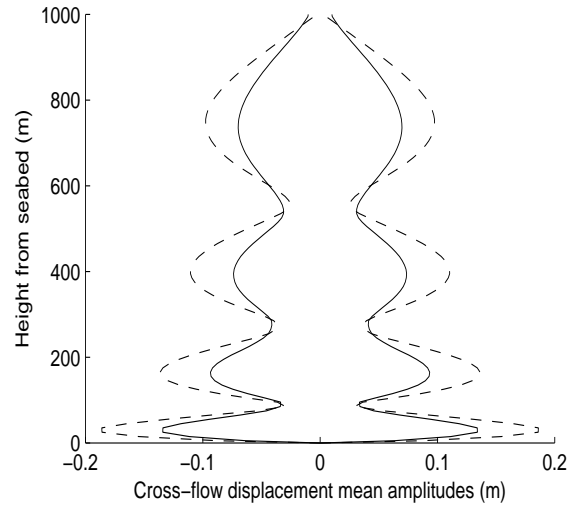


Figure 7.4: Cross-flow displacement for a variable sea current: open loop (dashed line) closed loop (continuous line)

Figures 7.7 and 7.8 show an important reduction of the vibration associated to the main frequency. They also show a slight amplification of other modes, because the lift force increases when the structure mean speed is reduced. These other frequencies remain of minor importance for the structure fatigue, according to their small amplitudes and to the fact that the displacement peaks do not coincide. Figure 7.9 shows a single mode open loop behavior due to the uniform current profile, which becomes multi-modal in closed loop, thus showing the attenuation of the vibrations for the structure natural frequency that is the closest to the vortex shedding natural frequency. Figure 7.10 shows this tendency for a case where the open loop has already a multi-modal behavior.

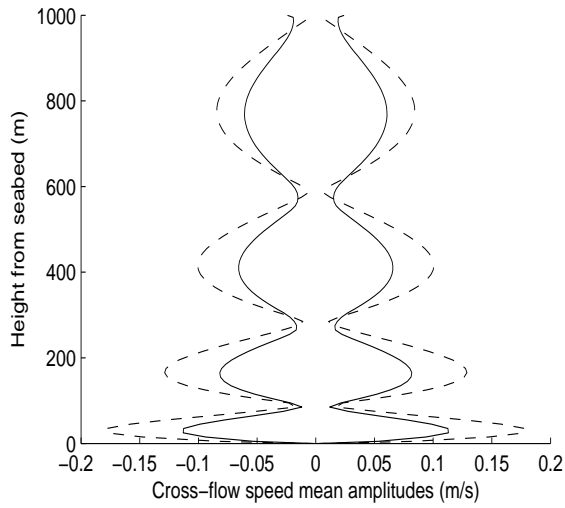


Figure 7.5: Cross-flow speed for a constant sea current: open loop (dashed line) closed loop (continuous line)

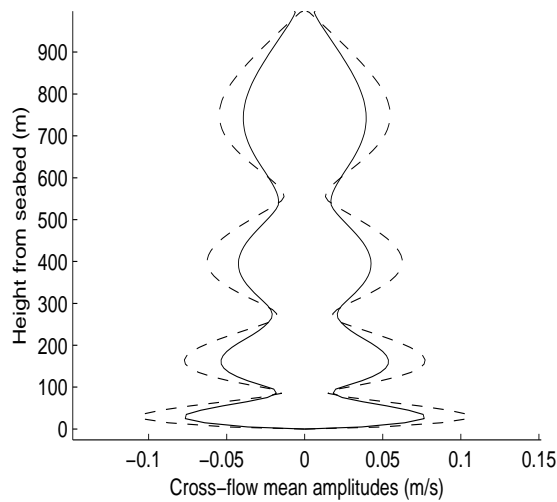


Figure 7.6: Cross-flow speed for a variable sea current: open loop (dashed line) closed loop (continuous line)

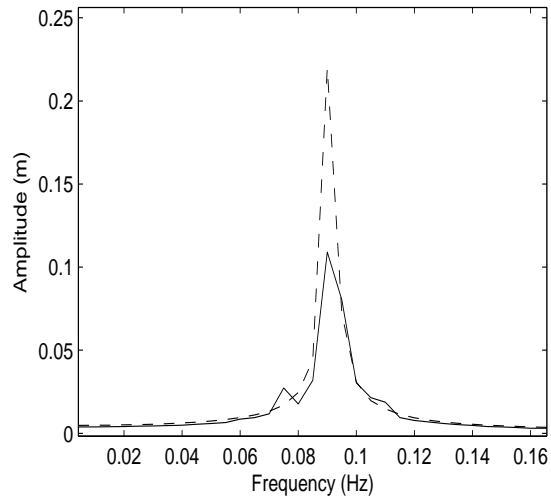


Figure 7.7: Cross-flow highest vibration Fourier transform for a constant sea current: open loop (dashed line) closed loop (continuous line)

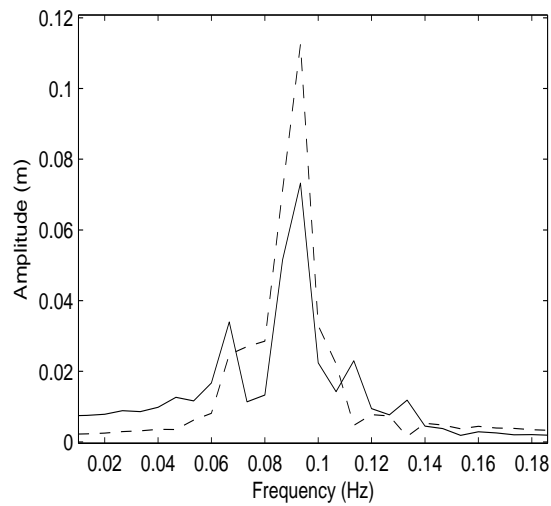


Figure 7.8: Cross-flow highest vibration Fourier transform for a variable sea current: open loop (dashed line) closed loop (continuous line)

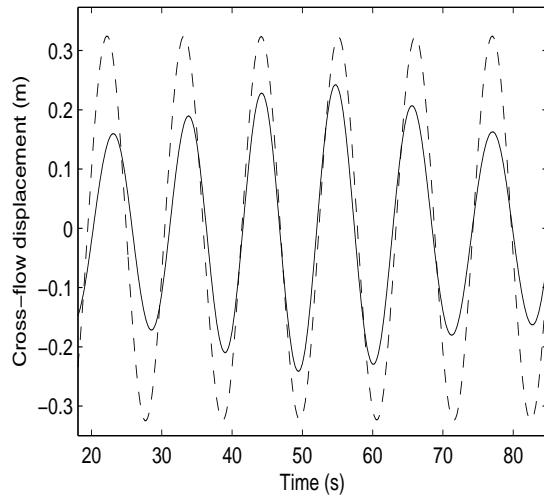


Figure 7.9: Cross-flow highest displacement for a constant sea current: open loop (dashed line) closed loop (continuous line)

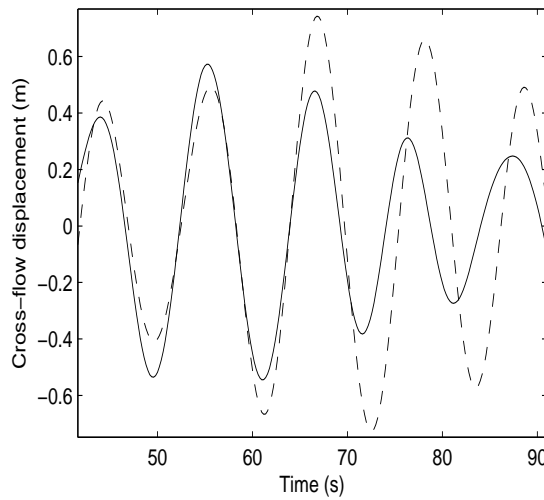


Figure 7.10: Cross-flow highest displacement for a variable sea current: open loop (dashed line) closed loop (continuous line)

Chapter 8

Reduced scale system

This chapter first presents, in section 8.1, the reduced scale system built at IFP Lyon. The main objectives of this experiment are to reproduce the phenomenon of vortex induced vibration in laboratory conditions and to test the proposed control strategy on a real system. This experimental set can be divided into three different parts: the hydraulic plant, the structure undergoing VIV and the control system. In section 8.2, experimental data are compared with numerical simulations, on a model that represents the experimental set. Section 8.3 is devoted to numerical simulations in open and closed loop. In section 8.4, the corresponding experimental results are presented and discussed.

8.1 Experimental set description

The reduced scale system is depicted in figure 8.1

8.1.1 Hydraulic plant

The hydraulic plant generates the flow around the structure. It can be divided into three parts:

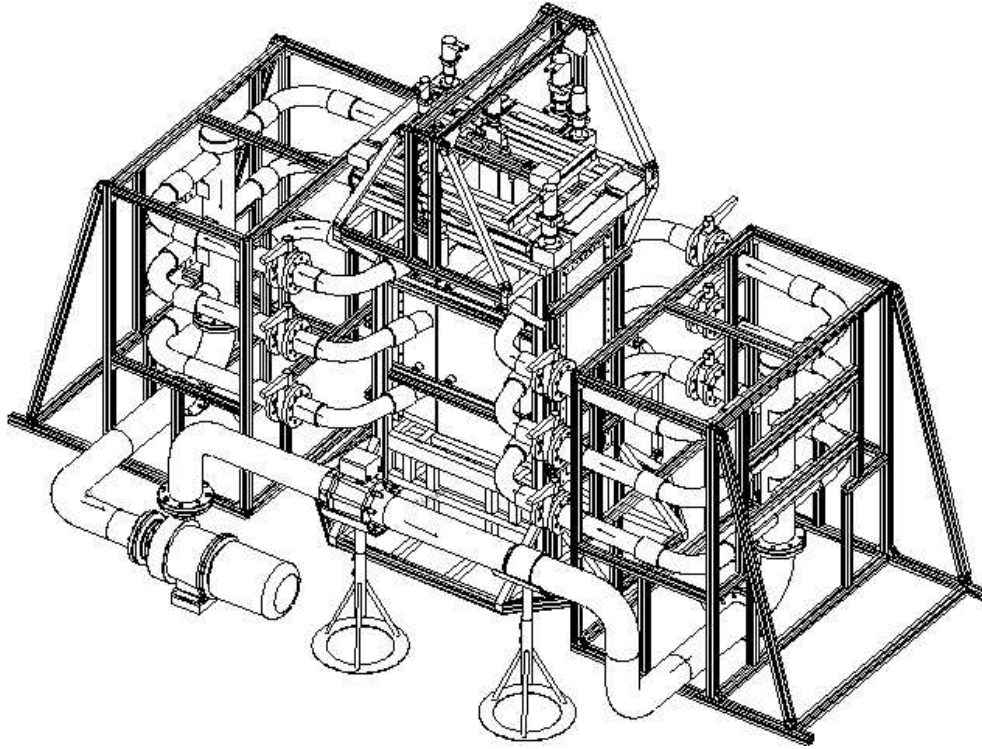


Figure 8.1: Experimental set overview

- Basin: it is the place where the studied structure is submerged. It has two honeycomb panels to avoid a turbulent flow. They separate the zone close to the studied structure and the zones of flow input and output.
- Flow lines: they link the pumping system to the basin, with six inputs and six outputs. The associated twelve valves are used to change the flow profile in the basin.
- Pumping system: it is made of a centrifugal pump and a variable-frequency drive. The flow range of the pump is limited by the available N_{psh} , the minimum and maximum rotation speeds of the pumping system. In the current configuration, the pumping system can deliver a flow between 20 and 60 m^3/h .

Table 8.1: Reduced structure dimensions and constants.

Type	Value	Unit
Height	1.3	m
Submerged part	1.1	m
Flow speed	0.04	m/s
External Diameter	11×10^{-3}	m
Internal Diameter	9×10^{-3}	m
Elastic Modulus	5.6×10^6	Pa
Bottom added Mass	80×10^{-3}	kg
Viton Density	1.96×10^3	kg/m ³
Water Density	10^3	kg/m ³
Upper bounder condition	Fixed top	-
Lower bounder condition	Free bottom	-

8.1.2 Structure undergoing VIV

The main objective during the design of the reduced scale structure was to reproduce the phenomenon of vortex induced vibration over a flexible structure. The chosen solution is a tube made of a special polymer called Viton, the characteristics of which are presented in table 8.1.

One punctual mass was added at the structure bottom end. Its main objective is to increase the tension along all the structure, thus to reduce the structure static deformation in the flow direction. The fact that the structure is almost vertical avoids that any part of the structure gets out of the region of laminar current. With the data presented in table 8.1, it is possible to calculate some systems characteristics: the structure has a Reynolds number around 430; its three first natural frequencies are respectively close to 0.13 Hz, 0.56 Hz and 1.25 Hz. The natural frequency of the vortex shedding ω is given in rad/s by

$$\omega = \frac{2\pi S_t U}{d} \quad (8.1)$$

where S_t represents the Strouhal number [10]. For the experimental set, the Strouhal number can be considered equal to 0.2, so the natural frequency of the vortex shedding is close to 4.4 rad/s or 0.7 Hz. These conditions have been chosen to produce a VIV at the same frequency than the structure

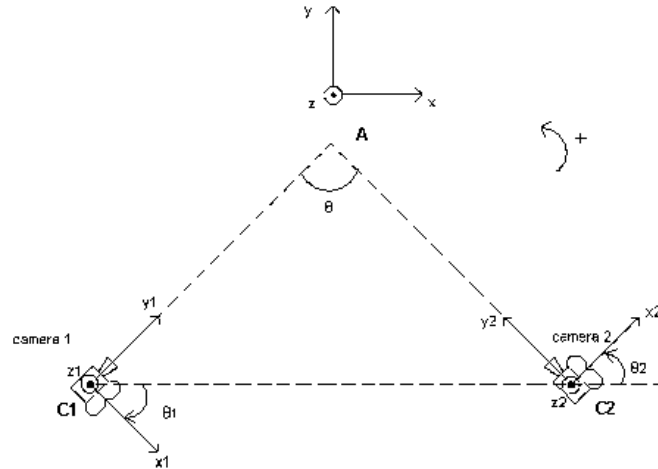


Figure 8.2: Stereovision system diagram

second mode, thus to test the theory in the less intuitive case, where the structure top and bottom ends are in phase opposition. In this case, the force at the structure top end should be applied with a phase shift of $+90^\circ$ with respect to the measured bottom end displacement.

8.1.3 Control system

The control system is physically made of three parts: cameras, computer and actuator. There are two cameras that have well-known angles and positions in a cartesian plane, as presented in figure 8.2. The measured point is the structure bottom end. Its position in the space is calculated by comparing the images from the two cameras and by using the stereovision principle presented by Sabri in [33]. The computer uses a binarization technique to localize the structure and its bottom end in each frame. Then, it calculates the tridimensional position of the structure bottom end by comparing the frames of the two cameras.

The used computer does not use a real-time operating system. The actuators are servo-motors able to introduce an external force over the structure, by forcing the displacement of its upper part in the three cartesian directions.

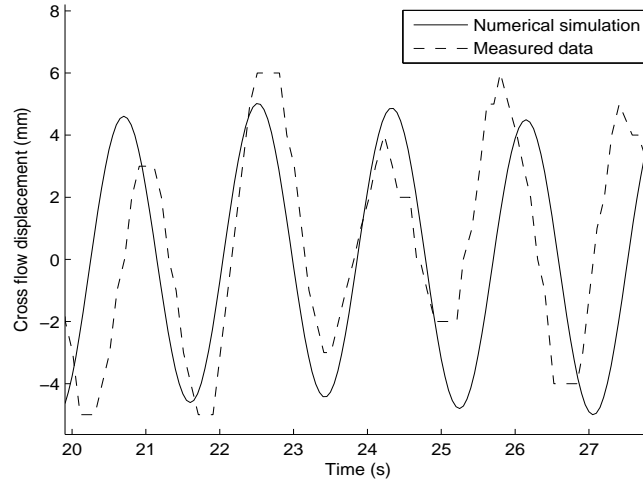


Figure 8.3: Open loop cross-flow displacement: numerical simulation and measured data

Even if the experimental set can apply external forces over the structure in the three directions, the lack of a convenient model to describe the structure undergoing VIV in the other directions limits the use of external forces to the direction of the main vibrations (horizontal cross-flow direction).

8.2 Comparative analysis between numerical and experimental results

The studied structure is presented in section 8.1.2. A numerical model is obtained through the discretization using the finite element method of equation (6.3) into 40 points. The results provided by this numerical model are compared to the experimental results in figures 8.3 to 8.6.

Figure 8.3 presents the open loop cross flow displacement of the structure bottom end. The measured vibration is slightly different to the vibration computed with the numerical model. The two signals have a similar frequency spectrum, even if the measured signal has a measure noise with components in a large range of frequencies (see figure 8.4).

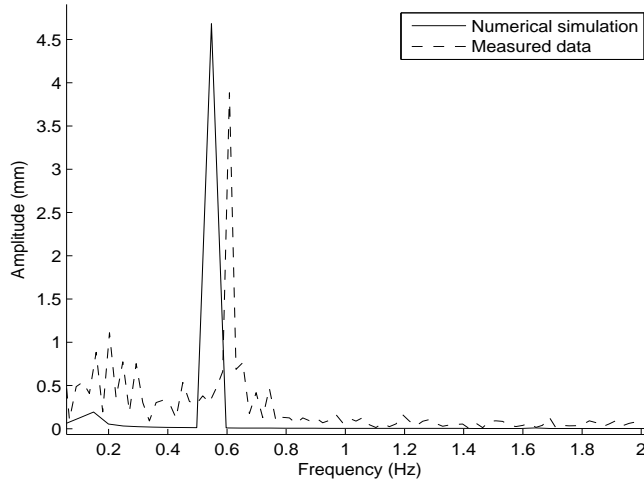


Figure 8.4: Fourier transform of the cross-flow displacement (open loop): numerical simulation and measured data

The numerical simulation and the measured data are also similar in the closed loop case. In both cases, there is a vibration reduction of at least 30%.

Figure 8.5 presents the closed loop cross flow displacement of the structure bottom end. As in the open loop case, the measured vibration is slightly different than the vibration computed with the numerical model. The two signals have a similar frequency spectrum, even if the measured signal has a measure noise with components in a large range of frequencies (see figure 8.6).

8.3 Numerical simulations

This section compares the open loop and closed loop results provided by the numerical model. In figures 8.7 to 8.10, the vibrations are compared, considering the following four aspects: cross-flow displacements, speeds, bottom end punctual displacement and its Fourier transform. The interest is to compare the vibration intensity and to observe the impact of the feedback control along the structure and on the other structure modes.

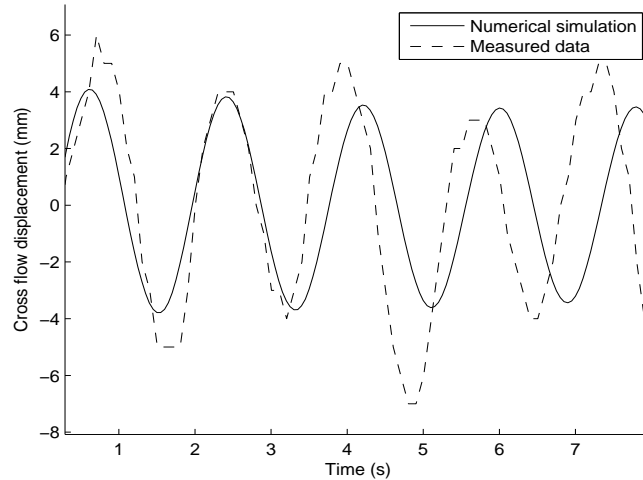


Figure 8.5: Closed loop cross-flow displacement: numerical simulation and measured data

The closed loop cross-flow displacements in figure 8.7 present a displacement reduction of 30% with the use of top end displacements smaller than 10% of the maximum punctual displacement. Section 8.4 presents similar results obtained on the experimental set.

The cross-flow speed presented in figure 8.8 shows an average speed decrease of 30% in the closed loop case. It is the same rate than for the displacement reduction. This point shows that the structure under active control keeps the same relation between displacement and speed, this happening because the structure continues to oscillate with the same main frequency than in open loop.

Figure 8.9 shows an important reduction of the vibration associated to the main frequency. Figure 8.10 confirms this single mode behavior, that is due to the uniform current profile.

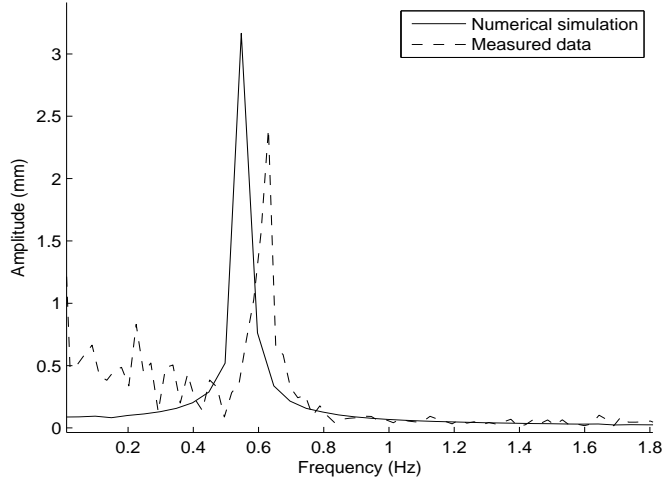


Figure 8.6: Fourier transform of the cross-flow displacement (closed loop): numerical simulation and measured data

8.4 Experimental results and discussion

This section presents the results obtained on the reduced scale system, using the same control system than for the numerical simulations of section 8.3. The current configuration of the experimental set only permits the measurement of the structure bottom end displacement. Thus in figures 8.11 and 8.12, the vibrations are compared by only considering displacements of the structure bottom, as well as its Fourier transform. The cross-flow displacements presented in figures 8.11 present a displacement reduction of about 35% at the measured point.

The experimental results kindly agree with simulations. In the tested cases, they are even slightly better than the numerical results. Some facts can justify these differences:

- The flow profile is considered as exactly uniform in the numerical simulations, however in practice it presents small variations along the vertical z-direction.
- There are inaccuracies in the structure data used to generate the numerical model.

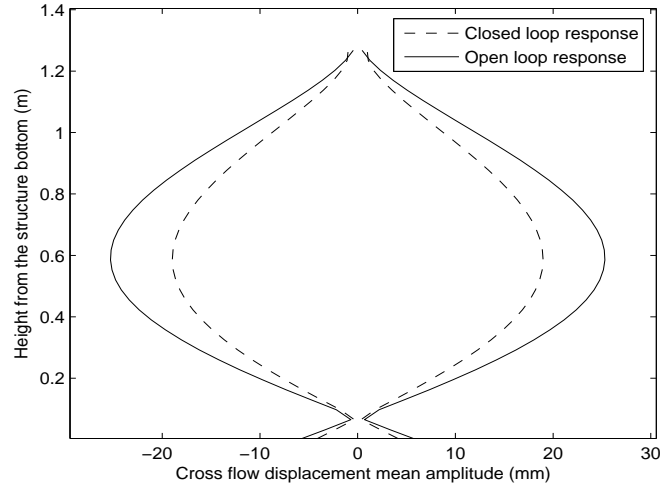


Figure 8.7: Cross-flow mean displacement amplitude (open and closed loop): numerical simulation

- The use of phenomenological model that was developed to represent the VIV on its limit cycle. The increase of lift force due to the reduction of the vibrations is maybe slightly smaller in reality than in the numerical simulations.

The reduced scale system was useful to validate the control strategy, the numerical simulations and the principle of a vibration reduction system using a measurement point away from the force application point. This validation has been made in presence of a strong measure noise generated by the camera discretization (see figure 8.11). This also shows the robustness of the approach. From an economical point of view, the main result is the reduction of 35% of the vibrations, with the use of a minimum energy control law. Such a reduction has an important impact over the service life, as it represents a fatigue reduction due to the VIV of more than 70%.

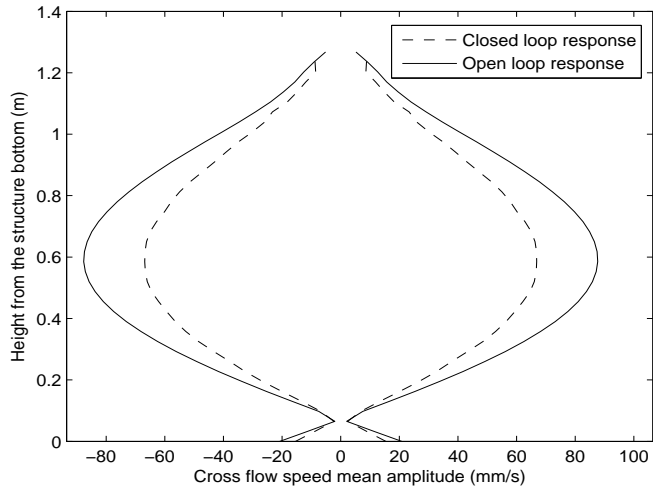


Figure 8.8: Cross-flow mean speed amplitude (open and closed loop): numerical simulation

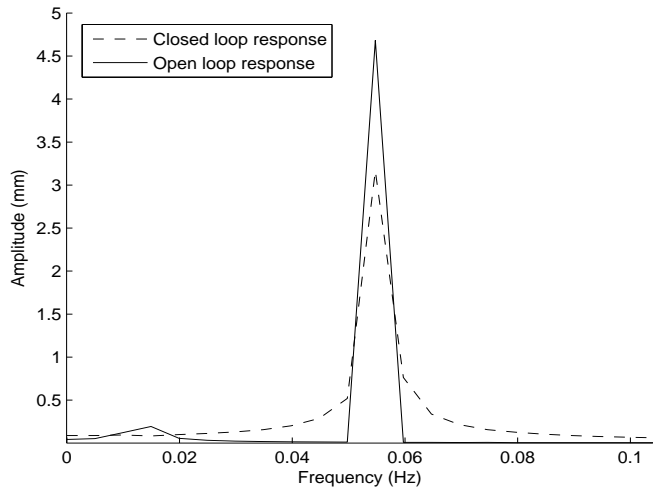


Figure 8.9: Fourier transform of the cross-flow bottom end vibration (open and closed loop): numerical simulation

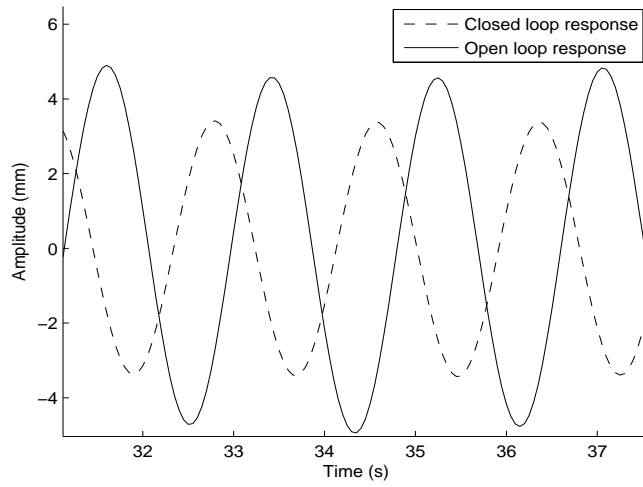


Figure 8.10: Cross-flow bottom end displacement (open and closed loop): numerical simulation

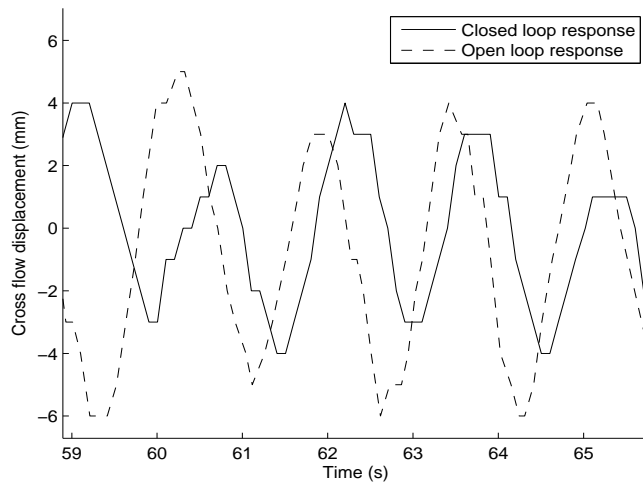


Figure 8.11: Measured cross-flow displacement: open and closed loop

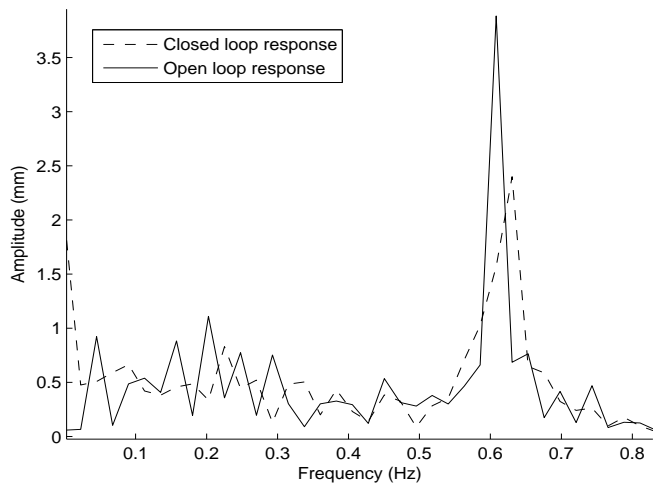


Figure 8.12: Fourier transform of the measured cross-flow displacement: open and closed loop

Chapter 9

Conclusion for the VIV control part

This research work presented the fundamental characteristics of long offshore structures undergoing vortex induced vibrations. The phenomenological model of the fluid-structure interaction that is used correctly represents real cases. A dedicated vibration control strategy has been developed. It is based on the modal analysis and the limit cycle behavior generated by the vortex shedding.

In the case of structures undergoing VIV, the objective of an active control is to reduce the structure displacements. This problem has been analyzed through the study of a system with a stable and constant reference position, associated to a special disturbance source. An accurate estimation of this disturbance source was not possible in the studied case, because of the impossibility to measure the sea current and the riser position all along the depth. However, the fact that these vibrations have specific frequencies and an effect all along the structure, guided the work toward a solution that reduces the displacement amplitudes associated to these special frequencies.

This system has interesting features: VIV reduction almost all along the riser, small top forces and small associated displacements, an adaptive concept using two sensors, that can be used to design the controller by on-line identification of the main vibration frequency and amplitude, thus eliminating the need to estimate which structure mode is excited.

The displacement and speed reductions of 35% all along the structure are rather good results, noticing that the control simply implies a punctual force that generates a displacement of the riser's top end (of about 10% of the maximum punctual displacement). The final result concerning the mechanical fatigue of the structure is a reduction of more than 70% of the mechanical fatigue associated to the VIV. These results were obtained with a simple and robust control system, that requires small actuators and a low power consumption.

Perspectives The control system is only based on the modal behavior of the structure. Further works could consist in analyzing the results of a larger test campaign on the experimental set. This campaign could test different structures and current profiles, to validate the control system for a larger group of cases. A perspective to improve the control performance is to consider in the control design the delay due to the mechanical wave propagation between the control application point and the measure point.

Bibliography

- [1] Abramowitz, M. and Stegun, I. A. (1972). *Handbook of Mathematical Functions with Formulas, Graphs, and Mathematical Tables*, ninth ed. Dover, New York.
- [2] Adachi, S. and Sano, H. (1998). *Active Noise Control System for Automobiles Based on Adaptive and Robust Control*, Proceedings of the IEEE International Conference on Control Application.
- [3] Angot, A. 2^oEd.(1982) *Compléments de mathématiques à l'usage des ingénieurs de l'électrotechnique et des télécommunications*, Masson, France.
- [4] Benner, P. (2009) *System-Theoretic Methods for Model Reduction of Large Scale Systems: Simulation, Control, and Inverse Problems*, Vienna International Conference on Mathematical Modelling, Vienna - Austria.
- [5] Blevins RD. (1990) *Flow-Induced Vibration*, Van Nostrand Reinhold.
- [6] Braaten, H., Lie, H., Skaugset, K. (2008) *Higher Order Modal Response of Riser Fairings* proceedings of the International Conference on Offshore Mechanics and Arctic Engineering, Estoril - Portugal.
- [7] Chauvin, J., Corde, G., Petit, N., Rouchon, P. (2007) *Periodic input estimation for linear periodic systems: Automotive engine applications*, Automatica, 43, **6**, 971-980.
- [8] Chowdhury, I. and Dasgupta, S. P. (2003). *Computation of Rayleigh Damping Coefficients for Large Systems*, Electronic Journal of Geotechnical Engineering.
- [9] El-Sinawi, A. H. (2004). *Active Vibration Isolation of a Flexible Structure Mounted on a Vibrating Elastic Base*, Journal of Sound and Vibration, **271**, 1-2, 323-337.

- [10] Facchinetti, M. L. (2003). *Un Modèle Phénoménologique des Vibrations Induites par Détachement Tourbillonnaire*, PhD Thesis, LadHyx - École Polytechnique.
- [11] Fard, M. P. (2001). *Modelling and Control of Mechanical Flexible Systems*, PhD Thesis, Norwegian University of Science and Technology.
- [12] Fliess, M., Lévine, J., Martin, Ph. and Rouchon, P. (1995). *Flatness and defect of nonlinear systems: introductory theory and examples*. Int. J. Control, 61(6):1327–1361.
- [13] Fortaleza, E., Creff, Y., Lévine, J. and Averbuch, D. (2007) *Méthode et Dispositif Améliorés de Limitation des Vibrations Induites par Vortex d'une Structure Allongée*, French Patent 07/09.119.
- [14] Fortaleza, E., Creff, Y., Levine, J.(2008) *Active Control of Vertical Risers Undergoing Vortex-Induced Vibrations*, Revue of International Conference on Offshore Mechanics and Arctic Engineering, Estoril - Portugal.
- [15] Fortaleza, E., Creff, Y., Levine, J.(2008) *Active Control and Motion Planning for Offshore Structures*. Fourth European Conference on Structural Control, Saint Petersburg - Russia.
- [16] Fortaleza, E., Creff, Y., Levine, J.(2009) *Active Control for the Re-Entry Operation of Flexible Risers*, Vienna International Conference on Mathematical Modelling, Vienna - Austria.
- [17] Greenberg, J. (2007) *Deepwater drilling equipment*, Kingdom Drilling, <http://www.kingdomdrilling.co.uk/drillops/equipment/DWRE02.pdf>.
- [18] Govardhan, R. and Williamson, C. H. K. (2000). *Modes of vortex formation and frequency response of a freely vibrating cylinder*, Journal of Fluid Mechanics, **420**, 11-14, 85–130.
- [19] Guckenheimer, J., Holmes, P. (1983) *Nonlinear Oscillations, Dynamical Systems, and Bifurcation of Vertical Fields*, Springer-Verlag, New York - USA.
- [20] Hoen, C. and Moe G. (1999). *Modal Decomposition of Measured Vortex Induced Response of Drilling Risers*, Proceedings of the Ninth(1999) International Offshore and Polar Engineering Conference, **3**, 1, 679–687.
- [21] Hogsberg, J. R. and Krenk, S. (2006). *Linear Control Strategies for Damping of Flexible Structures*, Journal of Sound and Vibration, **293**, 1-2, 59–77.

- [22] Howetal., B.V.E. et al. (2008). *Active control of flexible marine risers*, Journal of Sound and Vibration, doi:10.1016/j.jsv.2008.09.011
- [23] Inman, D.J. (2000). *Engineering Vibration*, Prentice Hall, second edition, New Jersey - USA.
- [24] Ismail, M. E. H., Muldoon, M. E. (1995). *Bounds for the small real and purely imaginary zeros of Bessel and related functions*, Methods and Applications of Analysis, **2**, 1, 1-21.
- [25] Ioki, T., Ohtsubo, K., Kajiwara, H., Koterayama, W., Nakamura, M. (2006). *On Vibration Control of Flexible Pipes in Ocean Drilling System*, International Offshore and Polar Engineering Conference, San Francisco - USA.
- [26] Keller-Ressel, M. *Wolfram MathWorld*. www.mathworld.wolfram.com/LyapunovFunction.html
- [27] Larsen, C.M. (2000) *Empirical VIV Models*, Workshop on Vortex-Induced Vibrations (VIV) of Offshore Structures. Sao Paulo -Brazil.
- [28] Le Cunff, C. Averbuch, D., Klopffer, M. *System and Method for Limiting Vortex-Induced Vibrations on an Offshore Production Riser*. French Patent FR0114814.
- [29] Levine, J. (2004) *Analyse et Commande des Systèmes Non Linéaires*. <http://cas.ensmp.fr/%7Elevine/Enseignement/CoursENPC.pdf>
- [30] Popov, Egor P. (1990) *Engineering Mechanics of Solids*. Prentice Hall - Pearson Ed, New York.
- [31] Sparks, C.P. (2002). *Transverse Modal Vibrations*, Oil, Gas and Technology -IFP Revue.
- [32] Sabri, R., Lévine, J., Biolley, F., Creff, Y., Le Cunff, C. and Putot., C. (2003) *Connection of the riser to the well-head using active control*, Deep Offshore Technology Conference, Marseille - France.
- [33] Sabri, R. (2004). *Installation des Conduites Pétrolières en Mer Profonde par Contrôle Actif*, PhD Thesis, Centre Automatique et Systèmes - École des Mines de Paris.
- [34] Petit, N., Rouchon P. (2001) *Flatness of Heavy Chain Systems*, SIAM Journal on Control and Optimization, 40:475-495.

- [35] Petit, N., Rouchon P. (2002) *Flatness of Heavy Chain Systems*, 41st IEEE Conference on Decision and Control. Las vegas - USA.
- [36] Slotine, JJ E. and Weiping, L. (1991) *Applied Nonlinear Control*, Prentice House.
- [37] Vandiver, J. K. (1993). *Dimensionless Parameters Important to The Prediction of Vortex-Induced Vibration of Long, Flexible Cylinders in Ocean Currents*, Journal of Fluids and Structures, **7**, 5, 423–455.
- [38] Violette, R., de Langre, E. and Szydlowski, J. (2007). *Computation of vortex-induced vibrations of long structures using a wake oscillator model: comparison with DNS and experiments*, Computers and Structures Journal, **85**, 11-14, 1134–1141.
- [39] Wiggins, S. (1990) *Introduction to Applied Nonlinear Dynamical Systems and Chaos*, Springer, New York - USA.
- [40] Woolsey, C. A. (2006). *Lecture Notes: Computer Aided Control System Design*, Virginia Tech Department of Aerospace and Ocean Engineering, www.aoe.vt.edu/~cwoolsey/Courses/AOE4004/+
- [41] Thull, D., Wild, D., Kugi, K. (2006). *Application of Combined Flatness- and Passivity-Based Control Concept to a Crane With Heavy Chains and Payload*, IEEE International Conference on Control Applications.
- [42] Vaz, G., Christiaan, K., Monroy, C. (2008). *Viscous Flow Computations on Risers- From 2D bare smooth cylinders towards 3D straked rough risers*, Revue of International Conference on Offshore Mechanics and Arctic Engineering, Estoril - Portugal.
- [43] Vikestad, K., Vandiver, J. K., Larsen, C.M. (2000). *Added Mass and Oscillation Frequency for a Circular Cylinder Subjected to Vortex-Induced Vibrations and External Disturbance*, Journal of Fluids and Structures, **14**, 7, 1071–1088.
- [44] Yamamoto, M., Morooka, C. K., Ueno, S. (2007). *Dynamic Behavior of a Semi-Submersible Platform Coupled With Drilling Riser During Re-Entry Operation in Ultra-Deep Water*, International Conference on Offshore Mechanics and Arctic Engineering, San Diego - USA.

Appendix A

Computations for the wake model in the resonant case

We here detail the study sketched in section 6.4.

The objective of this section is to study the stability of a limit cycle suggested in section 6.2, in the particular case where the structure natural frequency Ω is close to the natural frequency of the vortex shedding ωU . The rigid cylinder assumption gives $\partial^4 \Upsilon / \partial z^4 = \partial(T \partial \Upsilon / \partial z) / \partial z = 0$, and the unique natural pulsation Ω is the square root of the spring constant. The system can be written as

$$\begin{cases} \ddot{\Upsilon} &= -\Omega^2 \Upsilon - \tau U \dot{\Upsilon} + h U^2 Q \\ \ddot{Q} &= -\varepsilon U (Q^2 - 1) \dot{Q} - (\omega U)^2 Q + a \ddot{\Upsilon} \end{cases} \quad (\text{A.1})$$

It is important to note that the specific limit cycle studied in this section corresponds to cases where Ω and ωU are close to each other. So we can define the limit cycle frequency σ such $|\sigma^2 - \Omega^2| \ll 1$ and $|\sigma^2 - (\omega U)^2| \ll 1$.

To use the averaging method, we suggest the following change of coordinates:

$$\left\{ \begin{array}{l} H_1 = \Upsilon \sin(\sigma t) + \frac{\dot{\Upsilon}}{\sigma} \cos(\sigma t) \\ H_2 = \Upsilon \cos(\sigma t) - \frac{\dot{\Upsilon}}{\sigma} \sin(\sigma t) \\ Z_1 = Q \cos(\sigma t) - \frac{\dot{Q}}{\sigma} \sin(\sigma t) \\ Z_2 = -Q \sin(\sigma t) - \frac{\dot{Q}}{\sigma} \cos(\sigma t) \end{array} \right. \quad (\text{A.2})$$

So we can redefine the transverse displacement Υ , the wake state Q and their derivatives as:

$$\left\{ \begin{array}{l} \Upsilon = H_1 \sin(\sigma t) + H_2 \cos(\sigma t) \\ \dot{\Upsilon} = \sigma(H_1 \cos(\sigma t) - H_2 \sin(\sigma t)) \\ Q = Z_1 \cos(\sigma t) - Z_2 \sin(\sigma t) \\ \dot{Q} = -\sigma(Z_1 \sin(\sigma t) + Z_2 \cos(\sigma t)) \end{array} \right. \quad (\text{A.3})$$

The new differential system can be defined as

$$\left\{ \begin{array}{l} \dot{H}_1 = \frac{\cos(\sigma t)}{\sigma} (-(\Omega^2 - \sigma^2)(H_1 \sin(\sigma t) + H_2 \cos(\sigma t)) \\ \quad - \tau U \sigma (H_1 \cos(\sigma t) - H_2 \sin(\sigma t)) + h U^2 (Z_1 \cos(\sigma t) - Z_2 \sin(\sigma t))) \\ \dot{H}_2 = \frac{\sin(\sigma t)}{\sigma} ((\Omega^2 - \sigma^2)(H_1 \sin(\sigma t) + H_2 \cos(\sigma t)) \\ \quad + \tau U \sigma (H_1 \cos(\sigma t) - H_2 \sin(\sigma t)) - h U^2 (Z_1 \cos(\sigma t) - Z_2 \sin(\sigma t))) \\ \dot{Z}_1 = \frac{\sin(\sigma t)}{\sigma} (((\omega U)^2 - \sigma^2 - m U^2 g)(Z_1 \cos(\sigma t) - Z_2 \sin(\sigma t)) \\ \quad - \varepsilon U \sigma (Z_1 \sin(\sigma t) + Z_2 \cos(\sigma t))((Z_1 \cos(\sigma t) - Z_2 \sin(\sigma t))^2 \\ \quad - 1) + a(\Omega^2 (H_1 \sin(\sigma t) + H_2 \cos(\sigma t)) \\ \quad + \tau U a (H_1 \cos(\sigma t) - H_2 \sin(\sigma t)))) \\ \dot{Z}_2 = \frac{\cos(\sigma t)}{\sigma} (((\omega U)^2 - \sigma^2 - m U^2 g)(Z_1 \cos(\sigma t) - Z_2 \sin(\sigma t)) \\ \quad - \varepsilon U \sigma (Z_1 \sin(\sigma t) + Z_2 \cos(\sigma t))((Z_1 \cos(\sigma t) - Z_2 \sin(\sigma t))^2 \\ \quad - 1) + a(\Omega^2 (H_1 \sin(\sigma t) + H_2 \cos(\sigma t)) \\ \quad + \tau U \sigma (H_1 \cos(\sigma t) - H_2 \sin(\sigma t)))) \end{array} \right. \quad (\text{A.4})$$

Using the average method, the "slow" dynamic of equation (A.4) can be

defined as follows:

$$\left\{ \begin{array}{l} \dot{H}_1 = \frac{1}{2\sigma} (-(\Omega^2 - \sigma^2)H_2 - \tau U \sigma H_1 + hU^2 Z_1) \\ \dot{H}_2 = \frac{1}{2\sigma} ((\Omega^2 - \sigma^2)H_1 - \tau U \sigma H_2 + hU^2 Z_2) \\ \dot{Z}_1 = \frac{1}{2\sigma} (-(\omega U)^2 - \sigma^2 - hU^2 g)Z_2 - \varepsilon U \sigma Z_1 \left(\frac{Z_1^2 + Z_2^2}{4} - 1 \right) \\ \quad + a(\Omega^2 H_1 - \tau U \sigma H_2) \\ \dot{Z}_2 = \frac{1}{2\sigma} (((\omega U)^2 - \sigma^2 - hU^2 g)Z_1 - \varepsilon U \sigma Z_2 \left(\frac{Z_1^2 + Z_2^2}{4} - 1 \right) \\ \quad + a(\Omega^2 H_2 + \tau U \sigma H_1)) \end{array} \right. \quad (\text{A.5})$$

Using a new system of coordinates defined as

$$\left\{ \begin{array}{l} R_H^2 = H_1^2 + H_2^2 \\ R_Z^2 = Z_1^2 + Z_2^2 \\ \sin \theta_H = H_1/R_H \\ \sin \theta_Z = Z_1/R_Z \end{array} \right. \quad (\text{A.6})$$

we can rewrite the system (A.5) in the following way:

$$\left\{ \begin{array}{l} \dot{R}_H = \frac{U}{2\sigma} (-\tau \sigma R_H + hU R_Z (\sin \theta_H \sin \theta_Z + \cos \theta_H \cos \theta_Z)) \\ \dot{R}_Z = \frac{1}{2\sigma} \left(-\varepsilon U \sigma \left(\frac{R_U^2}{4} - 1 \right) R_U + a R_H (\Omega^2 (\sin \theta_H \sin \theta_Z \right. \right. \\ \quad \left. \left. + \cos \theta_H \cos \theta_Z) - \tau U \sigma (\sin \theta_Z \cos \theta_H - \cos \theta_Z \sin \theta_H) \right) \right) \\ \dot{\theta}_H = \frac{1}{2\sigma R_H \cos \theta_H} (-(\Omega^2 - \sigma^2) R_H \cos \theta_H \\ \quad + hU^2 R_Z (\sin \theta_Z - \sin \theta_H (\sin \theta_H \sin \theta_Z + \cos \theta_H \cos \theta_Z))) \\ \dot{\theta}_Z = \frac{1}{2\sigma R_Z \cos \theta_Z} (-(\omega U)^2 - \sigma^2 - hU^2 a) R_Z \cos \theta_Z \\ \quad + a R_H (\Omega^2 \sin \theta_H - \tau U \sigma \cos \theta_H - \sin \theta_Z (\Omega^2 (\sin \theta_H \sin \theta_Z \\ \quad + \sin \theta_H \sin \theta_Z) - \tau U \sigma (\sin \theta_Z \cos \theta_H - \cos \theta_Z \sin \theta_H))) \end{array} \right. \quad (\text{A.7})$$

It is possible to transform the products of the trigonometric functions into

sums and rewrite equation (A.7) as

$$\left\{ \begin{array}{l} \dot{R}_H = \frac{U}{2\sigma} (-\tau\sigma R_H + hUR_Z \cos(\theta_Z - \theta_H)) \\ \dot{R}_Z = \frac{1}{2\sigma} \left(-\varepsilon U\sigma \left(\frac{R_Z^2}{4} - 1 \right) R_Z + aR_H(\Omega^2 \cos(\theta_Z - \theta_H) - \tau U\sigma \sin(\theta_Z - \theta_H)) \right) \\ \dot{\theta}_H = \frac{1}{2\sigma} (-\Omega^2 + \sigma^2 + hU^2 \sin(\theta_Z - \theta_H) R_Z/R_H) \\ \dot{\theta}_Z = \frac{1}{2\sigma} \left(-(\omega U)^2 + \sigma^2 + hU^2 a + a(-\Omega^2 \sin(\theta_Z - \theta_H) - \tau U\sigma \cos(\theta_Z - \theta_H)) R_H/R_Z \right) \end{array} \right. \quad (\text{A.8})$$

The system can be represented with only three variables. So we propose to replace θ_Z by β defined by $\beta = \theta_Z - \theta_H$. The fact that this reduction is possible means that the system has one degree of freedom.

$$\left\{ \begin{array}{l} \dot{R}_H = \frac{U}{2\sigma} (-\tau\sigma R_H + hUR_Z \cos \beta) \\ \dot{R}_Z = \frac{1}{2\sigma} \left(-\varepsilon U\sigma \left(\frac{R_Z^2}{4} - 1 \right) R_Z + aR_H(\Omega^2 \cos \beta - \tau U\sigma \sin \beta) \right) \\ \dot{\theta}_H = \frac{1}{2\sigma} (-\Omega^2 + \sigma^2 + hU^2 \sin \beta R_Z/R_H) \\ \dot{\beta} = \frac{1}{2\sigma} \left(-(\omega U)^2 + \Omega^2 + hU^2 a - \sin \beta \left(hU^2 \frac{R_Z}{R_H} + a\Omega^2 \frac{R_H}{R_Z} \right) - a\tau U\sigma \cos \beta \frac{R_H}{R_Z} \right) \end{array} \right. \quad (\text{A.9})$$

The numerical solutions of the equilibrium point show that for values of $\omega U \simeq \Omega$, there is a stable equilibrium point for system represented by equation (A.9). These equilibrium points correspond in frequency and amplitude to the limit cycles described in 6.2 and observed in non dimensional numerical simulations, with this parameter set.